Ultrasonic Spectroscopy for in situ Particle Sizing and Crystallization Process Monitoring

Fei Sheng
B.Sc., M.Sc.

Submitted in accordance with the requirements for the degree of

Doctor of Philosophy

The University of Leeds
Institute of Particle Science and Engineering
School of Process, Environmental and Materials Engineering

November 2012

Acknowledgements

I wish to thank my academic supervisors Dr Xiaojun Lai, Professor Kevin J. Roberts and Professor Xuezhong Wang for offering me the opportunity of Ph.D. studies and their much valued assistance, advice and support throughout this research.

I would express my deepest gratitude to Professor Malcolm J. W. Povey for his inspirational suggestions and kind encouragement without which the completion of the work would have seriously suffered. Very appreciate Dr Valerie Pinfield and Professor Mi Wang for their contribution on the review work.

My sincerest appreciation to Dr Nik Watson and Dr Melvin Holmes for their advice and discussion on the acoustic work; Dr Tian Lin for his suggestions for the set-up of the MatLab program; Dr Richard Tweedie for his help on the calibration work of the instruments. I would like to specially thank to the colleagues at the University of Leeds, Dr Robert Hammond, Dr Tariq Mahmud, Dr Rehan Mohammed, Dr Antonia Borissova, Dr Vasuki Ramachandran, Dr Caiyun Ma, Dr Toshiko Izumi, Mr. Dave Merrifield, Miss Thai Hien Nguyen, Mr. Qassim Hussain, Miss Miram Barber, Miss Neepa Paul, Miss Siti Nurul Ain, Mr Akinola Falola and Mr Peter Baldwin for their helpful scientific discussions. I would also like to express my appreciation for the great help received from Mr. Simon Lloyd, Mrs. Ulrike Aufderhorst, Miss Judith Squires and Mrs. Kirn K. Jutlla.

Very special thanks to my dear friends Siyi Jiang, Haiyang Jiang, Zihua Wang, Chaoyang Ma, Yang Yang, Jingjing Liu, Wei Li, Dianzi Liu, Kai Yang, Fangzhong Su, Yuanyuan Li and Jiabin Jia for their care and support.

Finally, my heartfelt appreciation and words beyond gratitude goes to my parents for their constant love, encouragement and unconditional support through these years.

Abstract

The application of ultrasonic techniques for crystal size distribution (CSD) and solid volume concentration measurements in batch crystallization processes was investigated in situ and on-line, with emphasis on the crystallization of the copper sulphate pentahydrate crystallization system.

The fundamental crystal characteristics of copper sulphate pentahydrate including the solubility, metastable zone width, and induction time were assessed. The kinetic analyses carried out were independent of the acoustic measurement of the copper sulphate pentahydrate and provided the research background for the acoustic study.

The potential of ultrasonic spectroscopy was demonstrated using an experimental approach, focusing on the problem of cooling crystallization of copper sulphate pentahydrate from an aqueous solution in a 20 litre scale reactor. The set up of the physical properties matrix for the system allowed the ultrasound spectra to be converted into the particle size and particle volume information. Different cooling conditions were optimized due to the limitations of the instrument. The overall growth rate as a function of the relative solution supersaturation was determined from the combination of particle size and solid concentration.

A new method derived from the Modified Urick equation focusing on the on-line measurement of the crystal volume concentration without the phase separation was built up, which was modified from the prototype applied in the non-soluble oil-in-water system. The extended application on the copper sulphate pentahydrate crystal volume concentration during the dynamic process was successfully developed.

The third generation prototype acoustic spectroscopy Alphasizer developed by Malvern Ltd for on-line acoustic attenuation and velocity measurement was calibrated. Particle size distribution was successfully calculated from the manually calibrated attenuation spectra. The feedback closed loop supersaturation control based on Alphasizer was designed. The control algorithms and a communication system were built up.

Notation

Symbols	Definition	Units
α	particle diameter	m
α,b,c (Chapter 2)	axes length of unit cell	m
a,n	attenuation coefficient factors	1/m
A	single molecule	-
A_l, t_l	growth rate coefficients	-
A_n (Chapter 2)	critical cluster	-
(Chapter 3)	scattering coefficient	1/m
(Chapter 4)	surface area	m^2
b	cooling rate	°C/min
B	adiabatic bulk modulus of liquid	Pa
c	solution concentration	g/L
c*	normal equilibrium solubility of the substance	g/100g
c_r	solubility of particle of size r	g/100g
C_p	thermal specific of solution at constant pressure	$J/ kg\cdot K$
C_v	thermal specific of solution at constant volume	$J/ kg\cdot K$
D	distance between the transducers	m
d	electrodes	1/cm
f	sound frequency	Hz
G (Chapter 3)	rigidity modulus	Pa
(Chapter 4)	actual conductance	Siemens
(Chapter 6)	overall growth rate	m/s
h,k,l	Miller indices	-
I	sound wave intensity	W/m^2
J	rate of nucleation	$\#/m^3\cdot s$
K	cell constant	1/cm

Symbols	Definition	Units
k (Chapter 2)	Bolzmann constant	J/K
(Chapter 3)	sound wavenumber	-
k_n	nucleation rate constant	-
K_c	controller gain	-
K_p	process gain	-
M	molar mass of solid	kg/mol
n	order of nucleation	-
N	number of points in the attenuation spectrum	-
P	complex propagation constant	-
P_r	probability of having a particle of radius r	m
q	mass of crystalline substance	g
R	gas constant	-
S	supersaturation ratio	-
S_e	error of supersaturation	-
S_{sp}	set point of supersaturation	-
T (Chapter 2)	solution temperature	°C, K
(Chapter 3)	sound wave period	s
T_f	melting point of the solute	°C, K
t_{ind}	induction time	s
t_{therm}	thermal relaxation time	s
t_{vis}	viscous relaxation time	s
v	molecular volume	m^3/mol
x	mole fraction of the solute	%
x_g	geometric mean	µm
α	sound attenuation coefficient	dB/inch=0.4dB/cm
α, β, γ (Chapter 2)	angle of unit cell	°
β	volume thermal expansively	1/K

Symbols	Definition	Units
γ (Chapter 2)	interfacial tension between solid-liquid phase	J/m^2
(Chapter 3)	the specific heat of solution	-
ΔC_{max}	the maximum allowable supersaturation	g
ΔG	overall excess free energy	J
ΔG_s	sum of the surface excess free energy	J
ΔG_v	volume excess free energy	J
ΔH_f	molar enthalpy of fusion of the solute	J/mol
ΔL	path length of the wave	m
ΔS_f	molar entropy of dissolution	J/mol
ΔT_{max}	metastable zone width	°C
ζ_g	geometric standard deviation	-
η	shear viscosity of solution	Pa·s
θ	the angle of incidence	^{o}
κ	adiabatic compressibility of liquid	Pa
λ	ultrasound wavelength	m
λ_{th}	thermal wavelength	m
λ_{vis}	viscous wavelength	m
μ	bulk viscosity of solution	Pa·s
π	ratio of a circle's circumference to its diameter	-
ρ	density	kg/m^3
σ	relative supersaturation	-
τ	thermal conductivity	W/(m·K)
τ_I	integral time constant	min/repeat
τ_c	process time constant	-
υ (Chapter 2)	number of moles of ions	mol
(Chapter 3)	sound velocity	m/s
υ_l^s	velocity of longitudinal sound waves in the solid	m/s
υ_t	velocity of transverse sound wave	m/s

Symbols	Definition	Units
φ	particle volume	m^3
Φ	volume fraction of dispersed phase	%
ϕ	volume fraction of solid	%
χ, ψ	scattering coefficients in modified Urick equation	1/m
ω	radial frequency	Hz
Θ	process dead time	-

Abbreviation	Definition
CSD	Crystal size distribution
PAT	Process analytical techniques
ATR-FTIR	Attenuation total reflection fourier transform infrared spectroscopy
NIR	Near infrared spectroscopy
MSV	Ultrasizer
ECAH	Epstein and Carhart, Allegra and Hawley model
MSZW	Metastable zone width
SSD	Sum of the squares of the differences
PSD	Particle size distribution
URT	Ultrasonic resonator technology
UVM	Ultrasound velocity meter
RCI	Retreat curve impeller
XRD	X-ray diffraction
DSC	Differential scanning calorimetry
TGA	Thermogravimetric analysis
PXRD	Powder X-ray diffraction
FFT	Fast fourier transform
HCM	Hardware control module
ASM	Application specific module
PI	Proportional-Integral

Contents

List of Figures

List of Tables

Chapter 1 Introduction

Summary

The motivation behind this thesis is given and the overview of the PhD work is summarized. The contents of the thesis are detailed together with the chapter description.

1.1 Research background

Crystallization represents an important process of purification and separation in the chemical industry, which involves the formation of crystalline solids from the solution. Large quantities of high purity products of both organic and inorganic materials can be manufactured in crystalline form. Therefore, crystallization is commonly utilized in pharmaceuticals, fine chemicals, agrochemicals, food and cosmetics industries, aiming to produce high purity and high quality products [1, 2].

Crystals are produced in the wet product slurry, which contains the solid crystals and mother liquid. Several parameters of the crystal include the shape, purity, polymorphic form and the crystal size distribution (CSD) representing the quality of the crystals, which were determined by the process conditions. The CSD is considered as the most significant parameter in controlling the quality of the product, which determines the flow ability, dissolution rate and the downstream solid-liquid separation processes, i.e., filters, centrifuges and dryers. On the other hand, the supersaturation of the solution played an important role in controlling the nucleation and crystal growth during the crystallization process, which is the critical parameter for controlling the process.

However, due to the complex mixing conditions of the product with its mother liquid, plus the non-equilibrium state in the batch reactors, it is hard to determine the processing conditions. In order to solve these problems, the development and use of on-line process analytical techniques (PAT) for monitoring batch processes has become popular. Several on-line sensors were developed and applied in the process monitoring, which included the light scattering technique [3], light reflect technique [4], attenuated total reflection fourier transform infrared spectroscopy (ATR-FTIR) [5], near infrared spectroscopy (NIR) [6], and acoustic techniques [7-9]. These techniques were all used to predict the crystal size distribution or solution concentration during the crystallization process. Only the ultrasonic technique is able to reveal on-line the crystal size distribution and solution concentration simultaneously.

The acoustic technique can be generally divided into two aspects, ultrasound velocity measurement and ultrasound attenuation spectroscopy.

The acoustic velocity measurement method was developed by Povey, Pinfield and McClements [8, 10, 11] for the particle volume determination in the oil-in-water systems. This velocity model requires the particle size limited to the long wavelength region, which means the particle size is much smaller than the wavelength of the sound wave. In this project the model was developed and extended to be used in the soluble solution system, and the crystal volume that crystallized from the mother solution can be determined using sound velocity.

The ultrasonic attenuation spectroscopy was recently developed for on-line particle sizing plus particle volume concentration determination in the dispersions. This technique can be applied in the opaque and high concentration dispersion systems without dilution. The acoustic attenuation spectroscopy Ultrasizer (MSV) was developed by Malvern Ltd. The sound attenuation was measured as a function of frequency in the solution, and the model developed by Epstein and Carhart [12], Allegra and Hawley [13] (ECAH model) was used for the deconvolution of the attenuation spectra into the crystal size distribution and solid volume concentration of the crystals in the suspension. The size range is 0.01-1000 μm, and the measurements should be carried out with suspension of solid concentration between 0.1-80 v% depending on the sample characteristics [14]. However, 5 minute intervals for each measurement are a drawback for the fast dynamic process, this limited the crystallization as it could only measured accurately at low cooling rates.

In order to solve the time consuming problem of using MSV, a new prototype acoustic attenuation spectroscopy (i.e. Alphasizer) developed by Malvern Ltd was used in this project. The pulse generation system was installed in the Alphasizer, and the measurement interval was reduced to 20 seconds for each test. The Alphasizer could determine the crystal size distribution and crystal volume concentration during the crystallization process, similar to the MSV. The size range was still 0.01-1000 μm, and the measurements were carried out with suspension of solid concentration between 0.1-50 v% depending on the sample characteristics. The rapid data acquisition allowed the Alphasizer obtain more details in the dynamic system measurements. Furthermore, the group velocity measurement from the Alphasizer can be used to predict the crystal volume concentration depending on the velocity model developed in this project, which is a novel application for the acoustic technique. The solution supersaturation could be obtained as the suspended crystal volume is known, and the supersaturation closed loop control system based on the Alphasizer was set up in this project. The on line monitoring of the supersaturation could be realized using one acoustic instrument based on a new algorithm.

1.2 Research objectives

The main target of this research project is monitoring of the crystallization process based on ultrasonic techniques. Crystal size distribution and solution supersaturation measured by the sound attenuation or sound velocity can be used to predict the kinetic parameters of the crystallization system. The development of the new acoustic technique introduces a novel way to characterize and control the crystallizing process. The key research objectives are listed as follows:

- on-line monitoring the crystallization process through the acoustic attenuation spectrometer
- develop the acoustic velocity model for the on-line measurement of the particle volume concentration
- set up a new acoustic attenuation spectrometer and realize the supersaturation closed loop control based on the new logarithm

1.3 Scope of the thesis

The body of the thesis consists of nine chapters, which are described below:

Chapter 2 gives a review of the fundamental knowledge of crystal science and the crystallization process, where the definition and underlying principles of this field are presented, with emphasis on the nucleation and crystal growth study. The relationship between the kinetic parameters of the crystallization process and the solution supersaturation was reviewed.

Chapter 3 describes the principles of propagation of sound wave through homogeneous and heterogeneous media. The mechanisms of absorption and scattering of the sound wave by the media were presented. The dependant of the sound attenuation and sound velocity on the absorption and scattering was described in detail, and different models on the prediction of particle size and particle volume concentration based on the acoustic technique are presented and compared.

Chapter 4 lists the instruments and techniques used in this research project. The measurement theories and methods of the techniques are illustrated in this chapter. Especially for the ultrasound attenuation spectroscopy, the methods of manual optimization of the measurement strategy are presented.

Chapter 5 gives a fundamental crystal characterization of the material used in this project, i.e., copper sulphate pentahydrate. The measured kinetic parameters were calculated depending on the measurements of the metastable zone width and induction time, which provide the databases and background for the following measurements. The crystalline form of the crystals produced by the batch cell crystallization experiments was characterized and the crystal habit was illustrated.

Chapter 6 presents the study of the crystallization of copper sulphate pentahydrate in a

20 litre reactor based on the ultrasound attenuation spectroscopy MSV system. The crystallization process condition was optimized in order to fit the limitation of the instrument. Overall growth rate related to the supersaturation was extracted, and the growth mechanism was analyzed.

Chapter 7 describes the measurement of ultrasound velocity in the homogeneous and heterogeneous media. In the pure liquid, the variation of sound velocity is only caused by the absorption and relaxation process, and the classic function of sound attenuation related to sound velocity can be used to predict the bulk viscosity of the Newtonian liquid. In the particulate system, the variation of the sound velocity could indicate the adiabatic compressibility of the solid, and the particle volume concentration simultaneously. The modified scattering model on prediction of the crystal volume during the crystallization was developed.

Chapter 8 gives a description of the third generation process acoustic instrument (Alphasizer) for the in-line particle size distribution and solid concentration measurement of suspensions. The prototype instrument was calibrated under several different conditions using silica suspension. The optimal strategies under different solid volume concentration, different temperature for two different size silica samples were successfully modified. Precision size information can be determined by the Alphasizer based on the attenuation measurement. The function of the velocity measurement by the Alphasizer was used to determine the crystal volume during the crystallization process based on the model developed in Chapter 7. The in-process measurement and closed supersaturation loop control system was set up, the communication between the instruments and controlling software was successfully build up, and the controlling logarithm was designed based on the acoustic attenuation and acoustic velocity measurement.

Chapter 9 presents the conclusions of this project and some suggestions for the direction of future research.

Chapter 2 Crystallization Science and Process Characterization

Summary

A review of the crystal science and the fundamentals of crystallization process are given in this chapter with emphasis on the nucleation and crystal growth steps of crystallization process.

2.1 Introduction

The scope of this chapter is to give an overview of the field of crystallization, beginning with the definition of the different types of crystal, along with the basic parameters for crystal characterization, such as crystal chemical bonds, crystal morphology and crystal structure. The background on crystallization processes including solubility, supersaturation, nucleation, and crystal growth are all reviewed. The process of crystal formation from the solution including the nucleation and crystal growth aspects are analyzed from a thermodynamic and mechanistic perspective.

2.2 Crystallography

Crystals have always attracted the attention of scientists, because they differ in many ways from other solid state materials. The main difference is in the periodical arrangement of constituent species. In the crystalline state, the species are arranged in a pattern that repeats itself in three dimensions throughout the interior of the crystal [1], whereas the solids in amorphous have no long-range periodic structure at all, with all constituent species being completely disordered. The kinds of material in the crystalline state may have different physical and chemical properties, but they are common in their order structure.

A crystal is made by the smallest 3D-arrangement, the repetition of which is the entire crystal lattice. The minimum entity is called the unit cell. A unit cell contains one or several molecules, atoms or ions. Some parameters are used to describe the unit cell. The lengths of its three axes are called a, b and c. The three angles between them are α, β and γ, where α is the angle between the b and the c axes, β is the angle between the a and the c axes and γ is the angle between the a and b axes.

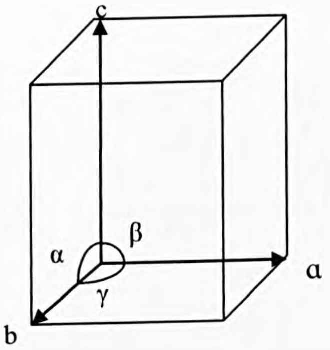

Figure 2.1: An example of unit cell of crystal[15].

The crystal lattice should have the following characteristics:

- periodically spaced
- infinite in extent
- all lattice points are identically surrounded
- mathematically described by translation vector

The variation of the parameter could determine several kinds of crystal system. In one type of system, different types of unit cells are possible depending on the place and number of the lattice points they contain. There should be 14 ways of arranging lattice points in three dimensions [16]. There are 7 systems needed to describe the unit cell, which is shown in Table 2.1. The 7 additional lattices are obtained by additional lattice points, which are in the centre of the unit cell, centre of each face or the centre of two basal faces. The 14 space lattice, called Bravias lattices, is shown in Figure 2.2.

Table 2.1: The seven crystal systems and their associated inter-relationships with the lattice parameters

Category	Edge Lengths	Internal Angles
Cubic	$a=b=c$	$\alpha=\beta=\gamma=90^\circ$
Tetragonal	$a=b\neq c$	$\alpha=\beta=\gamma=90^\circ$
Monoclinic	$a\neq b\neq c$	$\alpha=\beta=90^\circ\neq\gamma$
Orthorhombic	$a\neq b\neq c$	$\alpha=\beta=\gamma=90^\circ$
Rhombohedral	$a=b=c$	$\alpha=\beta=\gamma\neq 90^\circ$
Hexagonal	$a=b\neq c$	$\alpha=\beta=90^\circ,\gamma=120^\circ$
Triclinic	$a\neq b\neq c$	$\alpha\neq\beta\neq\gamma\neq 90^\circ$

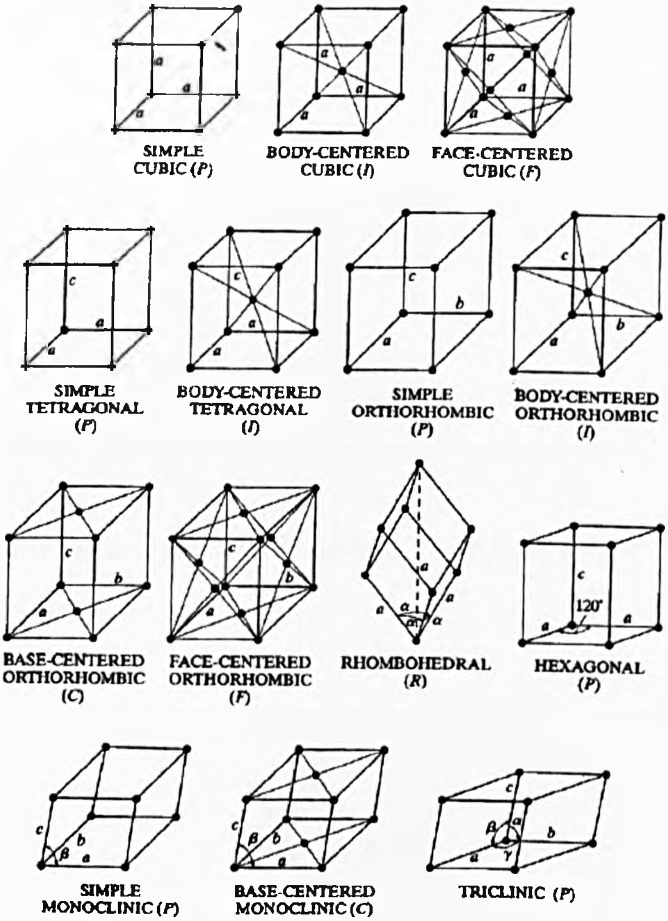

Figure2.2: Schematic diagram illustrating the main features associated with the 14 Bravais lattices (P=primitive cell, F=face centred, I=body centred, and C=base centered) [15]

In order to predict the face of the crystal, Miller suggested in 1839, that each face of a crystal could be represented by the indices h, k and l, which is defined by:

$$h = \frac{a}{X} \tag{2.1}$$

$$k = \frac{b}{Y} \tag{2.2}$$

$$l = \frac{c}{Z} \tag{2.3}$$

where a, b, and c are the unit cell lengths, and X, Y and Z are the intercepts on the unit cell axes, respectively.

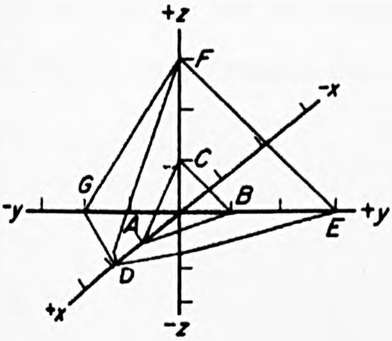

Figure 2.3: Intercepts of planes on the crystallographic axes [17]

The indices h, k and l of the plane ABC shown in Figure 2.2 are 1,1,1, which is written as (111). The indices h, k and l of the plane DEF shown in Figure 2.3 can be defined using the same theory as 1/2, 1/3, and 1/3, and multiplying by six, the face DEF, therefore is indexed as (322). On the other hand, the intercept of OG is negative, which gives the indices of the face DFG as $(3\bar{3}2)$.

2.3 Crystal chemistry

2.3.1 Chemical bonds

The crystalline solid is specified by the chemical bonding in the solid state. There are four main types of bonding in the crystalline solid, which are ionic, covalent, molecular and metallic. Most crystalline solids can be classified in these four types although some materials may be outside of these categories:

- ionic bonds involve the transfer of electrons (e.g. sodium chloride)
- covalent bonds involve the sharing of electrons (e.g. diamond)
- metallic bonds could be treated as a combination of both ionic and covalent boding (e.g. copper)
- inter-molecular bonds include the Van der Waals and hydrogen bonds, which are polar in nature but are much weaker than the other three bonds (e.g. organic compounds).

2.3.2 Polymorphism

A substance capable of crystallizing into different, but chemically identical crystalline forms is defined as a polymorph. Different polymorphs of a given substance are chemically identical but will exhibit different physical properties. Polymorphism can exist in most kinds of crystal structures and especially in molecular crystals, i.e. the organic compounds. Benzamide and naphthalene were the first observed polymorphs in molecular solids. In the inorganic compound, the calcium carbonate and silicon dioxide both typically contain polymorphisms.

Inter-conversion between two polymorphic forms may occur as a result of a change in conditions of temperature, pressure or solvent. A conversion result from temperature changes is said to be enantiotropy (changes into the opposite). It is a solid-state transition, involving a concerted displacement of the constituent atoms, ions or molecules. In this kind of polymorphic transformation the constituent molecules or ions of the meta-stable polymorphic structure rearrange their position in the solid state to obtain a more stable polymorphic structure.

$$Liquid \Leftrightarrow FormI \Leftrightarrow FormII \Leftrightarrow FormIII \tag{2.4}$$

A different type of inter-conversion between polymorphs may occur, involving a change in conditions of solvent, temperature or pressure. In this case, the transition involves a dynamic equilibrium with the liquid form (melt or solute in solvent) rather than a solid state transition.

$$FormI \Leftrightarrow Liquid \Leftrightarrow FormII \tag{2.5}$$

The transformation in the liquid can be explained relative to the solubility difference of the polymorphic forms, due to the stable form always having a lower solubility [18]. One classic example is the L-glutamic acid, which has two crystal forms, i.e. metastable form and stable form [19]. Because the crystallization occurs by starting with a saturated solution at a given temperature, cooling rapidly to produce a supersaturated solution, form which crystals grow, until the solution concentration is reduced to the solubility at that temperature. The meta-stable form would be the first to leave the solution until the solution concentration reached its solubility. The stable form starts to nucleate and grow and consumes the meta-stable form crystal. The crystallization process is not complete until the solution concentration reaches the solubility of the stable form, and the solid transforms completely in to the stable form.

2.3.3 Morphology and crystal habit

Crystal morphology is the general appearance of crystals which are described by the Miller indices of the faces which characterize the shape of the crystal. The morphology of the crystal is determined by the growth rates of the different crystal faces. The crystal structure and crystallization conditions such as supersaturation, solvent, additives, and pH value all affect the growth rates, and consequently affect the morphology of the crystal. Crystal habit refers to the external appearance of the crystal. The crystals may grow more rapidly or be stunted in one direction, thus an elongated growth of prismatic habit gives a needle shaped crystal (acicular habit) and a stunted growth gives a flat plate-like crystal (tabular, plate or flaky habit) shown in the Figure 2.4:

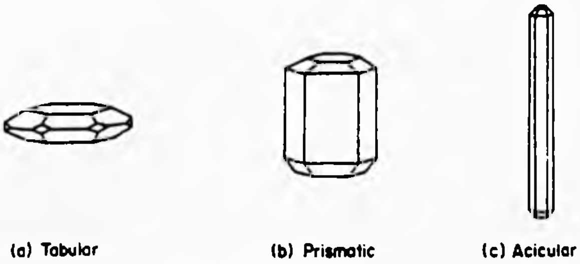

Figure 2.4: Crystal habit illustrated on a hexagonal crystal [17]

2.4 The crystallization process

2.4.1 Solubility

Solubility is the equilibrium limit value of the solute concentration dissolved in the solvent. In an ideal solution, the interaction between solute and solvent molecules is identical with that between the solute molecules and the solvent molecules themselves. The solubility in the ideal solution can be predicted using the van't Hoff equation:

$$\ln x = \frac{\Delta H_f}{R}\left[\frac{1}{T_f} - \frac{1}{T}\right] \tag{2.6}$$

where x is the mole fraction of the solute in the solution, T is the solution temperature, T_f *is the fusion temperature (melting point) of the solute,* ΔH_f *is the molar enthalpy of fusion of the solute which equal to* $T_f \times \Delta S_f$ *and R is the gas constant (8.314Jmol-1K-1)*

$$\ln x = -\frac{\Delta H_f}{RT} + \frac{\Delta S_f}{R} \tag{2.7}$$

where ΔS_f *is the molar entropy of dissolution*

In the particular solution, the solubility can also be predicted by the van't Hoff equation. However, if the solution exhibits non-ideal behaviour, the enthalpy ΔH_f should be replaced by the ΔH_d (of dissolution) [20]:

If the slope $-\Delta H_f/R$ keeps straight in the specific temperature region, it means there is no phase transition of the solute. Otherwise, the discontinuity in the solubility curve denotes the phase change. For instance, the solid phase deposited from an aqueous solution of sodium sulphate below 32.4 °C will consist of decahydrate, whereas the solid deposited above this temperature will consist of anhydrous salt.

2.4.2 Effect of particle size on solubility: Ostwald Ripening

The relationship between particle size and solubility was first derived for the vapour pressures in liquid-vapour systems by Thomson [21] in 1871, utilized later by Gibbs [22], and applied to solid-liquid systems by Ostwald [23] in 1900 and Freundlich [24] in 1926. The Gibbs-Thomson relationship between particle size and solubility can be expressed in the form:

$$\ln\left[\frac{c(r)}{c^*}\right]=\frac{2M\gamma}{\upsilon RT\rho r} \tag{2.8}$$

where c(r) is the solubility of particles of size (radius) r, c is the normal equilibrium solubility of the substance, R is the gas constant, T is absolute temperature, ρ is the density of the solid, M is the molar mass of the solid in solution and γ is the interfacial tension of the solid in contact with the solution. The quantity υ represents the number of moles of ions formed from one mole of electrolyte. For a non-electrolyte, $\upsilon = 1$.*

As a result of the particle size dependence on the solubility, some variations of the solute concentrations may occur. A consequence of this is that there is a tendency for the small particles to disappear, whereas the large particles (Crystals) grow larger. Although theoretically the particle size distribution should eventually become mono-dispersed, in practice for most solutes in water the solubility increase only starts to become significant for particle sizes smaller than about 1 μm.

2.4.3 Supersolubility

The state of supersaturation is an essential requirement for all crystallization operations. The terms 'labile' and 'metastable' were first introduced by Ostwald [25] in 1897 to classify supersaturated solutions in which spontaneous (primary) nucleation may occur. From the work of Miers and Isaac [26, 27] on the relationship between supersaturation and spontaneous crystallization, the diagram of solubility and supersolubility curves was worked out, and the supersolubility curve is almost always parallel to the solubility curve [26]. The width of the metastable zone would also be affected by the crystallization conditions, such as the cooling rate, the intensity of agitation, the presence of impurities, and the thermal history of the solution [28-31]

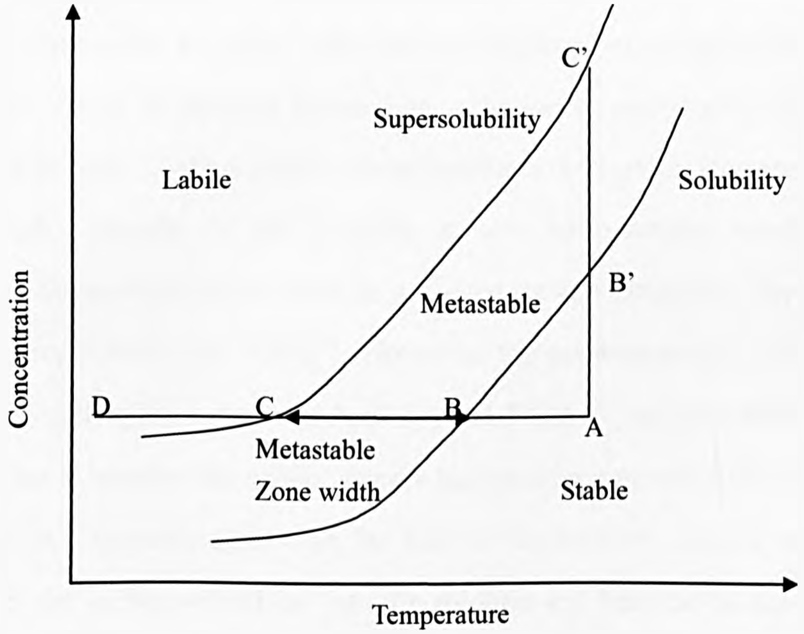

Figure 2.5: Schematic diagrams of solubility-supersolubility and metastable zone width

Despite the definite existence of the metastable region, the supersolubility is hard to define. The diagram shown in Figure 2.5 is therefore divided into three zones, one well-defined and the other two variable to some degree:

1. The stable (unsaturated) zone, where crystallization is impossible.
2. The metastable (supersaturated) zone, between the solubility and supersolubility curves, where spontaneous crystallization is improbable. However, if a crystal seed were placed in such a metastable solution, growth would occur on it.
3. The unstable or labile (supersaturated) zone, where spontaneous crystallization is probable, but not inevitable.

Point A in Figure 2.5 is used to represent the solution, if the solution is cooled down without loss of solvent (line ABC), spontaneous crystallization cannot occur until conditions the represented by point C are reached. At this point, crystallization may be spontaneous or it may be induced by seeding, agitation or mechanical shock. After further cooling to point D, spontaneous crystallization would occur. However, in some cases, the high viscosity of the solution at low temperatures would prevent crystallization. Supersaturation can also be achieved by vaporization of the solvent at the constant temperature (line AB'C'). However, the supersaturation value for the evaporation crystallization process is hard beyond Point C' and penetrates into the labile zone. This is because the surface from which evaporation takes place is usually supersaturated to a greater degree than the bulk of the solution. The crystals which crystallized on the surface would fall into the solution and become the seed, and the crystallization process would always happen in zone B' to C' for these cases.

When the solution concentration is higher than the equilibrium concentration, supersaturation is generated. The supersaturation is the driving force for the crystallization to occur, which needs to overcome the unfavorable energy associated with the creation of new interfaces when the solid phase first forms from the solution. The supersaturation is commonly defined as the concentration driving force, Δc, the supersaturation ratio, S, and a quantity sometimes referred to as the absolute or relative supersaturation, σ. The quantities can be defined by:

$$\Delta c = c - c^* \tag{2.9}$$

$$S = \frac{c}{c^*} \tag{2.10}$$

$$\sigma = \frac{\Delta c}{c^*} = S - 1 \tag{2.11}$$

where c is the solution concentration , and c is the equilibrium saturation at the given temperature.*

2.4.4 Nucleation

Before crystallization can occur, the existence of a number of minute solid bodies, i.e. embryos, nuclei or seeds in the solution is necessary, which acts as the centre of the crystallization. Nucleation can occur spontaneously or may be induced artificially. The crystallization process can be divided into two separate categories depending on the different nucleation mechanisms. Primary nucleation can occur spontaneously (homogeneous nucleation) or could be induced by foreign particles in the system (heterogeneous nucleation). Secondary nucleation occurs when the crystals of solute are already present in the solution.

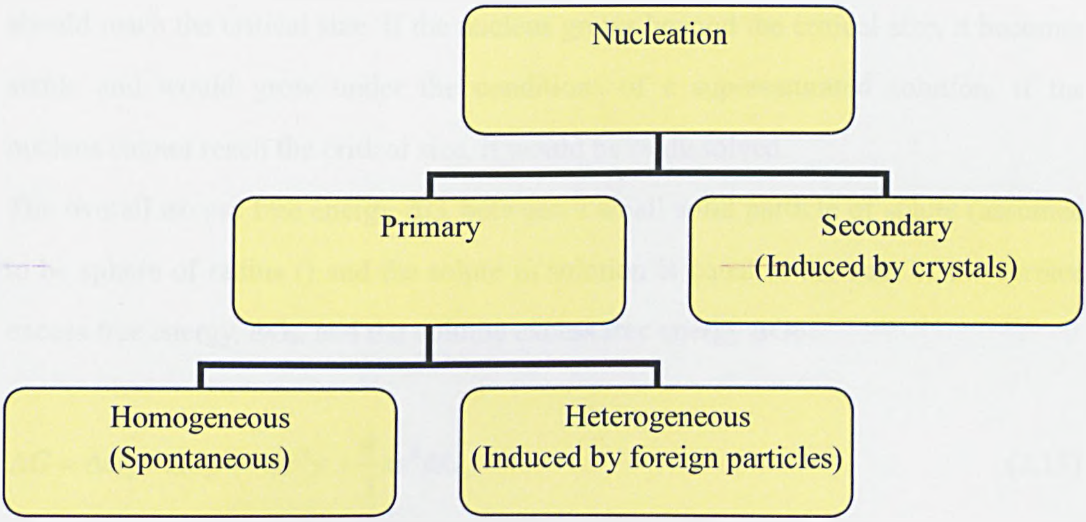

Figure 2.6: Schematic of the mechanisms of nucleation [32]

2.4.4.1 Homogeneous nucleation (HON)

The number of molecules in a stable crystal nucleus can vary from around ten to several thousand, the classical theory of nucleation assumes that the nucleus is formed in the solution by the successive attachment and detachment of single molecules [33].

$$\begin{aligned} &A + A \Leftrightarrow A_2 \\ &A_2 + A \Leftrightarrow A_3 \\ &A_{n-1} + A \Leftrightarrow A_n \end{aligned} \qquad (2.12)$$

where A *is one single molecule, and* A_n *is the critical cluster which denotes* n *molecules. Further molecular additions to the critical cluster would result in nucleation and subsequent growth of the nucleus.*

The classical theory of nucleation was carried out by Gibbs [34], Voolmer [35], and Becker and Doring [36], which was based on the condensation of a vapour to a liquid, and then extended to the crystallization from melts and solutions. The free energy changes are associated with the process of homogeneous nucleation. The nucleus must overcome the free energy barrier in order to become stable, which means it should reach the critical size. If the nucleus grows beyond the critical size, it becomes stable and would grow under the conditions of a supersaturated solution, if the nucleus cannot reach the critical size, it would be re-dissolved.

The overall excess free energy ΔG, between a small solid particle of solute (assumed to be sphere of radius r) and the solute in solution is equal to the sum of the surface excess free energy, ΔG_s, and the volume excess free energy ΔG_V.

$$\Delta G = \Delta G_s + \Delta G_V = 4\pi r^2 \gamma + \frac{4}{3}\pi r^3 \Delta G_v \qquad (2.13)$$

where ΔG_v *is the free energy change of the transformation per unit volume and* γ *is the interfacial tension, i.e., between the developing crystalline surface and the supersaturation solution in which it is located.*

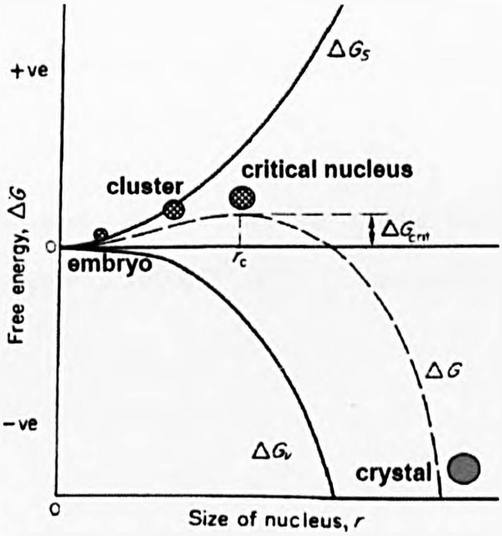

Figure 2.7: Free energy diagram for nucleation explaining the existence of a critical nucleus [37]

Figure 2.7 shows the effect of the sum of the free energy changes relating to the nucleus size. The maximum free energy value ΔG_{crit}, corresponds to the critical nucleus, r_c, for a spherical cluster which is obtained by maximizing Equation 2.13, setting $d\Delta G/dr=0$,

$$\frac{d\Delta G}{dr} = 8\pi r \gamma + 4\pi r^2 \Delta G_v = 0 \qquad (2.14)$$

therefore

$$r_c = \frac{-2\gamma}{\Delta G_v} \tag{2.15}$$

where ΔG_v is a negative quantity, from equations 2.13 and 2.15 we get

$$\Delta G_{crit} = \frac{16\pi\gamma^3}{3(\Delta G_v)^2} = \frac{4\pi\gamma r_c^2}{3} \tag{2.16}$$

The relationship between nucleus size and supersaturation can be expressed by the Gibbs-Thomson equation,

$$\ln S = \frac{2\gamma v}{kTr} \tag{2.17}$$

where S is the supersaturation, υ is the molecular volume, k is the Bolzmann constant, the gas constant per molecule (1.3805E^{-23} JK^{-1}), T is temperature; this gives

$$-\Delta G_v = \frac{2\gamma}{r} = \frac{kT\ln S}{v} \tag{2.18}$$

Hence, from Equation 2.16

$$\Delta G_{crit} = \frac{16\pi\gamma^3 v^2}{3(kT\ln S)^2} \tag{2.19}$$

The rate of nucleation, J, e.g. the number of nuclei formed per unit time per unit volume, can be expressed in the form of the Arrhenius reaction velocity equation commonly used for the rate of a thermal activated process [38],

$$J = A\exp\left(-\frac{\Delta G}{kT}\right) \tag{2.20}$$

where A is the pre-exponential factor

Combining equation 2.19 and 2.20

$$J = A\exp\left[-\frac{16\pi\gamma^3 v^2}{3k^3T^3(\ln S)^2}\right] \tag{2.21}$$

It is clear to see that the three main variables governing the rate of nucleation include the temperature, T, the degree of supersaturation, S, and the interfacial tension, γ.

2.4.4.2 Heterogeneous nucleation

When foreign particles exist in the crystallization system, it is defined as heterogeneous nucleation. Indeed, heterogeneous nucleation is a more common event in nature than homogeneous nucleation. Heterogeneous nucleation happens at lower supersaturation levels than homogeneous nucleation due to the lower free energy barrier for the heterogeneous case. The overall free energy change associated with the formation of a critical nucleus under heterogeneous conditions $\Delta G'_{crit}$, must be lower than the corresponding free energy change, ΔG_{crit}, associated with homogeneous nucleation, i.e.

$$\Delta G'_{crit} = \phi \Delta G_{crit} \tag{2.22}$$

where the factor ϕ is less than unity.

As shown in Equation 2.21, the interfacial tension, γ, is one of the important factors controlling the nucleation process. The interfacial energy diagram in the heterogeneous nucleation case is shown in Figure 2.8, which is a three phase system, including the γ_{cl} (between the solid crystalline phase, c, and the liquid l), γ_{sl} (between another foreign solid surface, s, and the liquid) and γ_{cs} (between the solid crystalline phase and the foreign solid surface).

$$\gamma_{sl} = \gamma_{cs} + \gamma_{cl} \cos\theta \tag{2.23}$$

The angle θ is the angle of contact between the crystalline deposit and the foreign solid surface, which corresponds to the angle of wetting in liquid-solid systems.

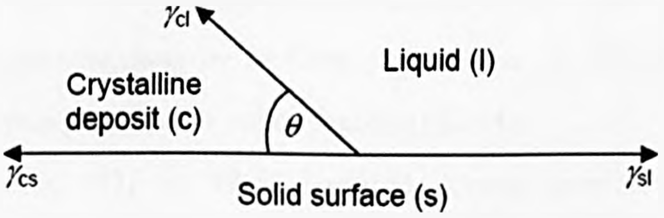

Figure 2.8: Interfacial tensions at the boundaries between three phases [37]

The factor ϕ in Equation 2.22 can be expressed as [39]

$$\phi = \frac{(2+\cos\theta)(1-\cos\theta)^2}{4} \tag{2.24}$$

For the case of complete non-affinity between the crystalline solid and the foreign solid surface (corresponding to that of complete non-wetting in liquid-solid systems), θ is equal to 180°, the overall free energy of nucleation is the same as that required for homogeneous or spontaneous nucleation. For the case of partial affinity (the partial wetting of a solid with a liquid), $0 < \theta < 180^\circ$, the nucleation is easier to achieve because the overall excess free energy required is less than that for homogeneous nucleation. For the case of complete affinity (complete wetting) θ equal to 0, the free energy of nucleation is zero. This case corresponds to the seeding of a supersaturated solution with crystals of the required crystalline product, which means no nuclei have to be formed in the solution.

2.4.4.3 Secondary nucleation

When the crystal of the solute is already present or deliberately added, nucleation would occur at a lower supersaturation. This process is defined as the secondary nucleation. This phenomenon was mentioned in the early paper by Ting and McCabe in 1934 [40] in the research of magnesium sulphate, similar observations were made in studies of copper sulphate by McCabe and Stevens in 1951 [41]. Some other research on secondary nucleation can be found in [42-44].

Strickland-Constable [45] in 1968 described several possible mechanisms of secondary nucleation, including the initial breeding, dendrite breeding, attrition breeding, and fluid shear breeding.

In initial breeding, the secondary nuclei originate from the seed crystals. Tiny crystallites are formed on the crystal surface during the growth of seed crystals or due to fragmentation during storage and act as nucleation centres when introduced into the solution.

Dendrite breeding is caused by needle-like or dendritic crystals which form at high levels of supersaturation. These crystals fragment in the solution and serve as nucleation sites.

Attrition breeding occurs at high stirring speeds due to macroabrasion of crystals which results in fragments that serve as nucleation sites. The rate of nucleation by this mechanism is a function of the crystal hardness, the concentration of the suspension and the retention time.

Fluid shear breeding refers to the breakage of dendritic crystals grown on the crystal surface due to the shearing flow around them.

2.4.4.4 Nucleation kinetics determination

Nylt's [29] equation was developed to describe the kinetics of a real crystallization process, which is simple and based on the measurement of metastable zone width (MSZW).

$$J = k_n \Delta c_{\max}^{n} \qquad (2.25)$$

where J *is the nucleation rate,* k_n *is the nucleation rate constant and* Δc_{max} *is the maximum allowable supersaturation (or MSZW). The exponent, n, is frequently referred to as the apparent order of nucleation, which has no fundamental significance.*

If the maximum allowable supersaturation Δc_{max} is expressed in terms of the maximum allowable undercooking ΔT_{max} (MSZW),

$$\Delta c_{\max} = \left(\frac{dc^*}{dT}\right)\Delta T_{\max} \qquad (2.26)$$

where $\Delta T_{max}=T_{sat}-T_{cry}$, T_{sat} *and* T_{cry} *are the saturation temperature and crystallization temperature, respectively, and* dc^*/dT *is the temperature dependence of solubility.*

In fact the nucleation rate may be expressed in terms of the rate at which supersaturation is created by cooling,

$$J \equiv A = qb \tag{2.27}$$

where A is the supersaturation rate, b is the cooling rate –dT/dt, q is the mass of crystalline substance deposited per unit mass of 'free' solvent present when the solution is cooled by 1 °C, which is a function of the concentration change and of the crystallizing.

$$q = \varepsilon\left(\frac{dc^*}{dT}\right) \tag{2.28}$$

where ε is a correction factor for the change in concentration.

Hence, Equation 2.25 can be rewritten as

$$\varepsilon\left(\frac{dc^*}{dT}\right)\left(-\frac{dT}{dt}\right) = k_n\left[\left(\frac{dc^*}{dT}\right)\Delta T_{\max}\right] \tag{2.29}$$

taking logarithms,

$$\log b = (n-1)\log\frac{dc^*}{dT} - \log\varepsilon + \log k_n + n\log\Delta T_{\max} \tag{2.30}$$

Plotting logb against logΔT_{max} should give a straight line with a slope equal to the order of nucleation n with the intercept yielding the nucleation constant k_n, which was derived by Nyvlt [46].

2.4.4.5 Induction time and interfacial tension calculation

When the solution reached supersaturation, the crystal phase could emerge from the soluble phase. However, a certain induction time t_{ind} is necessary prior to the formation of the new phase. This time could be influenced by the level of supersaturation, agitation rate, presence of impurities, viscosity, etc. The induction time t_{ind} is the sum of the time needed to reach steady-state distribution of molecular clusters, 'relaxation time', t_r; for formation of a stable nucleus, t_n; and the time required for the critical nucleus to grow to a detectable size, t_g.

$$t_{ind} = t_r + t_n + t_g \tag{2.31}$$

As the induction period can be influenced by so many external factors, it cannot be regarded as a fundamental property of a system. However, it has frequently been used as a measure of the nucleation event, making the simplifying assumption that it can be considered to be inversely proportional to the rate of nucleation:

$$t_{ind} \propto J^{-1} \tag{2.32}$$

The classical nucleation relationship (Equation 2.21) would therefore be written as:

$$\log t_{ind} \propto \left[\frac{\gamma^3}{T^3(\log S)^2}\right] \tag{2.33}$$

which suggests that, for a given temperature, a plot of $\log t_{ind}$ versus $(\log S)^{-2}$ should yield a straight line, the slope of which should allow the value of the interfacial tension, γ, to be calculated.

2.4.5 Crystal Growth

After the stable nuclei formed, they began to grow into crystals of a visible size. There are several potential steps during crystal growth from aqueous solution shown in Figure 2.9

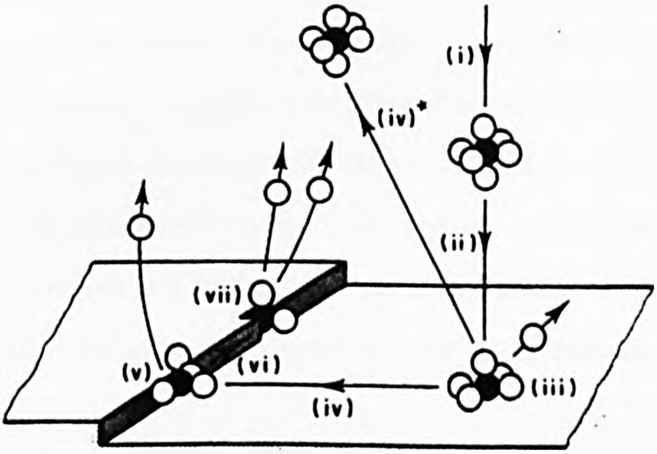

Figure 2.9: Schematic of crystal growth incorporating several steps: diffusion (i, ii, iv, vi), adsorption (iii), attachment (v), integration (vii) and desolvation (iii, v, vii) [32]

The steps involved in crystal growth are:

(i) Solute molecule move from the bulk of the solution toward to the boundary layer on the crystal surface.

(ii) Diffusion through the boundary layer to the surface of the crystal according to Fick's Law was due to the concentration gradient being close to the growing surface.

(iii) Adsorption onto the surface and partial or total desolvation.

(iv) Diffusion along the crystal surface to energetically favourable incorporation sites, (iv)* diffusion away from the crystal surface.

(v) Attachment to the surface step and partial or total desolvation.

(vi) Diffusion along the surface step.

(vii) Integration into the crystal at a kink and total desolvation.

As the steps involved in the crystal growth are supersaturation-related, three types of growth mechanisms were investigated to describe the crystal growth theory.

2.4.5.1 Birth and spread (B+S) models

The crystal would grow from the surface nucleation since the supersaturation was sufficient to form surface nuclei. The adsorption of the crystalline entities onto the crystal surface will occur at the point of the greatest attractive forces, described as the kink site [47]. Under ideal conditions, this step-wise build-up will continue until the whole plane face is completed (Figure 2.10a and b). Before the crystal face can continue to grow, i.e. before a further layer starts, the centre of crystallization must exist, which is called the monolayer island nucleus or the two-dimensional nucleus (Figure 2.10c)

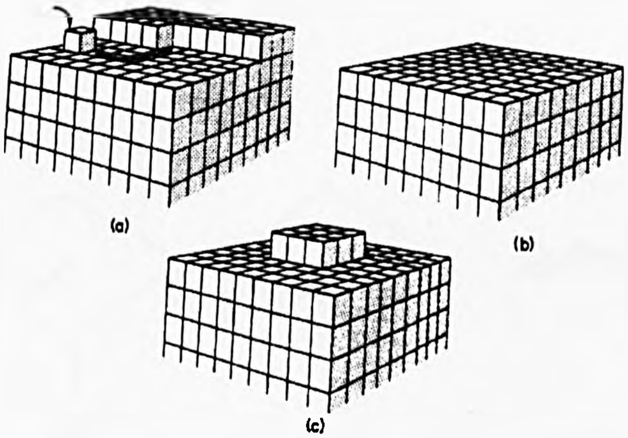

Figure 2.10: A mode of crystal growth without dislocations, (a) migration towards desired location; (b) completed layer; (c) surface nucleation [17]

After the two-dimensional nucleus formed on the crystal surface, it started to spread out resulting in growth on the crystal face [48, 49]. Each new layer was dependent on the formation of a nucleus on the crystal surface which determined the growth rate of the layer. When more than one nucleus was formed on the layer, it still spread out, and the growth is referred to as polynuclear. The growth rate has the relationship with the relative supersaturation of,

$$R_{B+S} = A_1\sigma^{5/6}\exp\left(\frac{A_2}{\sigma}\right) \tag{2.34}$$

where A_1 and A_2 are the system-related constants, σ is the relative supersaturation

2.4.5.2 Screw dislocation model

Most crystals contain dislocations which cause steps to be formed on the faces and promote growth. The screw dislocation is considered to be important for crystal growth, since it obviates the necessity for surface nucleation. This leads to the spiral growth on the surface of the crystal, which is called the screw dislocation model or BCF theory [50] Due to no surface nucleation being required for the screw dislocation model, the model accounts for the much higher growth rates than the other models predict observed at low supersaturation.

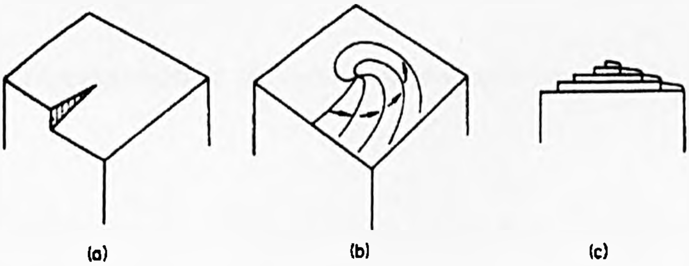

Figure 2.11: Development of a growth spiral staring from a screw dislocation [37]

Burton, Cabrera and Frank developed a kinetic theory of growth in which the curvature of the spiral near its origin was related to the spacing of successive turns and the level of supersaturation [50]. By the application of Boltzmann statistics they predicted kink populations, and by assuming that surface diffusion is an essential step in the process they were able to calculate the growth rate at any supersaturation [17]. The relationship of growth rate and relative supersaturation by the BCF model may be written as:

$$R_{BCF} = A\sigma^2 \tanh(B/\sigma) \tag{2.35}$$

where A and B are complex temperature-dependent constants which include parameters depending on step spacings.

At low supersaturation, the BCF equation predicts the growth rate related to relative supersaturation as [51]:

$$R \propto \sigma^2 \tag{2.36}$$

whereas at high supersaturation, the relationship should be:

$$R \propto \sigma \tag{2.37}$$

2.4.5.3 Rough growth model

The rough surface growth describes the crystal face growth under high supersaturation, under conditions of rough crystal surface. A rough crystal surface would provide many sites for the crystallizing substance to integrate onto the surface with lowest energy. The number of sites can be large and randomly distributed over the surface. The growth rate at a rough surface is, therefore, much faster compared to a smooth surface. At high supersaturation, the growth rate related to relative supersaturation as:

$$R \propto \sigma \tag{2.38}$$

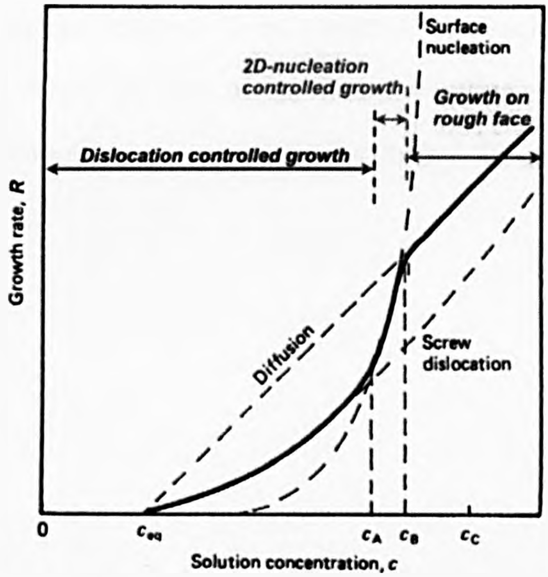

Figure 2.12: Growth rate and supersaturation relationship [32]

The relationship of the growth rate of the crystal and the supersaturation presented in Figure 2.12 could illustrate the different dominant mechanisms [37]

At low supersaturation ($c<c_A$), shows $R \propto \sigma^2$, which indicates the crystal growth is dominated by the screw dislocation mechanism.

At slightly higher supersaturation ($c_A<c<c_B$), shows $R \propto \sigma^{5/6} \exp(1/\sigma)$, indicating the two-dimensional surface nucleation (B+S model) dominates.

At high supersaturation ($c>c_B$), $R \propto \sigma$, means fast growth on a rough surface above the roughening transition point (c_B)

2.5 Closing remarks

In this literature review chapter, the fundamental knowledge of crystallography was described, several important parameters used for crystal characterization were defined. For the overall crystallization process, each step during the process, including the nucleation and crystal growth, were explained in detail. Different theories involved in the crystallization kinetics analysis from supersaturated solution were reviewed, which were used to define the key parameters controlling and characterizing the process and the information to be retrieved for the process design.

Chapter 3 Acoustic Spectroscopy and Velocity Techniques for Crystallization Process Characterization

Summary

This chapter describes the principles of the propagation of sound waves through homogeneous and heterogeneous media. The mechanisms of absorption and scattering of the sound wave by the media are presented. Models for the calculation of particle size and particle volume concentration are described.

3.1 Introduction

This chapter will introduce the fundamental knowledge of the ultrasound wave, including the basic definitions and the wave propagation theory. The propagation of the sound wave in the homogenous medium and inhomogeneous medium are both described, and the mechanisms which occur during propagation have been investigated in detail. The effect of the different kinds of scattering and absorption, plus the relaxation process on the sound wave from the medium are explained separately. The evolution of the theory of propagation of sound through particulate media follows with an emphasis on the models of instruments used this project for the de-convolution of sound attenuation plus the suspended particle volume analysis by sound velocity. The limitations of the theories are compared, and the most suitable equation is selected for the calculation of the targets depending on the experimental results in this project after reviewing the theories.

3.2 Ultrasound wave

Sound is a form of energy in the process of being transmitted through matter by means of mechanical vibrations. It can propagate through gases, liquids and solids. Ultrasound is sound with the frequency, f, over 20,000 cycles per second [52], and the unit for the cycles per second is hertz (Hz). T, is defined as the period, which is the time interval oscillatory motion repeats the medium elements (atoms, ions or molecules). If the direction of individual element oscillations is perpendicular to the direction of the wave motion, it is called a transverse wave, whereas when the direction of the individual element oscillations corresponds to the direction of the wave motion, it is called a longitudinal wave or compression wave. The type of wave motion is dependent on the material it has to penetrate. Transverse waves cannot propagate through the gas or liquid phase. However, transverse waves can occur on the liquid-solid interface and then propagate through the solid phase. In the liquid and gas phase, the sound waves propagate as the longitudinal waves.

The sound wave can be characterized by several fundamental parameters, including the frequency f, the radial frequency ω, the period T, the wavelength λ, and the wavenumber k.

$$T = \frac{1}{f} \tag{3.1}$$

$$\lambda = \frac{\upsilon}{f} \tag{3.2}$$

$$\omega = 2\pi f \tag{3.3}$$

$$k = \frac{2\pi}{\lambda} \tag{3.4}$$

$$P = k + i\alpha \tag{3.5}$$

where υ *is the sound velocity, the wavenumber k means the real part of the complex propagation constant which is a phase change per unit distance, P is the complex propagation constant,* $i = (-1)^{0.5}$ *and* π *is the ratio of a circle's circumference to its diameter.* α *is the attenuation of the sound wave (Neper* m^{-1}*)*

3.3 Ultrasound wave propagation in homogeneous systems

3.3.1 Attenuation in pure Liquid

3.3.1.1 Viscous and thermal absorption

When the ultrasound propagates through the homogeneous liquid, the attenuation of the ultrasound wave is always caused by the viscous and thermal absorption. Both of these mechanisms were taken account in the calculation models by the researchers [53-55]. Both the viscous drag and thermal conductivity cause an exponential decay in the sound amplitude with increasing the distance. However, the thermal conduction is proportional to the ratio of the specific heats γ, which is the ratio of the heat capacity at constant pressure to the heat capacity at constant volume. The value of specific heat ratio for liquid is very close to 1, due to its low compressibility. This means the thermal conductivity contribution for the sound attenuation in the liquid is small, and usually negligible, e.g. the sound attenuation contributed by viscous absorption and thermal absorption are $8.1\times10^{-15}\times f^2$ and $3.0\times10^{-18}\times f^2$, receptivity [56]. Only the in the case of liquid metals, which thermal conduction makes a greater relative contribution.

The sound attenuation of the wave through the viscous thermal non-conductive liquid can be expressed based on the Navier-Stokes Equation [55].

$$2\left(\frac{\alpha\upsilon}{\omega}\right)^2=\frac{1}{\sqrt{1+\omega^2t_{vis}^2}}-\frac{1}{1+\omega^2t_{vis}^2} \tag{3.6}$$

where υ *is the sound velocity,* ω *is the radial frequency,* α *is the attenuation coefficient,* t_{vis} *is the viscous relaxation time, which involves the bulk viscosity and the shear viscosity, and given by*

$$t_{vis} = \frac{\eta}{\rho \upsilon^2}\left(\frac{4}{3} + \frac{\mu}{\eta}\right) \tag{3.7}$$

where η is the shear viscosity of the solution, ρ is the density of the solution, υ is the sound velocity and μ is the bulk viscosity of the solution.

The relation of sound attenuation and frequency reveals a Gaussian distribution function, the maximum of the attenuation at the critical frequency. This is corresponding to a timescale approximately equal to the viscous relaxation time.

The attenuation of sound can be expressed by the sound velocity and viscosity data based on Equation 3.8 as assumed the $\omega^2 << \omega_{th}^2$. For instance, ω_{th} and ω_{vis} are 10^{12}Hz and 10^{15}Hz for water.

$$\alpha = \frac{\omega^2}{2\rho \upsilon^3}\left(\frac{4}{3}\eta + \mu\right) \tag{3.8}$$

where α is the attenuation coefficient, η is the shear viscosity of the solution, ω is the radial frequency, ρ is the density of the solution, υ is the sound velocity and μ is the bulk viscosity of the solution.

Assuming the liquid is incompressible and the thermal conduction contribution is negligible. The sound attenuation obey the Stokes law [57], and can be expressed without the bulk viscosity [58]

$$\alpha = \frac{2\omega^2 \eta}{3\rho \upsilon^3} \tag{3.9}$$

where α is the attenuation coefficient, η is the shear viscosity of the solution, ω is the radial frequency, ρ is the density of the solution, and υ is the sound velocity.

When the adiabatic wave propagates through the liquid, the pressure variation occurs as the wave propagation causes the temperature gradients. A certain amount of heat follows from the region of high temperature (compression) to an adjacent one of low temperature (rarefaction). This results the in loss of sound energy from the heat conductivity.

Vigoureux [59] showed the absorption due to heat conductivity has the same form of equation relating the sound attenuation and sound frequency as the viscous absorption (Equation 3.6). However, the relaxation time is different [56].

$$t_{therm} = \frac{\tau}{\rho \upsilon^2 C_v}\left(\frac{\gamma - 1}{\gamma}\right) \tag{3.10}$$

where τ *is the thermal conductivity of the solution,* C_v *is the thermal specific of the solution at constant volume,* ρ *is the density of the solution,* υ *is the sound velocity and* γ *is the ratio of the specific heats of the solution.*

If considering both the thermal absorption and the viscous absorption of the sound wave in the single phase liquid, the sound attenuation relating to the sound frequency can be expressed as:

$$\alpha = \frac{\eta \omega^2}{2\rho \upsilon^3}\left[\frac{4}{3} + \frac{\mu}{\eta} + \frac{(\gamma - 1)\tau}{\eta C_P}\right] \tag{3.11}$$

where C_p *is the thermal specific heat in the constant pressure of the solution,* α *is the attenuation coefficient,* η *is the shear viscosity of the solution,* ω *is the radial frequency,* ρ *is the density of the solution,* υ *is the sound velocity,* μ *is the bulk viscosity of the solution,* γ *is the ratio of the specific heats of the solution and* τ *is the thermal conductivity of the solution.*

3.3.1.2 Molecular relaxation

For the polyatomic molecules, the molecule possesses a number of degrees of freedom, which includes external and internal. The translational energy obtained from the sound wave can be passed to the external degree of freedom directly from molecule to molecule by collisions with virtually no time delay. The energy from the external degree of freedom can be transmitted to the internal degree of freedom by the excitation of vibrational relaxation and rotational isomerism. These processes are called thermal relaxation, which are both essentially due to the disturbing influence of the temperature changes caused by the propagation of an ultrasonic wave through the liquid [60, 61].

Another molecular relaxation process is caused by the periodic pressure change and is not affected by temperature variation, which is called molecular structural relaxation. The molecules are squashed and relocated in the crystal lattice after the sound wave propagates in the liquid. This process is a relaxational one and results in absorption of the energy of the sound wave [62].

For the associated polar liquids, the relaxation caused by the chemical reaction should account for the total attenuation of the sound wave during the propagation in the pure liquid [63]. The classic hydrogen-bond material, i.e., alcohol, was used to measured the contribution of the intermolecular reaction to the sound attenuation [64, 65].

3.3.2 Sound velocity in pure liquid

The relation of the sound velocity and the properties of the materials it propagates was first pointed out by Strutt in 1877 [66]. Wood then pointed out the physical properties of the medium, i.e., the density and elasticity would influence the sound velocity [67, 68]. The adiabatic compressibility of the liquid is the reciprocal of the bulk modulus of elasticity.

$$\upsilon = \sqrt{\frac{B}{\rho}} = \sqrt{\frac{1}{\kappa\rho}} \tag{3.12}$$

where B is the adiabatic bulk modulus of liquid, κ is the adiabatic compressibility of liquid, and ρ is the density of the liquid. This equation is also called the Laplace equation in the physical chemistry research area [69].

3.3.3 Sound wave propagate in the solid

Both longitudinal and transverse sound waves exist when the sound wave propagates in solid materials.

The velocity of longitudinal sound waves in the solid υ_l^s can be expressed [70, 71] as:

$$\upsilon_l^s = \sqrt{\left[B + \left(\frac{4}{3}\right)G\right] \Big/ \rho} \tag{3.13}$$

where G is the rigidity modulus, B is the adiabatic bulk modulus of liquid, and ρ is the density of the liquid.

The velocity of a transverse sound wave υ_t propagating in the solid is given by [72]:

$$\upsilon_t = \sqrt{\frac{G}{\rho}} \tag{3.14}$$

where G is the rigidity modulus, and ρ is the density of the liquid.

The sound velocity propagated in a solid is always much higher than the velocity in a liquid, which is typically 3000- 6000 m/s, where as the velocity propagated in a liquid is around 1500 m/s [73].

3.4 Sound propagating in a suspension

3.4.1 Elastic scattering

Elastic scattering occurs when all the incoming ultrasonic energy is conserved and none of the energy is converted into other forms of energy such as heat. Five factors listed below determine the elastic scattering of sound waves:

- mismatch in the compressibility or density of the two phases
- size of the particle
- angle of scattering
- concentration of particle
- phase of the particle and continuous phase

3.4.1.1 The mismatch in compressibility or density

For the elastic scattering to occurs, the acoustic impedance of the particle and surrounding liquid should be different. Otherwise, the sound wave would transmit into the particle rather than the reflected by the particle. The acoustic impedance of the phase is determined by its compressibility and density. This explains why the difference between the compressibility and density of the two phases are the basic requirement for elastic scattering to occur.

3.4.1.2 The size of the particle

The discussion of the effect of the size of particle on the elastic scattering always introduces the scattering cross section, S_{scat}. It is the area multiplied by the incident intensity which gives the decrease of intensity as a result of scattering. It is proportional to the attenuation coefficient for scattering. The diameter, D, of the particle related to the wavelength in the fluid is important, and it is expressed by the dimensionless number $\pi D/\lambda$ (i.e. the kD/2, k is the wave number) depending on the assumption that the particle is spherical.

The dependence of $\pi D/\lambda$ on the S_{scat} is illustrated in Figure 3.1:

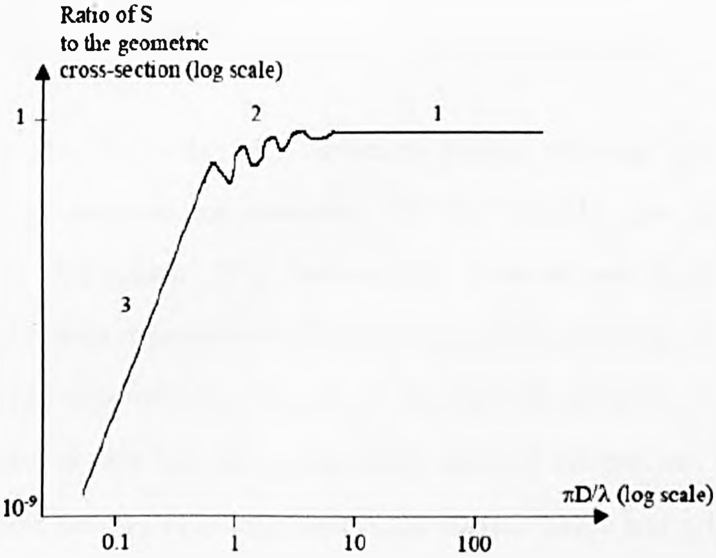

Figure 3.1: The dependence of Sscat on πD/λ [63]

- $\pi D/\lambda >> 1$ (Region 1), i.e., particle size is much larger than the wavelength of the sound wave.

This region is called the specular region or geometric region, where the particle acts as a mirror. The scattering cross section is independent of frequency, which is equal to the geometric cross sectional area.

- $\pi D/\lambda \approx 1$ (Region 2), i.e., particle size is similar to the wavelength of the sound wave.

This region is called the stochastic region or diffraction region. The interaction between the sound wave and the particle is complicated in this region. The scatted wave is critically dependent upon the dimensions, shape and acoustic properties of the particle. The shaking in the relation to S_{scat} and $\pi D/\lambda$ is due to the interference from the reverberation inside the particle and the incident wave. No matter whether the particle is solid, liquid or gas phase, shaking is always present.

- $\pi D/\lambda << 1$ (region 3), i.e., particle size is much smaller than the wavelength of the sound wave.

This region is the classic Rayleigh scattering region, with the upper limitation of $\pi D/\lambda=0.5$. Most acoustic measurements on the particle size and volume are investigated in this region. It is because the particles are much less than one millimeter in diameter in most dispersions, whereas the wavelength of the sound wave is larger than one millimeter. In the case of the crystallization process, this Rayleigh scattering region always happens, in the early stage of the process. In the Rayleigh scattering region, the S_{scat} is independent of the particle shape and proportional to the fourth power of the frequency. The attenuation is more strongly dependent on the frequency than it is for most mechanisms for attenuation by absorption, which is depending on the square of the frequency. Furthermore, the S_{scat} is also dependent on the volume of the particle.

3.4.1.3 The angle of scattering

The angle of scattering depends on the scattering region. In the case of solid particle suspensions, the sound is mainly scattered backwards and sideways and is mostly independent of the particle size and shape in the Rayleigh region. In the stochastic region, forward scattering is increased at the expense of sideways scattering, whereas in the geometric region forward scattering dominates.

3.4.1.4 The effect of the concentration of particles

The effect of the concentration of the particles on the attenuation was discussed by Waterman and Truell [74]. The effect is complete and needs to be discussed in a different section. In the low particle concentration region, the attenuation from scattering is proportional to the concentration of the particles. As the particle concentration increases, the attenuation reaches as the maximum value and then decreases, which obeys the original theory. This is because at high concentrations, some of the dispersed phase would not act as the scatterer since it was in the shadow of the other particles.

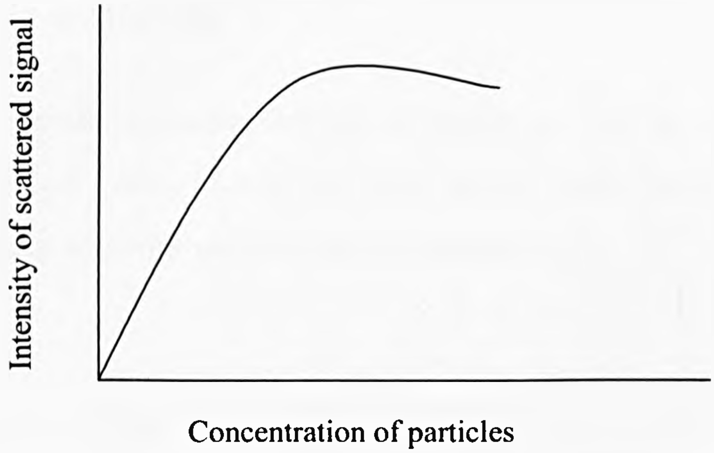

Figure 3.2: The schematic illustration of the dependence of scattering on the concentration of particles

3.4.1.5 Effect of the phase of the particles

In addition to the effects of compressibility and density characterizing different phases, the phase of the particle is particularly important to the resonance phenomena. The resonance effects are caused by the interference between the incoming wave and the scattered wave, which is very strong for the gas particles. Several models of resonance exist, e.g. the expansion and contraction of the particle depending on the monopole oscillation. Multi-pole oscillations can also occur in which the shape of the particle changes. The scattering cross section of bubbles at resonance in water can be almost a thousand times greater than the geometric cross section. For comparison, the cross section for a rigid sphere does not reach unity until its diameter approaches the wavelength. In practice, this means that it is critical to avoid the existence of air bubbles for the acoustic attenuation measurement of the suspension.

3.4.2 Inelastic scattering

Compared to the elastic scattering, inelastic scattering involves the conversion of some of the ultrasonic energy to heat, etc. There are two main inelastic scattering mechanisms, thermal scattering and visco-inertial scattering.

3.4.2.1 Thermal scattering

Thermal scattering occurs when the thermal properties or compressibility of the dispersed phase differ from those of the continuous phase. As the ultrasonic wave propagates through the dispersion, it causes periodic fluctuations in the local pressure and temperature as the material expands and contracts. Because of the adiabatic compressibility (change in volume per unit change in pressure) or thermal properties (change in volume per unit change in temperature) are different between the particle and the surrounding liquid, when the sound wave propagates through the suspension, the temperature change of the particle does not match the change in the liquid. For example, the oil droplets dispersed in water will usually have a lower heat capacity than the water and will range more widely in temperature. The heat will therefore flow from the droplet to the surrounding liquid. Because the heat flow from the droplet is not compensated for by the heat flow into the droplet during a compression-expansion cycle, some of the ultrasonic energy is converted into heat, which is referred to as the thermal absorption. On the other hand, the particle expands or contracts relative to the surrounding liquid which would lead to the generation of a monopole thermal wave which propagates away from the particle equally in all directions. Thus some of the ultrasonic energy is scattered in directions which are different from the original one. This is referred to as the monopole scattering.

Two parameters determine the importance of the thermal scattering. One is the wavelength of the thermal wave from the particle. The thermal scattering has the maximum value when the thermal wavelength, λ_{th} is similar to the particle size [75]. The thermal wavelength is given by

$$\lambda_{th} = \sqrt{\frac{4\pi\tau}{f\rho_f C_p}} \tag{3.15}$$

where τ *is the thermal conductivity of the liquid,* C_p *is the thermal specific of the liquid at constant pressure,* ρ_f *is the density of the liquid, and* f *is the frequency of sound*

The other parameter determining the importance of thermal scattering is the difference in temperature between the particle and the continuous phase. This is related to the term $\left((\beta_1/\rho_1 C_{p1}) - (\beta_2/\rho_2 C_{p2})\right)^2$, where β is the thermal expansion coefficient and the subscripts refer to the two phases. The larger the value of this term, the larger the effects on the total attenuation from the thermal scattering.

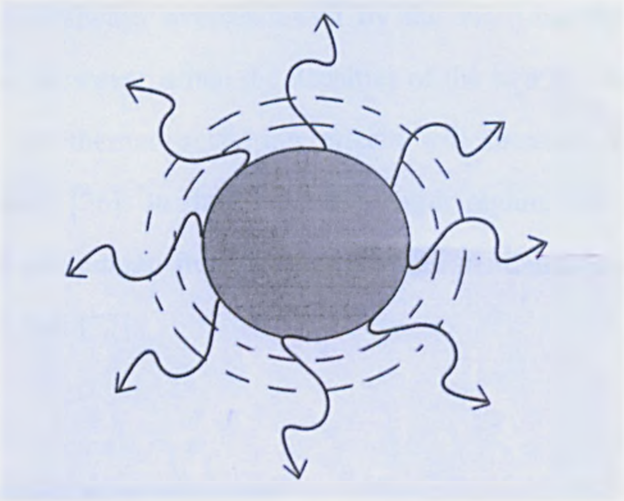

Figure 3.3: Thermal contrast

Cyclic variations in temperature driven by oscillating wave pressure cause differential expansion and contraction between the two phases, this results in acoustic re-radiation in the form of a monopole field. In addition, heat flows away from the particle, again with monopole field geometry, representing energy lost from the acoustic wave [9]

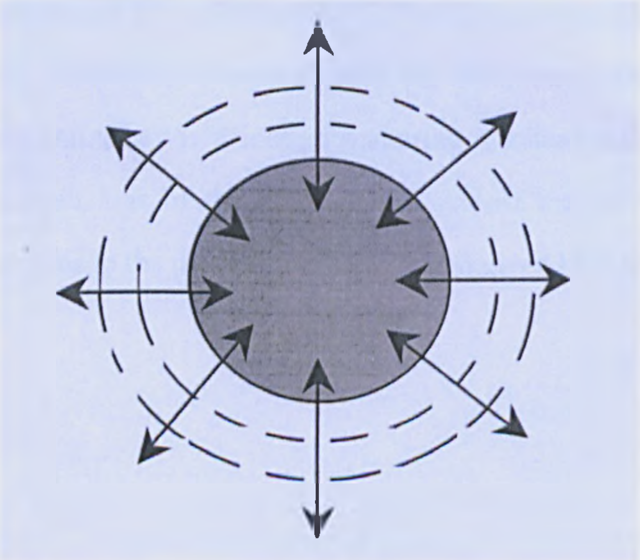

Figure 3.4: Compressibility contrast

The particle expands and contracts with respect to the continuous phase in response to cyclic pressure variations in the wave, local fluid flows and re-radiation of sound result [9]

Thermal scattering is always overshadowed by the visco-inertial scattering in the suspension systems. However, when the densities of the two phases in the dispersion are quite similar, the thermal scattering effects will increase, e.g., sound waves propagate in the milk [76]. In the long wavelength region, the thermal scattering dominates the total attenuation from scattering when the densities of the two phases are similar to each other [77].

3.4.2.2 Visco-inertial scattering

Visco-inertial scattering would occur when a density difference exists between the particle and the continuous phase. When the ultrasound wave propagates in the suspension, the particle would move backwards and forwards relative to the surrounding liquid due to it having a different inertia. The oscillation of the particle generates a scattered wave which moves away from the particle with a cosine dependence on angle. Thus some of the ultrasonic energy is scattered in directions which are different from the original wave. This process is referred to as dipole scattering. The damage of this oscillation by the viscous drag of the surrounding liquid refers to the ultrasound energy loss to the heat, this process is known as visco-inertial absorption. The visco-inertial scattering reaches maximum value when the viscous wavelength λ is of the order of the size of the particle. The viscous wavelength is analogous to the thermal wavelength and given by a similar equation

$$\lambda_{vis} = \sqrt{\frac{4\pi\eta}{f\rho_f}} \tag{3.16}$$

where, η is the shear viscosity of the liquid, ρ_f is the density of the liquid, and f is the frequency of sound.

Visco-inertial effects are usually more important than thermal effects in suspensions and emulations [78]. For instance, McClements [8] plotted the viscous wavelength and thermal wavelength versus frequency, which showed that viscous wavelength is 2.6 times more than thermal wavelength in aqueous dispersions [79].

In most suspensions, one or two of the above mechanisms usually dominate the overall attenuation in a particular frequency range. At relatively low frequencies referred to as the long wavelength region, the inelastic scattering mechanisms including visco-inertial and thermal scattering usually dominate, but at higher frequencies when in the intermediate wavelength region, the dominating mechanisms are the absorption from the two phases plus the relaxation process and the scattering losses from the pulsation and oscillation of the particle [80-82].

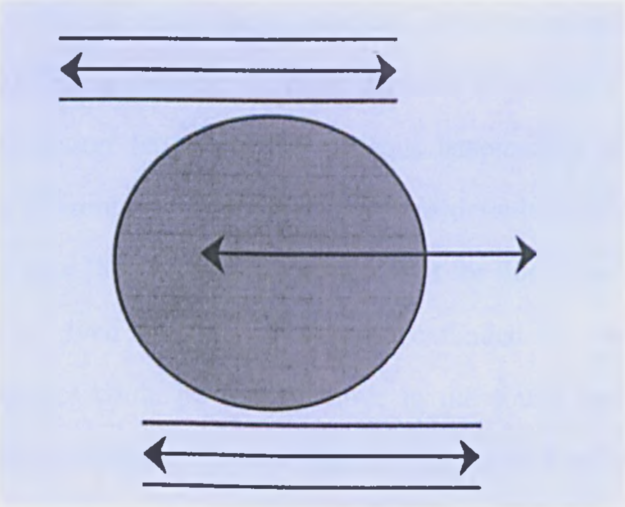

Figure 3.5: Density contrast

Cyclic variations in local pressure gradient associated with the passage of the wave cause forward and backward motion of the particle with respect to the continuous phase, resulting in frictional losses commonly modeled by viscous (shear) waves [9]

3.5 Particle size analysis depending on the sound attenuation model

3.5.1 The evolution of the theory

The relationship between particle size and sound velocity has been predicted by many mathematical models. The review and comparison have been carried out by many research groups [9, 83-86]. These advantages and the limitations of the models have been described in these articles. The following section gives a brief explanation of the history of these models.

The absorption of sound in a suspension of small particles was first considered theoretically by Sewell in 1910 [87]. Sewell considered the case of small rigid spherical particles to be immobile, i.e. the particles do not oscillate in the sound field. This immobile condition is satisfied by water droplets in the air at audio frequencies. However, this assumption failed for the aqueous suspensions at MHz due to the particles following the motion of the fluid to a considerable extent. This was proved by Hartmann and Focke [88], Sewell did not account for this effect. A modification of Sewell's theory was given by Lamb [58], who extended the theory that the rigid incompressible particles could be free to move in the sound field. Urick [89] then derived an identical relationship for the viscous loss term from consideration f the viscous drag associated with a spherical particle. The cases of kaolin and sand in water suspensions gave good agreement with the Urick's theory. Urick's theory was then modified and introduced by Urick and Ament [90, 91]. The Urick and Ament model assumed that the particle size was much less than the wavelength, and the particle did not re-scatter the acoustic energy and occupied no volume, which is only suitable for dilute systems. The attenuation contributed by the thermal diffusion was taken into account by Isakovitch in 1948, who pointed out the sound propagation in a suspension could generate the temperature gradients in a particle and fluid interface which can affect the attenuation value. In 1953, Epstein and Carhart [12] presented a description of the counting of thermal losses into attenuation in detail. However, their theory was applied only for aerosols. Later, Allegra and Hawley [92] extended the theory to suspension and emulsion cases in 1971, which assumed that the sound wave was scattered by a single particle, then estimate the attenuation from many particles. Different kinds of multiple scattering models were investigated by various researchers, including Waterman and Truell [74], Lloyd and Berry [93], Twersky [94], and Javanaud and Thomas [95]. The Waterman and Truell model and the Lloyd and Berry model are the main multiple scattering models applied. In order to solve the effect of particle interactions in non-dilute media with a phenomenological approach rather than a mathematical treatment of existing theories using the standard multiple scattering equations, Harker and Temple [96, 97] compared two different approaches to describe the problem. In the phenomenological approach, the effective velocity was dependent on an effective density and effective compressibility and attenuation was given by the concentration multiplied by an average scattering factor. In a second approach, the coupled phase model, the hydrodynamic interactions occurring in non-dilute media were introduced via a solid fraction and a particle shape-dependent effective viscosity parameter.

The wavenumber k_s is given by:

$$k_s^2 = \omega^2\left[(1-\varphi)\kappa_f + \varphi\kappa_p\right]\frac{\rho_f\left\{\rho_p(1-\varphi+\varphi U)+\rho_f U(1-\varphi)\right\}}{\rho_p(1-\varphi)^2+\rho_f\left[U+\varphi(1-\varphi)\right]} \tag{3.17}$$

with

$$U = Q + iR \tag{3.18}$$

$$Q = \frac{1}{2}\left(\frac{1+2\varphi}{1-\varphi}\right) + \frac{9\lambda_{vis}}{4a} \tag{3.19}$$

$$R = \frac{9}{4}\left(\frac{\lambda_{vis}}{a} + \frac{\lambda_{vis}^2}{a^2}\right) \tag{3.20}$$

where κ is the compressibility, and the subscription of f and p mean the fluid and particle phase, respectively. U is the complex quantity that depends on the particle size a (particle diameter), particle volume φ and viscous wave wavelength λ_{vis}.

This model was applied to the long wavelength regime under a limited relatively high concentration. The thermal contrast between the two phases was not accounted for in this model, which means this model was not suitable for the thermal absorption [98]. Some modifications were introduced in the cell model of Dukhin and Goetz [79] where hydrodynamic interactions between particles were taken into account. This modification made this model suitable for the suspensions systems with high density contrast at concentrations up to 10 v% [99].

Hipp investigated the particle to particle interaction in high concentration suspensions, and developed a multiple scattering model dependent on the Epstin and Carhart, Allegra and Hawley Model (ECAH), which accounted for the effect of interaction of neighboring particles [100].

3.5.2 The ECAH model

The ECAH model is the landmark in the study of ultrasonic spectroscopy in particulate systems. Both the thermal and visco-inertial loss effects were considered in this model. It is assumed in this model that the particles are monodispersed, spherical and isotropic. By considering three conservation equations for mass, momentum and energy, a complex propagation equation for the velocity and attenuation in a suspension was derived. In the case of a solid particle with diameter equal to 'a' in liquid, at the solid-liquid boundary of an isolated sphere suspended particle around the liquid, six waves are generated when an incident plane compression wave impinges on the boundary into the solid, and away from the surface back into the fluid. These are the compression wave, the thermal wave and the transverse wave into and out of the particle. The wave equations are solved using spherical co-ordinates in terms of a series of expansions of spherical Bessel functions and spherical harmonics with undetermined coefficients, A_n, B_n, C_n, A'_n, B'_n, C'_n. Six equations are obtained with six unknown coefficients for each order n. These equations are in terms of the various wave potentials, spherical Bessel and Hankel functions, the densities and thermal and elastic properties of the two phases [75, 101].

The ultrasonic properties of an ensemble of particles are described by a complex propagation constant P,

$$\left(\frac{P}{p}\right)^2 = 1 - \frac{24i\varphi}{p^3a^3}\sum_{n=0}^{\infty}(2n+1)A_n \tag{3.21}$$

where $P = \omega/\upsilon_p + i\alpha_p$*,* υp *is the ultrasound velocity of the scattering material, and* α_p *is the ultrasound attenuation of the scattering material,* $p = \omega/\upsilon_f + i\alpha_f$ *is a propagation constant of the continuous phase,* φ *is the dispersed phase volume fraction, a is the particle diameter,* ω *is the angular frequency, i is* $1^{1/2}$*, and* A_n *is the complex scattering coefficient. In order to calculate the velocity and attenuation, the scattering coefficient* A_n *should be computed and then inserted into the equation.*

The ECAH model is written for the mono-dispersed suspension or emulsion. However the poly-dispersion can be introduced assuming that the total attenuation in poly-dispersion is due to the combined effects of the particles of different sizes [9, 102]. The determination of the particle size distribution (PSD) is separated into two steps. Firstly, the attenuation is measured as a function of frequency. Secondly, these experimental measurements are compared with the theoretical predictions of the ultrasonic properties of the dispersion, and the PSD which gives the best fit between the theoretical attenuation and experimental result is determined by a model dependent method [103]. The fit is established by calculating the sum of the squares of the differences (SSD) between theory and experiment,

$$SSD = \sum_{i} \left[\alpha_{theory}(f_i) - \alpha_{experimental}(f_i)\right]^2 \tag{3.22}$$

where the $\alpha_{theory}(f_i)$ *and* $\alpha_{experimental}(f_i)$ *are the theoretical predicted and the measured attenuation value at frequency* f_i*, respectively. The geometric mean* x_g *and the geometric standard deviation* ζ_g *are then varied until the computer finds the minimum SSD, and then the PSD of* $P_{(r)}$ *can be determined. It is assumed that the particle size distribution follows some common form which can simply be modelled mathematically by log-normal fit [75, 80, 104],*

$$P_{(r)} = \frac{1}{\chi_g \ln(\zeta_g)\sqrt{2\pi}} \exp\left[\frac{\ln^2(\zeta_g)}{2}\right] \exp\left[\frac{\left(\ln(r) - \ln(\chi_g)\right)^2}{2\ln^2(\zeta_g)}\right] \tag{3.23}$$

where $P_{(r)}$ *is the probability of having a particle of radius r.*

The closeness of the fit for all the frequencies is given by the figure of merit [14],

$$Merit(\%) = \sqrt{\sum_{i=1}^{N} \left(\frac{\alpha_{theory} - \alpha_{experimental}}{\alpha_{experimental}}\right)^2 \frac{100}{N}} \tag{3.24}$$

where N is the number of points in the attenuation spectrum.

3.6 Particle volume analysis depending on the sound velocity

The ultrasonic velocity measurements have been proved useful in determining the dispersed phase volume fractions in emulsions and suspensions, especially in optically opaque cases. It was also used to determine the adiabatic compressibility of dispersed phases. In order to extract the information, the theoretical formulations are required [11]. There are a large number of equations available in the literature which can be used for this purpose, which includes the Ament equation in 1953 [91] (Ahuja applied in 1972 [13]), Urick equation in 1948 [89], Urick and Ament equation in 1949 [90], Kuster and Toksoz equation in 1974 [105, 106], and Johnson and Plona equation in 1982 [107]. The development of the velocity theory is similar to the evolution of the sound attenuation theory. The different mechanisms which affect the sound velocity were accounted by researchers step by step. The most important factors which cause velocity dispersion in suspensions and emulsions are those due to viscous and thermal transport processes which occur at the interfaces of the two phases. Of these two, the viscous processes are usually the most important for suspensions and emulsions. For the particles which are not negligible in size compared to the ultrasonic wavelength, especially in the case that there is a large density difference between the two phases, the inertial effect would be counted for the velocity variation. In the case of determining the particle volume using sound velocity, one significant simplification is to assume that the wavelength of sound in the fluid is much greater than the size of the particle. This is not a very restrictive condition, although it does exclude the consideration of suspended particles whose size is of the order of, or greater than, the wavelength of sound.

There are three regions within the long wavelength limit shown in Figure 3.6. At the very long wavelengths ($\lambda \rightarrow \infty$, $r \rightarrow 0$, $f \rightarrow 0$), where r is the radius of the particle, the velocity is independent of frequency and particle size. This region is convenient for phase volume determination because it is simpler if particle size and frequency dependent effects can be ignored. However, this region is affected by the thermal properties of the system, which means the thermal effects need to be counted in the velocity variation. The significance of the parameter $f^{0.5}r$ is that it is proportional to the thermal and shear wavelengths in liquids. In the long wavelength limit, the ultrasound velocity and the attenuation per wavelength ($\alpha\lambda$) vary with $f^{0.5}r$.

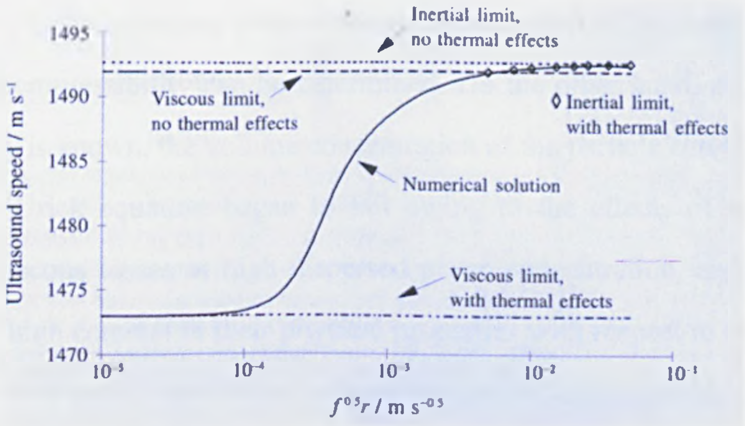

Figure 3.6: Ultrasound velocity as a function of the scaling parameter $f^{0.5}r$ for a 20 v% sunflower oil-in-water emulsion at 30 °C [108]

3.6.1 Urick equation

Consideration of the dependence of the sound velocity on the properties of the material through which it propagates in the emulsion or suspension was first given by Urick in 1948. Urick indicated the sound velocity was determined from an effective density and compressibility of the mixture by taking a volume weighted average of the densities and compressibilities of the two phases:

$$\upsilon = \sqrt{\frac{1}{\rho_{eff}\kappa_{eff}}} \tag{3.25}$$

where

$$\rho_{eff} = \rho_p\varphi + \rho_f(1-\varphi) \tag{3.26}$$

$$\kappa_{eff} = \kappa_p\varphi + \kappa_f(1-\varphi) \tag{3.27}$$

The subscripts p and f refer to the particle and fluid phases, respectively, κ is the adiabatic compressibility, ρ is the density and φ is the volume concentration of the particles

According to Urick's equation, if the volume concentration of the particle is known, the adiabatic compressibility can be determined. On the other hand, as the adiabatic compressibility is known, the volume concentration of the particle can be determined. However, the Urick equation began to fail owing to the effects of scattering and thermal and viscous losses at high dispersed phase concentration, and for particles which exhibit high contrast in their physical properties with respect to the continuous phase or for very small particles at a high number of concentrations. Because in Urick's assumption, the most suitable case was no acoustic scattering, no thermal processes, and the particle diameter is much smaller than the wavelength in the diluted system.

3.6.2 Solid fat content model

The solid fat content model was developed by Dickinson, McClements and Povey in 1990 [109]. This model was used to directly determine the solid content from the ultrasound velocity for single scattering cases.

The monitoring of the solids content during the crystallization process in the oil in water system was investigated by Dickinson et al. [109, 110] using the solid fat content model. The oil-in-water system was separated into three states. One is the wholly liquid state part, another is the wholly solid state part, and the state of solid liquid mixtures. The relation of sound velocity and temperature was calculated first in pure liquid or a pure solid state system to determine the temperature effect without phase transfer. In the liquid and solid mixture region, the solid contents can be determined using Equation 3.28

$$\phi = \frac{\frac{1}{v^2} - \frac{1}{v_l^2}}{\frac{1}{v_s^2} - \frac{1}{v_l^2}} \Phi \tag{3.28}$$

where ϕ is the calculated volume fraction of solid present in the entire system; Φ is the volume fraction of the dispersed phase; v is the measured velocity of sound; v_s is the extrapolated velocity of sound for an emulsion containing wholly solid droplets, and v_l is the extrapolated velocity of sound for an emulsion comprised wholly of liquid droplets

This equation is first derived by Miles et al. [111] using Taylor series expansions of the compressibility and density in the Wood equation. McClements claimed this equation could be derived from the Urick equation if it was assumed that fractional difference in density between phases were much smaller than fractional differences in compressibility [112]. Some solid-liquid mixture oil-in-water system was investigated by McClements et al. [113-115], Dickinson et al. [116]. The kinetics of crystallization of solid and liquid mineral droplets can be determined by the sound velocity [117-119]. However, there are two drawbacks to this model when calculating the particle volume in the dissolvable two phases crystallization system. The first one is the solid fat model does not count the thermal effect due to it being derived from the Urick equation. This second drawback is that for the dissolvable system, the velocity of the liquid phase would change along with the variation of the particle volume due to the nucleation and crystal growth occurring.

3.6.3 Modified Urick equation

Neglecting the thermal scattering is the main limitation of applying the Urick equation in the practice system due to the significance of the thermal effects shown in Figure 3.6. In the modified Urick equation, the thermal effects are counted in the scattering parameters [102]:

$$\frac{1}{\upsilon^2} = \frac{1}{\upsilon_f^2}\left(1 + \chi\varphi + \psi\varphi^2\right) \tag{3.29}$$

where

$$\chi = \left[\frac{\kappa_p - \kappa_f}{\kappa_f} + \theta + \frac{\rho_p - \rho_f}{\rho_f}\right] \tag{3.30}$$

and

$$\psi = \left[\frac{\kappa_p - \kappa_f}{\kappa_f} + \theta\right]\left[\frac{\rho_p - \rho_f}{\rho_f}\right] + \frac{2\left(\rho_p - \rho_f\right)}{3\rho_f^2} \tag{3.31}$$

$$\theta = \left(\gamma - 1\right)\frac{\rho_p C_{pp}}{\rho_f C_{pf}} R^2 \tag{3.32}$$

where

$$R = \left[\frac{\dfrac{\beta_p}{\rho_p C_{pp}} - \dfrac{\beta_f}{\rho_f C_{pf}}}{\dfrac{\beta_f}{\rho_f C_{pf}}}\right] \tag{3.33}$$

where υ *is the velocity in the solution,* υ_f *is the velocity in the continuous phase,* φ *is the volume fraction of the particle.* χ *and* ψ *are scattering coefficients. The subscripts p and f refer to the dispersed and continuous phases, respectively.* β *is the volume thermal expansively* (K^{-1})*, Cp is the specific heat at constant pressure* ($J\ kg^{-1}\ K^{-1}$)*, and* γ *is the ratio of the specific heats of the solution.*

3.7 Conclusion

The fundamental theories of sound propagation in the homogeneous and inhomogeneous solution were reviewed in the chapter. For the case of homogenous solutions, the classic relationship between the sound attenuation and sound velocity was revealed, which resulted in the calculation of bulk viscosity. In the case of particulate systems, various mechanisms of sound attenuation velocity were discussed. A review of the particle size characterization depending on the ultrasonic attenuation spectroscopy for the two phase systems demonstrated the theoretical certification for the particle size analysis in the experiments. On the other hand, after comparison and analysis of the sound velocity theory on the particle volume calculation in the two phase system, the mathematical model was defined for the experimental work in the following chapters.

Chapter 4 Experimental Instruments and Methods

Summary

This chapter lists the instruments and techniques used in this research project. The measurement theories and method of the techniques are described with focus on the acoustic techniques.

4.1 Introduction

A series of ultrasound instruments were employed in this project for the research of the copper sulphate pentahydrate crystallization system. Two aspects of ultrasonic techniques were developed for the measurements, including the acoustic attenuation spectrometer and acoustic velocitimeter. Both these techniques were studied and described in this chapter from a scientific perspective. For the acoustic attenuation spectrometer, the measurement of accurate attenuation data is necessary for the implementation of the theory for particle size analysis, which is illustrated in this chapter. The acoustic instruments using a continuous sound wave generation system and pulse wave generation systems were compared, and different crystallization experiments were designed based on the characteristics of the acoustic instruments presented in the following chapters.

Copper sulphate pentahydrate is the material for the crystallization process research in this project, the characterization work on it is carried out in Chapter 5. The instruments for crystal characterizing are presented and studied in this chapter.

4.2 Solution concentration and particle volume prediction measurement depending on sound velocity

4.2.1 ResoScan

The ResoScan system (TF Instruments Ltd) is a compact bench-top instrument enabling high resolution sound velocity measurement, depending on the ultrasonic resonator technology (URT). The sound waves are generated by an oscillating wall (transducer) and reflected by a solid wall (reflector), the inference phenomena of the sound waves occurs in the spacing between the transducer and reflector, and the frequency is adjusted within a narrow range, to find the standing wave condition. As the transducer is precisely parallel to the reflector at a fixed distance D, acoustical resonances can be observed in the space between the transducer and reflector. The distance D should be an integral multiple of half wavelength of the waves, which gives:

$$D = n\left(\frac{\lambda}{2}\right) \tag{4.1}$$

where λ is the wavelength of sound wave, n means the positive integers.

The sound waves with certain wavelengths, i.e. certain frequencies, are enhanced by reflection and interference as shown in Figure 4.1. In these cases, the sound waves form a field of standing waves at defined resonance frequencies. The lowest resonance frequency, i.e. the fundamental resonator frequency f_1, corresponds to a half wavelength of sound and permits the calculation of the sound velocity υ from the distance D and the observed fundamental resonance frequency f_1. The frequency is adjusted within a narrow range to find the standing wave condition

$$f = \frac{v}{\lambda} = \frac{nv}{2D} \tag{4.2}$$

when $n=1$, f is called fundamental frequency f_1.

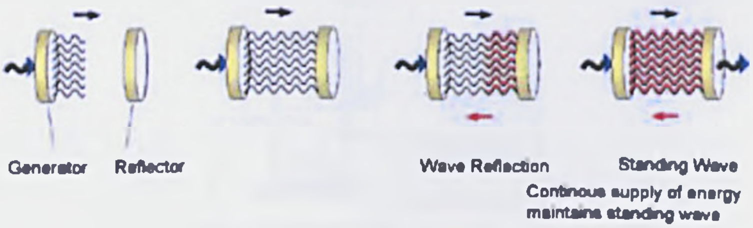

Figure 4.1: Schematic diagram of the generation of standing wave in the cell of ResoScan [120]

The ultrasonic cell of the ResoScan is made of titanium and gold, and the ultrasonic transducers are fabricated from high quality lithium niobate. The cell is equipped with two identical, vertically aligned chambers with capacities from 0.17 ml to 0.25 ml. The path length is 7.0 mm with a fundamental frequency of approximately 9 MHz.

The operating temperature was under 5 °C to 85 °C, and the maximum heating rate and cooling rate was 1 °C/min and 0.5 °C/min, respectively. The cooling rate was set as 0.5 °C/min, and the acoustic velocity data was recorded after the system temperature get stable.

4.2.2 Ultrasound velocity meter (UVM)

The ultrasound velocity meter (Cygnus Instruments Ltd) employs a straightforward implementation of the pulse-echo technique to measure the sound velocity. A simple start/stop timer is used to obtain the time-of-flight. The start point of the time-of-flight is recorded as the pulse is excited by the transducer. After the pulse travels through the sample in the cell, it is reflected by the reflector wall, and then travels back to the transducer. The returning pulse is detected and the timer is stopped.

Due to the distance the pulse travels being fixed and known, the velocity can be easily obtained by:

$$v = \frac{2D}{t} \tag{4.3}$$

where D is the distance between the transducer and reflector, t is the time-of-flight of the pulse

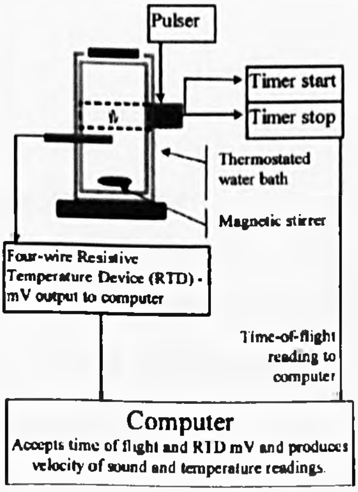

Figure 4.2: Schematic diagram of the ultrasonic velocity meter [102]

All the circuitry can be integrated into a single small box (Figure 4.2) which uses serial communications to send data to the controlling computer. The calculation of time-of-flight and temperature is carried out in the computer. The transducer of the UVM is made of lead zirconium titanate and covered with epoxy plate (to protect the surface of the transducer). The pulse may last a few microseconds and consist of two or more cycles. The central frequency of the pulse is 2.5 MHz.

The cell is 200 ml, and the temperature dependency can be measured quickly and accurately (±1 ms^{-1}, ±0.1 ms^{-1} precision; ±0.1 °C, ±0.01 °C precision) and over a wide temperature range (-20 °C to 90 °C). The temperature in this project was fixed at desired temperatures within 25 °C to 30 °C.

4.3 Crystallization process monitoring depending on the sound attenuation measurement using the Ultrasizer (MSV)

The Ultrasizer (MSV) system is the acoustic spectrometer for particle sizing developed by Malvern Instruments Ltd. It is employed in this project in studying the on-line crystallization of the copper sulphate pentahydrate system. The crystal size and crystal volume concentration can be measured simultaneously by MSV during the process.

4.3.1 Principle of measurement

As sound waves move through the suspension or emulsion, they lose energy by different kinds of mechanisms, each serves to reduce the intensity of the wave, which is known as attenuation of the wave.

The attenuation coefficient can be measured at a particular sound frequency using the following formula:

$$\alpha = \frac{1}{\Delta L} In \frac{I_0}{I_1} \tag{4.4}$$

where α is the attenuation, I_0 is the incident intensity, I_1 is the sound wave intensity after passing through the sample, and ΔL is the path length of the wave.

By passing a wide range of frequencies through the sample and measuring the wave intensity at different positions, it is possible to build up a picture of how attenuation and frequency are related. Either 50 or 100 frequency points can be used to measure the wave intensity. The dynamic transducers installed in the MSV enable the measurement in variable path length to get the acoustic attenuation shown in Figure 4.3. There are several advantages of using the dynamic transducers: there is no need to measure the background attenuation separately, the total attenuation of the suspension or emulsion is the sum of the attenuation of pure solution and particles, and acoustic wave has different decay processes in different samples. On the other hand, the dynamic transducer also introduces some disadvantages, such as time consuming and alignment problems. In order to maximise the signal to noise ratio, the path length is required to be variable. For the strongly attenuated samples, the path length should be small, whereas the weakly attenuated samples need a large path length. On the other hand, the variable path length is suitable for the wild frequency bandwidth. For the high frequency measurement, the path length should be smaller than the low frequency measurement, as the acoustic attenuation of high frequency is larger than the low frequency attenuation.

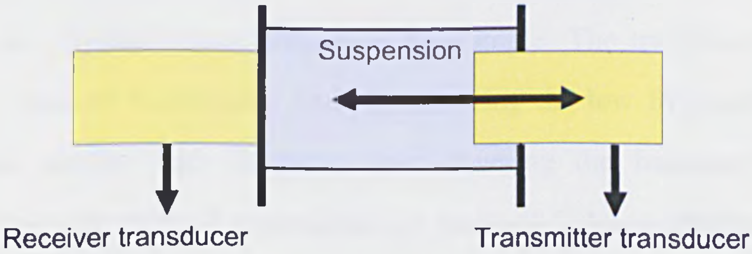

Figure 4.3: Schematic diagram of acoustic attenuation measurement

MSV employs the discrete frequency acoustic wave for the attenuation measurement. For one particular frequency, the sound velocity and attenuation are recorded after the sound wave propagates through the sample. The transducer then turns to another frequency point and repeats the measurement again. The acoustic attenuation spectrum consists of serial attenuation data at different frequencies. When the sound wave propagates in the sample, the wave will interact with the background solution and the particles. Part of the wave will be reflected back to the transmitter as well as part of it being refracted in other directions such as beam spread, and some energy of the wave will be absorbed by the background solution. Only the part of the wave which is caught by the receiver transducer is recorded for the attenuation measurement. Thus, the interval of the complete measurement is dependent on the sample physical properties which determine the scattering mechanism and the frequency points used for the measurement.

The volume based particle size distribution model installed in MSV is the benchmarking model, i.e., the ECAH model, which is applied in the area of acoustic spectrum relating to particle size analysis described in Chapter 3. After the measured acoustic spectrum was analysed, MSV could output both the particle size distribution and the suspended particle volume.

4.3.2 Instrument specification

MSV can be used for the on-line measurement of the acoustic attenuation of the sample over the frequency range of 1-150 MHz. The frequency range used is dependent on the physical characteristics of the sample. The transducer assembly consists of two pairs of transducers, one pair covering the low frequency range of 1-20 MHz, and another high frequency pair covering the frequency range of 15-150MHz. These two pairs of transducers are made of Lithium Niobate and Lead Zirconate-Titanate (PZT). The two pairs of transducers are installed coaxially on both sides of the chamber with the volume of 500 ml. The path length of the transmitter (dynamic) transducer is from 0.51-10.16 cm (0.2-4 inches). One complete measurement need around 4 mins.

The specified particle size range of the instrument is 0.01-1000 μm, and measurements should be carried out with a suspended particle volume concentration of 0.1-80 v% depending on the sample characteristics[14].

MSV can be operated under the temperature range of 5-100 °C, and when the temperature over 50 °C, it required the external cooling system for protecting the transducers. The wild operation temperature range allowed MSV to make dynamic measurement, such as in the crystallization process.

MSV could either install the batch cell or the flow-through cell. The interchangeable of these two cells allow the instrument to be used for off-line and in-line acoustic measurements separately. Both cells are equipped with temperature sensors (PT100), which take record of the temperature during the measurements. The batch cell is equipped with a four blade marine-type impeller with variable speed in the range 40 to 2000 rpm. The instrument operational range when equipped with flow-through cell is limited by the pressure inside the cell which would not exceed 1 bar gauge.

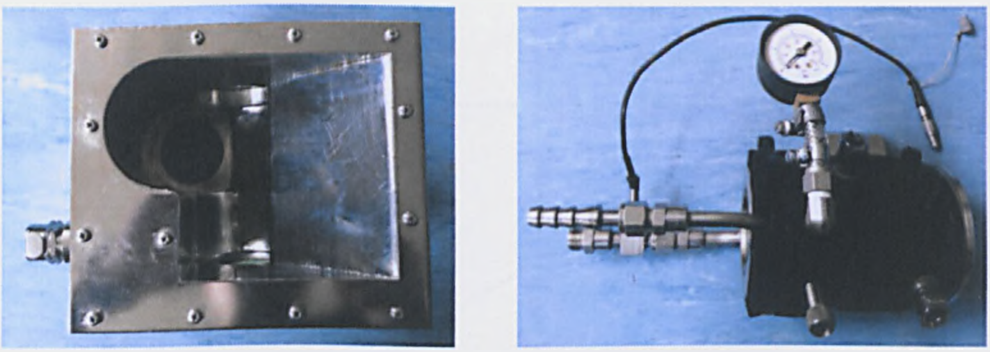

Figure 4.4: MSV batch cell (a) and flow-through cell (b)

4.3.3 Optimization of measurement strategy

4.3.3.1 Automatic strategy

There are two pairs of transducers, a high frequency pair and a low frequency pair. For each pair, the frequency range is split into two sub-channels. Each of these four sub-channels is optional, chosen for optimizing the measurement. The path length is adjusted for each sub-channel so that 4 different path lengths can be used over the entire frequency range. The change of the frequencies between the sub-channels can also be selected. The spacing of the low frequency is always much larger than the spacing for the high frequency due to the fact that low frequency has smaller attenuation and needs more passing spacing to detect the attenuation signal. The spacing of the region a, b, c and d should be reduced gradually. The f_a and f_e are defined as the frequency limits, where f_a was originally set to 1 MHz and f_e is 150 MHz, which are variable for measurement optimisation. The changeover frequencies f_b, f_c and f_d are all variable for the measurement.

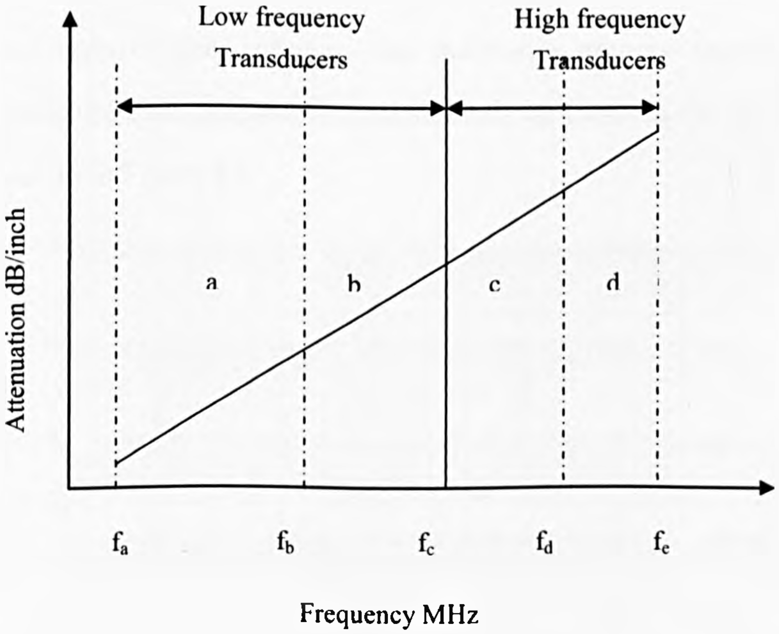

Figure 4.5: Schematic diagram of the MSV sub-channel split (logarithm to logarithm scale)

Depending on the selected changeover frequency points and the spacing for each channel, MSV could supply the automatic optimal measurement strategy. This automatic optimal strategy assumes the background is pure water, and the scattering from the particle is not high. It is well suited to the silica suspension with low concentration. However, after changing the background solution, or increasing the suspension particle concentration, some errors will exist in the spectrum. Typically, one automatic optimal strategy search takes around 4 minutes, and the acoustic attenuation already has a dramatic change for the dynamic system. In addition to not being able to measure the correct strategy, the time consumption will miss the monitoring of the changes to the crystal during the crystallization process. In the measurement of the acoustic attenuation spectrum of the crystallization process, the automatic optimal strategy is only used for the first measurement before the crystal comes out, which supplies an essential estimate of the attenuation of the sample, and then the manual optimization is needed for the correct strategy search.

4.3.3.2 Manually optimized strategy

A typical incorrect optimal strategy from automatic strategy searching in copper sulphate pentahydrate crystallization can commonly be found in the spectrum as in the sample presented in Figure 4.6.

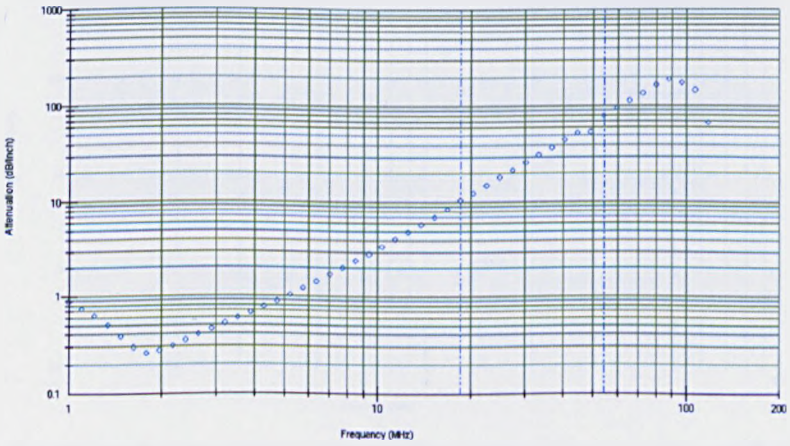

Figure 4.6: An example of acoustic attenuation with incorrect strategy

Three sub-channels were used for the strategy measurements. The error in the lower end of the low frequency is due to the sample attenuation being close to the noise threshold. Increasing the measurement frequency would eliminate the error which existed in the low end frequency. For this example, the minimum frequency used is increased from 1 MHz to 2 MHz. It was also found that in solid suspensions, frequencies less than 10 MHz made less contribution to attenuation[121] that they make less difference to the particle size distribution analyzed results. The attenuation at the lower end frequency (1-10 MHz) could be cut directly to modify and improve the spectrum. Deviation at the high frequency end of the spectrum could be an indication that the sample attenuation is outside the dynamic range of the instrument. Reducing the measurement frequency is a better way to modify the spectrum. Changing the transducer passing spacing could modify the spectrum at the high frequency end as well. However, it is more difficult to optimize the passing space. Because the high frequency end channel should have the smallest passing space, the maximum value was under 0.8 inch.

The irregularities existing in the spectrum itself, particularly at the boundary between the sub-channels, either increasing transducer passing spacing (Figure 4.7) or reducing the maximum frequency of the sub-channel towards a lower value (Figure 4.8) should modify the spectrum. The parameters of the improved spectrum are listed in Table 6.1 and compared with irregular strategy.

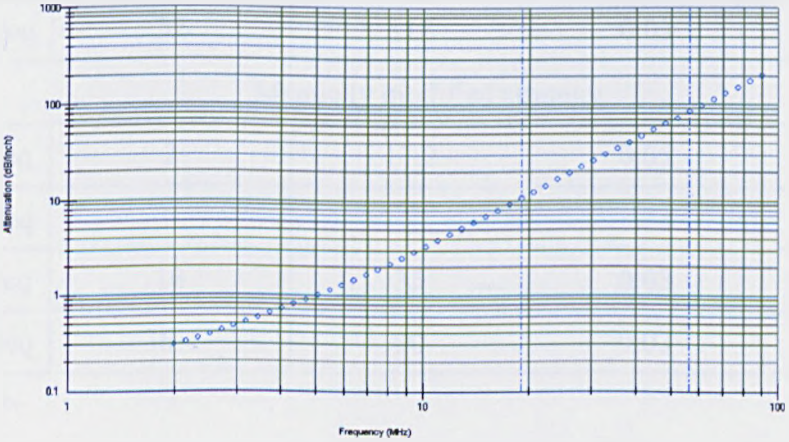

Figure 4.7: Modify the irregularity at the boundary between the sub-channels by increasing the transducer passing spacing

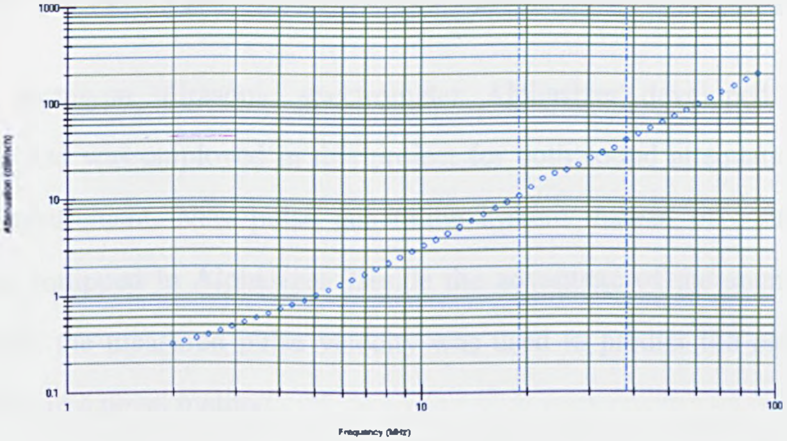

Figure 4.8: Modify the irregularity at the boundary between the sub-channels by reducing the sub-channel maximum frequency

Table 4.1: Comparison of the automatic strategy and manually modified strategy

Channels	Min Freq (MHz)	Max Freq (MHz)	Position 1 (inch)	Position 2 (inch)
Automatic strategy				
1 Low Freq	1	17.2	0.05	4
1 High Freq				
2 Low Freq	18	49.6	0.03	1.1
2 High Freq	52	118	0.03	0.35
Manually modified strategy				
1 Low Freq	2	17.2	0.05	4
1 High Freq				
2 Low Freq	18	35	0.03	1.1
2 High Freq	36.4	90	0.03	0.35

4.4 Sound attenuation and velocity measurement by the new prototype ultrasonic spectrometer Alphasizer

The new prototype ultrasonic spectrometer Alphasizer developed by Malvern Instruments Ltd was employed in this project for both sound attenuation and sound velocity measurement. New pulse generation system instead of continuous wave system was equipped in Alphasizer. Beside the advantage of the sound attenuation measurement, the measured pulse velocity was used to predict the particle volume concentration in a novel method.

4.4.1 Principle of measurement

The principle of the acoustic wave generation of the Alphasizer is different from the MSV. The measurement method of MSV, fully described above is based on the acoustic frequency sweep. The frequency sweep is a pseudo continuous wave method. Each frequency has sufficient duration for a stable condition to exist in the sample acoustic field. This pseudo frequency sweep method has the advantage of generating a stable and accurate acoustic signal whilst the long time required previously caused the failed measurement in the fast dynamic process.

The Alphasizer uses a short wide bandwidth pulse, i.e. a single pulse containing a wide range of different frequencies. This meant a wide bandwidth signal can be obtained at a very short interval.

Figure 4.9: Schematic diagram of a typical broadband pulse

It is not like the MSV in that every signal from each frequency will be analyzed individually and then combined with the entire spectrum. One pulse contains the whole information for different frequencies. After the pulse travels through the sample, it is analyzed using the Fast Fourier Transform (FFT) signal-processing technique to determine the values of time (t) and Amplification (A). The time and amplification are used to calculate the group velocity and sound attenuation, respectively. The signals received contain a series of pulses corresponding to the reverberations of the transmitted pulse in both the transmitting and receiving transducers. The first pulse received by the receiving transducer is selected for the calculation of the sound velocity and sound attenuation by FFT.

In order to improve the Signal to Noise Ratio (SNR), 1000 bursts are taken by the Alphasizer for one measurement. The average result determines the output information from the Alphasizer which increases the measurement accuracy. The burst repetition rate is dependent on the application and ranges from 1 kHz to 5 kHz.

The application of the wide bandwidth pulse of the Alphasizer implements the rapid measurement for a wide frequency range, and a type of acoustic spectrum can be collected after only around 20 seconds, dependent on the number of frequencies used. Compared to the MSV which needed 4 to 5 minutes for each measurement, the Alphasizer obviously has the advantage to be applied to the fast dynamic process, i.e. the crystallization process.

4.4.2 Instrument description

The Alphasizer contains one pair of transducers including a receiver and transmitter, which cover the frequency range from 5 MHz to 100 MHz, and the total bandwidth is 95 MHz. The frequency range can be selected by the user manually. The more frequency points used, the more accurate the data obtained. Meanwhile, more measurement time was consumed. The specified particle size range of the instrument is 0.01 to 1000 μm, and the measurements should be carried out for suspensions with solid concentration in the range of 0.1 v% to 50 v% which depends on the sample's physical characteristics. The transducers consisted of a 35 MHz lead zirconate-titanate (PZT) half wave resonator and damped with a tungsten loaded epoxy and encapsulated in a stainless steel enclosure. The instrument can be regularly operated under -5 °C to 120 °C, and external cooling is required for the transducer at temperatures over 50 °C

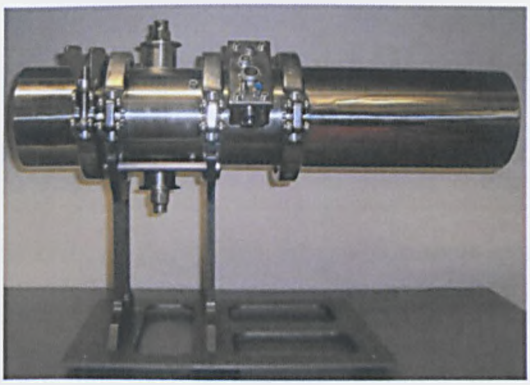

Figure 4.10: Photograph of Alphasizer

The Alphasizer still adopts the go through sample transducer like the MSV, which means the transmitting transducer will move through the sample during measurement. The modification of the transducer spacing still follows the same method described in Section 4.3.3.2. The spacing between the transducers can be switched from 0.75 mm to 50 mm to optimize the SNR along with the change of frequencies used and the sample characteristics. The reason for this is the requirement of the large frequency range used for particle size analysis. The attenuation of sound intensity as a function of distance is roughly proportional to the square of the frequency. This means the high frequencies required much shorter path length in order for a good SNR compared with low frequencies. In water for example, the measurement at 100 MHz needed a few millimetres while hundreds of millimetres were required for 1 MHz [122].

The Alphasizer software consists of two Active X (COM objects) modules, a hardware control module (HCM) which controls the Alphasizer and acts as a library of functions. The control functions include the measurement electronics, temperature controller, and bed position. The library function provides simulation, the ECAH model and the algorithm for inversion. A second application specific module (ASM) drives the HCM and generates the commands for the spacing and frequencies chosen for measurement. The ASM has an interface with file handling and data display functions, and TCP IP or RS232 interface functions allow users to operate the Alphasizer from a remote computer or another application supporting Active X such as Excel, MatLab, and Origin, etc.

4.5 On-set of crystallization predicted by electrolytic conductivity probe

The electrolytic conductivity is the ability of a solution to pass an electric current. Compounds dissolved in water would take up as an ionized state. These electrically charged ions enable the passage of current through the solution. In general, conductivity can be used to determine the purity of a solution or to indicate the total concentration of all the various ions dissolved in the solution. If the solution only consists of a single compound dissolved in pure water then the conductivity level can be referred to standard tables or graphs that convert this to a concentration of the solute. The unit of the measurement for conductivity is the Siemen/cm, which is a very high level of conductivity. In practice, mill-siemens (mS/cm) is usually used for the solution concentration measurement of inorganic solution whereas the micro-siemens is used for the purity measurement of water. Resistivity is the reciprocal of conductivity and is often used for pure water measurement when results are reported in mega ohms (MΩ/cm).

In practice, the conductivity is calculated from the actual conductance G (S), measured between the plates, multiplied by the cell constant K (cm^{-1}). The cell constant is the ratio of the distance between the electrodes d (cm) and their surface area A (cm^2), which is fixed for each conductivity cell,

$$C = GK = G\frac{d}{\mathrm{A}} \tag{4.5}$$

The electrolytic conductivity value of the solution is solute concentration and solution temperature dependent. There is a visible drop in the conductivity value as the solute concentration decreases as the crystals come out of the solution at a known temperature. On the other hand, the existence of the crystals in the solution would introduce some disturbance in the conductivity data, which is another way of finding the on set of the crystallization. Some conductivity ranges of common solutions are presented in Table 4.2

Table 4.2: Conductivity ranges of common solutions [123]

Solution	Conductivity μS/cm
Pure water	0.05
Distilled water	1 to 10
Sea water	30,000 to 50,000
5% Sodium chloride solution	70,000
10% Sulphuric acid solution	140,000

4.6 Set-up of the crystallization systems

4.6.1 20 litre crystallizer

The copper sulphate pentahydrate crystallization experiments were carried out using the 20 litre jacked glass reactor developed by HEL Ltd, MSV system, Hubber thermo-stated batch, a data interface board (A/D), and WinISO process control software (HEL Ltd). The reactor equated with the thermometer (PT100) and retreat curve impeller (RCI).

Because the Alphasizer system only had a flow-through cell installed the calibration work (described in detail in Chapter 8) was carried out using the 20 litre reactor as well.

A progressing cavity pump (Mono Pumps Ltd.), capable of delivering 1-10 litre/min flow rates was used for pumping the slurry through the system (crystallizer to MSV/Alphasizer, and then back to the crystallizer). It is a positive displacement pump which consists of an eccentrically revolving helix which propagates fluid forwards via the cavities resulting from the helix rotation. The operation of the mono pump is illustrated in Figure 4.11. This pump applies low levels of shearing to the fluids, which would not break the crystals.

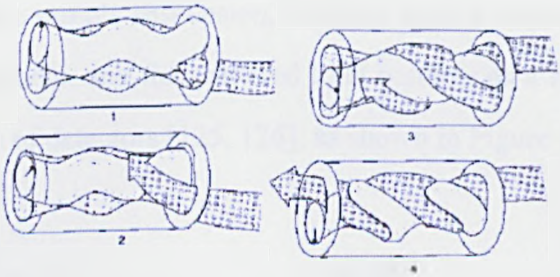

Figure 4.11: Principle of operation of a progressing cavity pump [124]

4.6.2 1 litre crystallizer

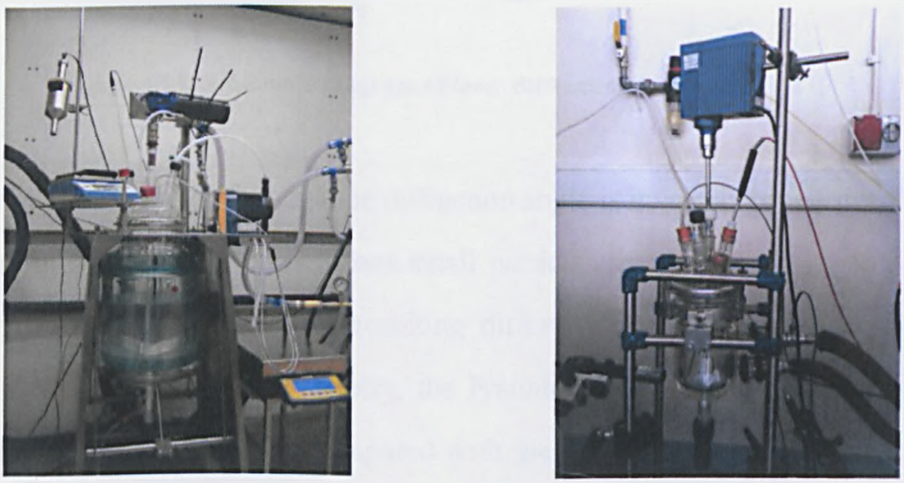

(a)

(b)

Figure 4.12: Photograph of (a) 20 litre crystallizer and (b) 1 litre crystallizer

The fundamental crystallization research experiments were carried out in the 1 litere crystallizer (HEL Ltd), combined with the Jenway 3540 pH and electrolytic conductivity meter (Jenway Ltd), Julabo FP50-HE Refrigerated/Heating Circulator (Julabo Ltd), and WinISO process control software (HEL Ltd). Thermometer (PT100) and retreat curve impeller (RCI) are equipped in the reactor for crystallization experimental requirements.

4.7 Particle size measurement using the Mastersizer 2000 (Malvern Instruments Ltd)

The Mastersizer developed by Malvern Instruments Ltd was used to predict the particle size distribution as a reference. Light scattering techniques were employed in the Mastersizer. In the sample suspension, the laser light is scattered at various angles by the suspended particle, and the scattered light patterns as a function of angles are measured by a series of detectors [125, 126], as shown in Figure 4.13.

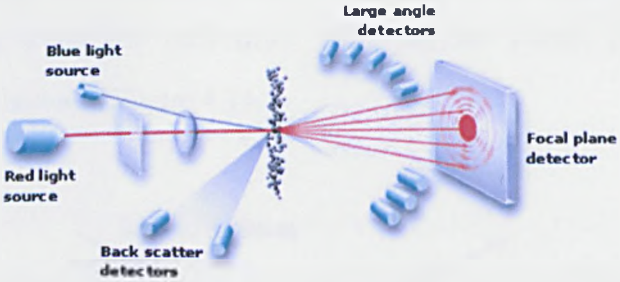

Figure 4.13: Schematic diagram of laser diffraction instrument [127]

This method relies on the fact that the diffraction angle is inversely proportional to the diameters of the particles. This means small particles scatter light at greater angles compared to larger ones and the resulting diffraction pattern is used to measure particle size. In light scattering theory, the Fraunhofer theory [128] is used for the particles with large dimensions compared with the wavelength of light, whereas the more complex Mie light scattering theory [129] is used for the particles with dimensions near the wavelength of light in order to determine the complete particle size distribution. The Mie light scattering theory is used in the Mastersizer, which gives accurate particle size distribution results over a size range of 0.02-2000 μm [130]. However, the concentration sample (over 1 v%) must be dilute prior to analysis, which limited the instrument implemented for the on-line measurement

4.8 Crystal identification by X-ray diffraction (XRD)

Because there are several forms of hydrates existing in nature for the copper sulphate compounds, the identification of the copper sulphate pentahydrate after crystallization experiments is necessary to define the crystal form. XRD was used for the crystal identification in this project.

Bragg presented a simple explanation of diffracted beams from a crystal in 1912 [131]. It is supposed that the incident radiation waves are reflected from parallel planes of atoms in the crystal with each plane reflecting only very a small fraction of the radiation. The angle of incidence is equal to the angle of reflection. The diffracted beams are found when the reflections from parallel planes of atoms interfere constructively as shown in Figure 4.14.

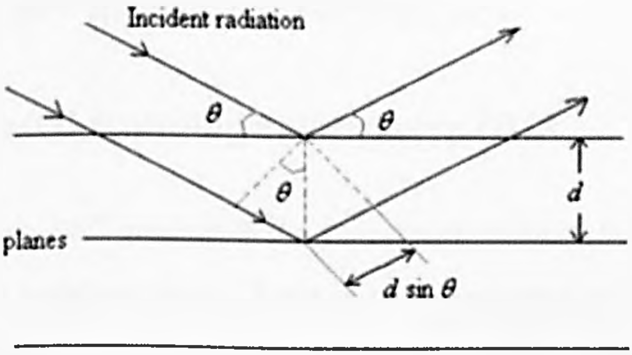

Figure 4.14: Derivation of Bragg's equation, d is the spacing of parallel atomic planes

Consider d is the space of parallel lattice planes, the path difference between the two reflected waves is 2dsinθ, where θ is the angle of incidence. Constructive interference of the radiation occurs when the path difference is an integer number (n) times the wavelength λ,

$$2d\sin\theta = n\lambda \tag{4.6}$$

The combination of constructive and destructive interference leads to intensity peaks only at certain incidence angles. A typical diffraction pattern contains many peaks, each due to diffraction from a given set of crystal planes. The number of peaks depends upon the crystal structure and the wavelength employed. Structural information is contained in both the positions (angles) and the intensities of the peaks. From Bragg's Law, the interplanar spacing (d) controls the peak positions, so peak positions reveal the size and shape of the unit cell. In addition, the intensity of a diffraction peak from the planes is proportional to the crystal structure factor, which means the peak intensities contain information about the types, number and positions of atoms within the unit cell [132].

The powder XRD, D500 (Siemens) was used in the project for identification of the copper sulphate pentahydrate crystal. Samples were examined using flat plate Bragg-Bentono geometry with the scan range of 10-50°.

4.9 Some other analytical techniques

4.9.1 Differential scanning calorimetry (DSC)

For a thermal event, DSC yields both the temperature at which the event occurs and the corresponding enthalpy change. Some of the more common aspects of material properties and behaviour on which DSC provides information include melting point, crystallization, solid-solid phase transformations, chemical reactions, measurement of heat capacity (C_p), and changes in C_p e.g. accompanying glass transition.

A Mettler-Toledo 820e DSC with a Ts0801R0 automatic sampler was used to investigate the thermal behaviour of copper sulphate pentahydrate, which is operated at a N_2 gas flow of 200 ml/min in a temperature range from 25 to 250 °C at a heating rate of 4 °C/min.

4.9.2 Thermogravimetric Analysis (TGA)

TGA involves the measurement of changes in sample mass as a function of temperature and/or time. The sample atmosphere can be controlled during measurements, specifically pressure, humidity, inert atmosphere or oxidative atmosphere, etc. Thus a wide range of processes and interactions can be investigated, ranging from adsorption to loss of solvent or thermal decomposition.

A Mettler-Toledo (MODEL: TGA) is employed coupled with DSC in this project to measure the solubility of copper sulphate pentahydrate. The copper sulphate solution was kept at 30 °C over 10 hours to make sure the solvent evaporated and the crystalline water was reserved in the crystal lattice.

4.9.3 Optical microscopy

A standard reflected light Olympus IMT-2 microscope (Olympus UK Ltd) with a CCD video camera (JVC model KY-f1030) was used for the examination of crystal morphology. The microscope was connected to a PC with a KY-LINK JVC image grabbing package. Images were analyzed with LEICA IM500 image analysis software for size measurement.

4.9.4 Density measurements

Density measurements of solutions were carried out using a density and sound analyzer DSA48 (Anton Paar).

4.10 Materials

Copper sulphate pentahydrate samples and silica samples both purchased from Aldrich were used in this project. The characterization of the copper sulphate pentahydrate crystals was carried out and fully described in Chapter 5.

4.11 Conclusions

Each instrument used in this project has been introduced in this chapter, along with a full description of the measurement theories. The measurement strategies are also studied in this chapter, especially the measurement strategy optimization of the acoustic sound attenuation spectrometers including the MSV which played an important role during the on line crystallization monitoring in Chapter 6. The optimal strategy modification method is also adapted to the Alphasizer, and this is the fundamental operation background for the calibration work of the Alphasizer presented in Chapter 8. The set-up of the two crystallization systems for the 1 litre crystallizer and 20 litre crystallizer are also described in this chapter.

Chapter 5 Fundamental Characterization of Copper Sulphate Pentahydrate Crystals

Summary

This chapter gives the characterization of copper sulphate pentahydrate. The measured kinetic parameters of the material provide the databases for the measurements using acoustic techniques.

5.1 Introduction

The copper sulphate pentahydrate system is the main material investigated in this project. The fundamental crystallization parameters should be measured independently of the measurement of ultrasonic instruments to provide the databases of copper sulphate pentahydrate crystallization process and research background for the following measurements. The characterization of the crystal focus on the parameters determines the crystallization process, i.e. the solubility, metastable zone width, and induction time. Kinetic parameters of nucleation were determined depending on the classic crystallization analysis equations. The crystalline form is characterized after the batch crystallization experiments, which prove the identity of the products.

5.2 Solubility of copper sulphate pentahydrate

5.2.1 Measurement of solubility

The kinds of methods which were employed to measure the solubility of salt in water include ultraviolet spectroscopy, chromatographic method, and gravimetric. Some new devices and measurement methods are developed by the pharmaceutical companies for the rapid automatic solubility measurement [133-136]. However, the traditional gravimetric method is the most commonly used for the measurement of inorganic compounds.

Copper sulphate pentahydrate is a crystalline compound containing five co-ordinate water molecules. They may held by (a) co-ordinate covalent bonds, (b) hydrogen bonds, or (c) uniform or random arrangement in a crystal lattice [137]. Four water molecules bound covalently through oxygen to copper whereas the fifth one was attached via hydrogen bonding to sulphate ions. Gentle heating of copper sulphate pentahydrate causes loss of the lattice water and one water molecule attached to copper yielding copper sulphate trihydrate. The copper sulphate pentahydrate would dehydrate to monohydrate containing one water molecular attached to the copper under high temperature conditions. Depending on the heating rates, four of the co-ordinating water molecules were released along the range 100-150° C, whereas the most strongly bonded water molecule was released above 150° C[138, 139].

DSC was used to measure the temperature of the physical and chemical variation of copper sulphate pentahydrate crystal, i.e. loss of the crystalline water, and transition of different hydrates of copper sulphate crystal, which is presented in Figure 5.1.

The first endothermic peak in the DSC measurement was defined as the temperature of dehydrate of the weak bonded water molecule, and the second big endothermic peak presented the left dehydrate of the four water molecules. The exothermic peak shows the transition of different forms of crystals with different hydrates.

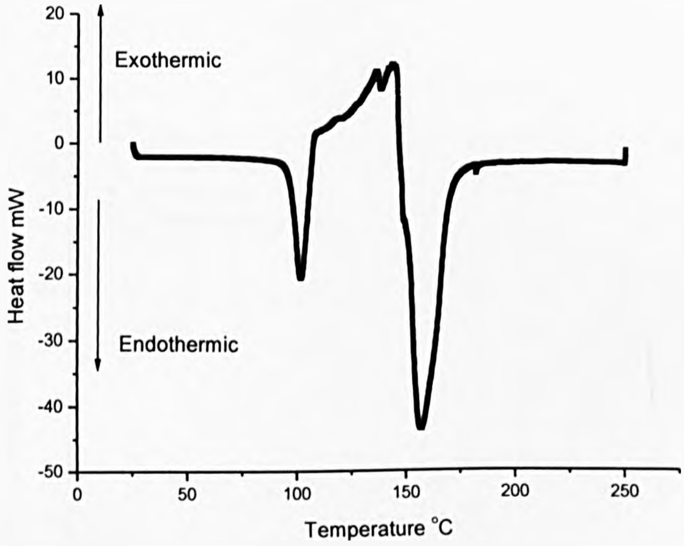

Figure 5.1: DSC measurement of copper sulphate pentahydrate

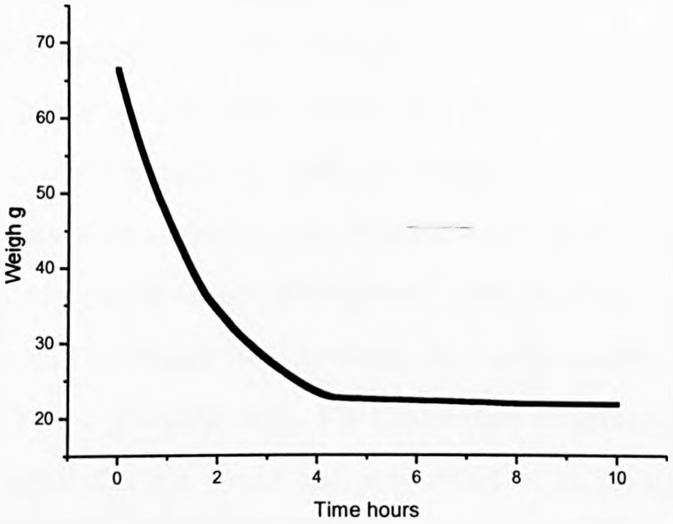

Figure 5.2: TGA measurement of 30 °C saturated copper sulphate solution

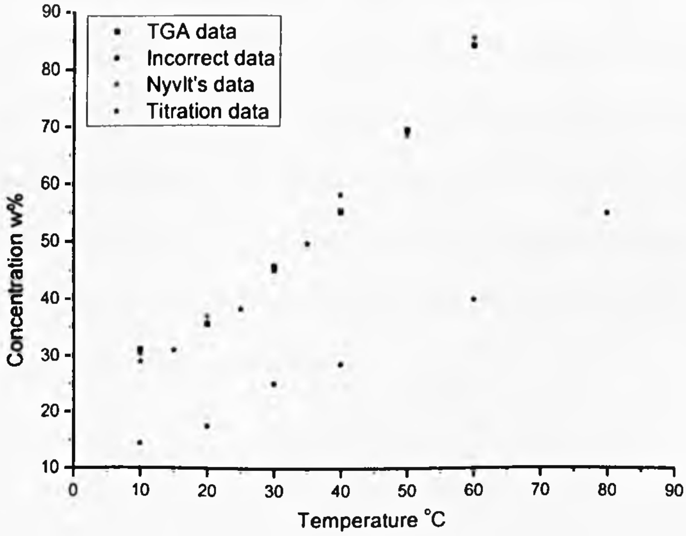

Figure 5.3: Solubility data comparison of copper sulphate pentahydrate

According to the temperature of losing crystalline water at around 100 °C, the TGA was set to fix the temperature at 30 °C to vaporize the solution water and keep the crystalline water in the crystal lattice. Before the TGA test, the saturated copper sulphate solutions were prepared at different temperatures. The copper sulphate pentahydrate crystals were added into the distilled water under agitation at a fixed temperature until the crystal cannot be dissolved, and then the solution was kept overnight to make sure the solution was saturated. The sample is filtered, and the clear solution after filtration is put in the TGA. The final weight remaining after drying (see Fig 5.2) is the weight of crystal which had been dissolved in the known volume of saturated solution. This is the solubility at the specified temperature.

The solubility data of copper sulphate pentahydrate measured by TGA is presented in the Figure 5.3 and compared with the data in the literature, the value is nearly double that of the value used by Sohnel [140] which was taken from Mullin's data [141]. However, the TGA result is very close to Nyvlt's data [142, 143]. In order to verify the correct solubility, several crystallization experiments were carried out, no crystals came out using Mullin's solubility data, which proved the underestimation of the solubility of copper sulphate pentahydrate. The TGA measurement of solubility is repeatable for the copper sulphate sample used in this project, and the data fits the titration measurement data well using ethylenediaminetetraacetic acid (EDTA) by Jiang [144]. On the other hand, the solubility data of copper sulphate pentahydrate measured by TGA had a good agreement with the data measured by the electrical conductivity probe which is described below.

5.2.2 Van't Hoff analysis of solubility data

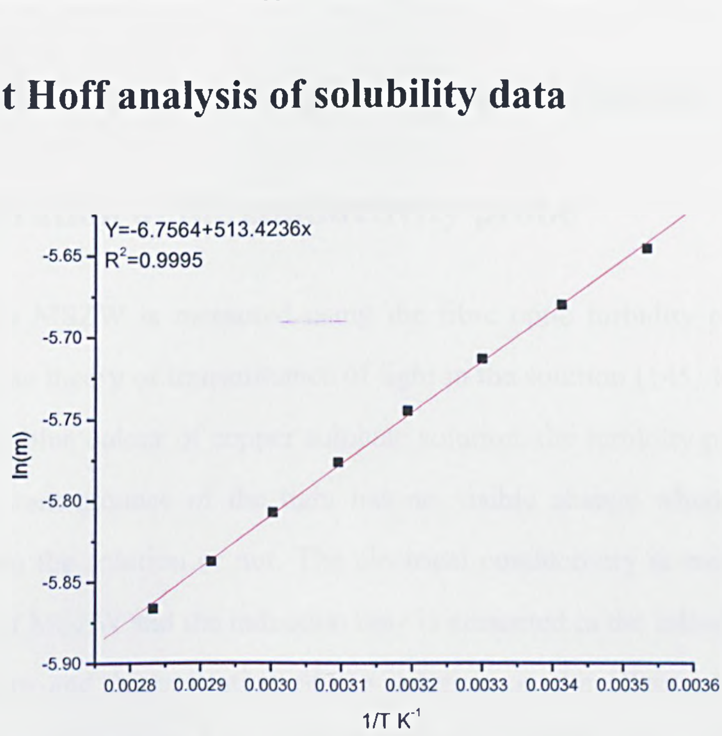

Figure 5.4: Van't Hoff equation fitting of copper sulphate pentahydrate depending on the solubility data measured by TGA

According to the Van't Hoff equation presented in Equation 2.7, the relationship between the logarithm of the mole fraction of solute in solution against the reciprocal of the absolute temperature was plotted in Figure 5.4. There was no change in the slope which meant the given solution had no polymorphic form of solid, which means there was no other hydrate appearing and only copper sulphate pentahydrate crystals came out during the solubility measurement using TGA.

5.3 MSZW of copper sulphate pentahydrate

5.3.1 Calibration of the conductivity probe

Commonly, the MSZW is measured using the fibre optic turbidity probe which is dependent on the theory of transmittance of light in the solution [145, 146]. However, due to the dark blue colour of copper sulphate solution, the turbidity probe could not be used. The transmittance of the light has no visible change whether the crystal comes out from the solution or not. The electrical conductivity is employed for the measurement of MSZW and the induction time is presented in the following section.

The temperature and concentration of the solution on the effect of the electrical conductivity was investigated by former researchers[147]. Diego studied several compounds in a wide range of concentrations and temperatures to find the model to fit the relation around conductivity, solution concentration and solution temperature [148, 149]. The electrical conductivity rises linearly as the solution concentration increases [150, 151] for the inorganic salt solution under a limited concentration, which is dependent on the characteristics of the material. Furthermore, the temperature has the similar effect on the electrical conductivity [152, 153]. Due to the ability of indicating the concentration change of the solution, the electrical conductivity was employed to detect the on-set of crystallization [154]. The electrical conductivity is also used to measure the MSZW, induction time [155, 156], and supersaturation [157, 158].

Before the MSZW measurement, the conductivity probe was calibrated for the copper sulphate solution under different conditions. The conductivity data of solutions with different solute concentrations were measured at different temperatures. The measurements were carried out in the pure solutions, so all the solutions were prepared with concentration under solubility corresponding to the experimental temperature.

Similar results were found in the literature, the conductivity was changing linearly to the temperature at a fixed solution concentration, 2ms/cm changing per 1° C. Similarly, the conductivity was changing linearly to the concentration change at a fixed solution temperature. However, the increase of conductivity at high solution concentrations was smaller than the increase in the low solution concentrations at a fixed temperature as shown in Figure 5.5. For instance, from the serial conductivity value of copper sulphate solution with different solution concentration from 25 w% to 60 w% under the fixed temperature 50 °C shown in the Figure 5.5, it is easy to find that the increase of conductivity is getting small as the solution concentration goes up. The conductivity at 60 w% is nearly equal to the data at 55 w%, whereas the conductivity of solution at 30 w% is around 5 ms/cm higher than the result of solution at 25 w%. Same concentration change under the same temperature shows different trend at different solution concentration. Actually, the solution conductivity at 60 w% is the maximum value for the solution under 50 °C. When the solution concentration sequentially goes up, the conductivity will keep constant and then decrease. This means the 60 w% is the maximum conductivity solution concentration for the copper sulphate at 50 °C.

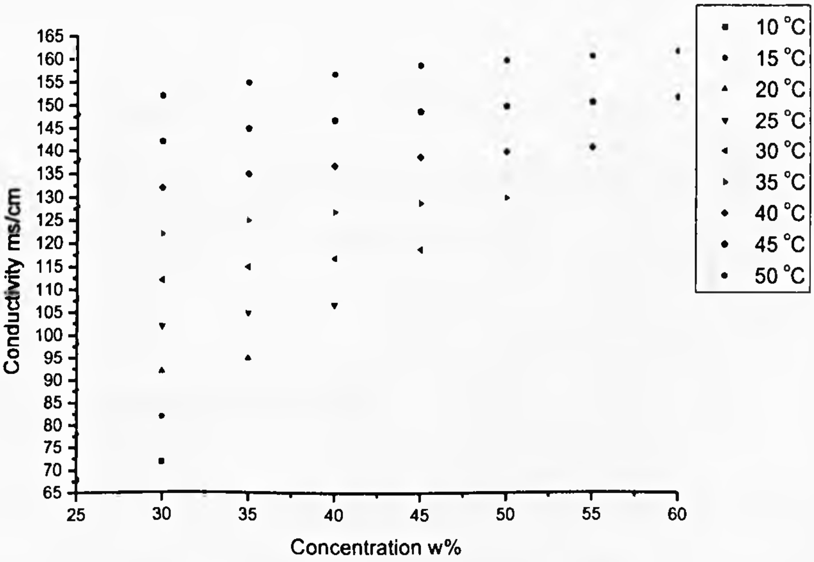

Figure 5.5: Conductivity of copper sulphate solution under different conditions

When the solution concentration is below the maximum concentration, the solution conductivity would increase along with an increase in the solution concentration, whereas the conductivity would decrease with increase in the solution concentration when the solution was beyond the maximum concentration. This phenomenon agrees with the Casteel-Amis equation [159], which described the relationship between the electrical conductivity with the solution concentration and solution temperature. In solution, copper sulphate forms Cu^{2+} and SO_4^{2-} ions which exist as separate entities and are individually surrounded by water molecules. Being separated, the Cu^{2+} and SO_4^{2-} ions are in a state capable of carrying current, and the conductivity is directly proportional to the solution concentration. However, if the solution concentration is too high, the attraction between the ions breaks down the water molecule barrier and the total number of ions in the solution is at the maximum. At this point, the conductivity of the solution reaches a maximum value. Any further increase in the concentration of the solution results in more and more ions coming together, which produces fewer ions available to conduct current.

For the conductivity measurement of copper sulphate solution under the pre-set solution concentration, the technique is still useful to predict the on set of crystallization although the conductivity in the high solution showed no dramatic change.

There is a visible change in the conductivity as the crystallization occurs, which is due to (a) large consumption of the solution concentration by nucleation; (b) obvious disturbance of the conductivity data from the particle.

5.3.2 Measurement of MSZW

The MSZW measurement of copper sulphate solution was set up in the 1 a litre of reactor combined with the electrical conductivity probe. The copper sulphate solutions with different solute concentrations of 45 w%, 50 w%, 55 w%, and 60 w% were prepared, the stirrer speed was fixed at 200 rpm to avoid bubbles which will drop the conductivity value [160].

The prepared solutions were cooled down at different cooling rates, which were set to

0.1 °C/min, 0.25 °C/min, and 0.5 °C/min. The conductivity value first linearly decreased as the temperature decreased due to no solution concentration change. When the crystallization occurred, the solution concentration was decreased, and the drop of the solution concentration brought drop of the conductivity value as well. The crystals therefore can be detected by the probe when the slope of the change of the conductivity increased. The crystallization accelerated the decreasing of the conductivity data. It also brings some interruption to the conductivity data by the existence of the crystal. Fortunately, it has no effect on the determination of the on-set of crystallization. On the other hand, the temperature at which all crystals dissolved can be defined as the change of the slope of the conductivity decrease.

The conductivity measurement processes of copper sulphate with solution concentration of 50 w% were monitored under different cooling rates shown in the Figure 5.6 – 5.8. From the straight lines drawn on the conductivity data, it is apparently to see that the slops of straight lines are different after the crystallization occurs. The onset of the crystallization points can be determined from the slop change during the crystallization processes. For the same reason, the dissolution temperature can be evaluated. The conductivity measurements for 50 w% copper sulphate solution were repeated for the solution with four different concentrations of 45 w%, 55 w% and 60 w%.

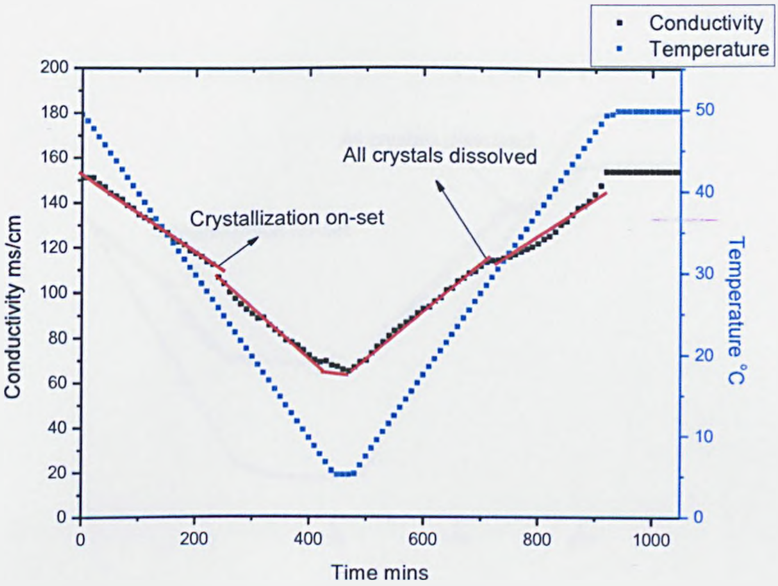

Figure 5.6: Conductivity and temperature measurement against time of 50 w% copper sulphate solution at 0.1 °C/min cooling rate

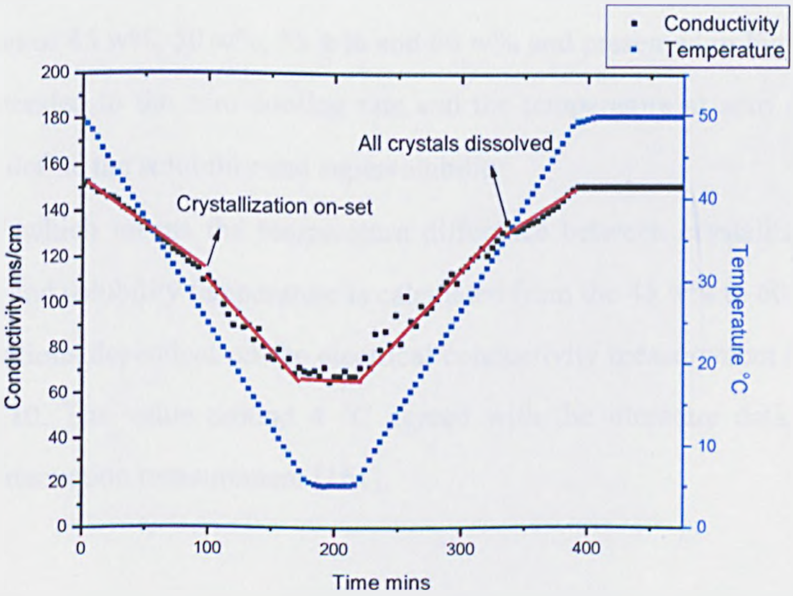

Figure 5.7: Conductivity and temperature measurement against time of 50 w% copper sulphate solution at 0.25 °C/min cooling rate

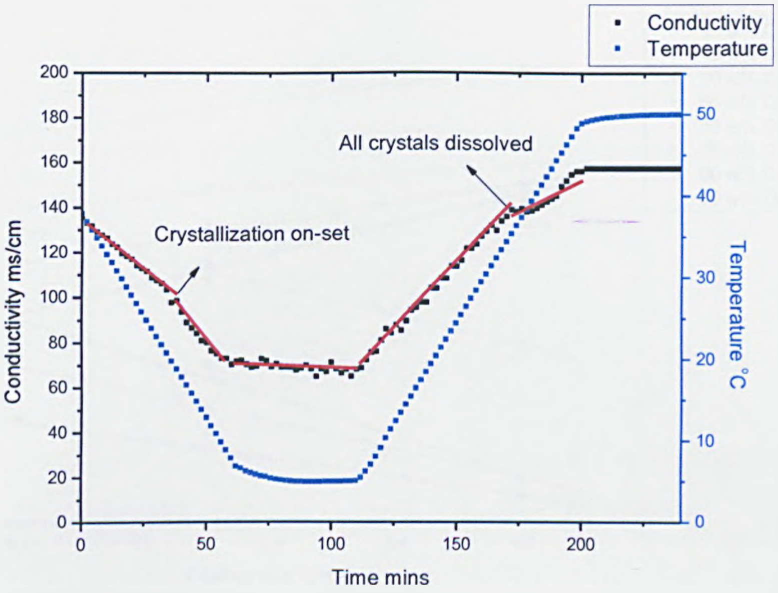

Figure 5.8: Conductivity and temperature measurement against time of 50 w% copper sulphate solution at 0.5 °C/min cooling rate

The temperature difference (T_{max}) between the on set of crystallization and the point at which all the crystals dissolved under different cooling rates of each concentration solution were recorded for the these copper sulphate solution with solution concentration of 45 w%, 50 w%, 55 w% and 60 w% and presented in Figure 5.9. The plot was extended to the zero cooling rate and the temperature at zero cooling rate was used to define the solubility and supersolubility.

The MSZW which means the temperature difference between crystallization onset temperature and solubility temperature is calculated from the 45 w% to 60 w% copper sulphate solutions dependent on the electrical conductivity measurement is presented in Figure 5.10. The value around 4 °C agreed with the literature data well using ultrasound attenuation measurement [161].

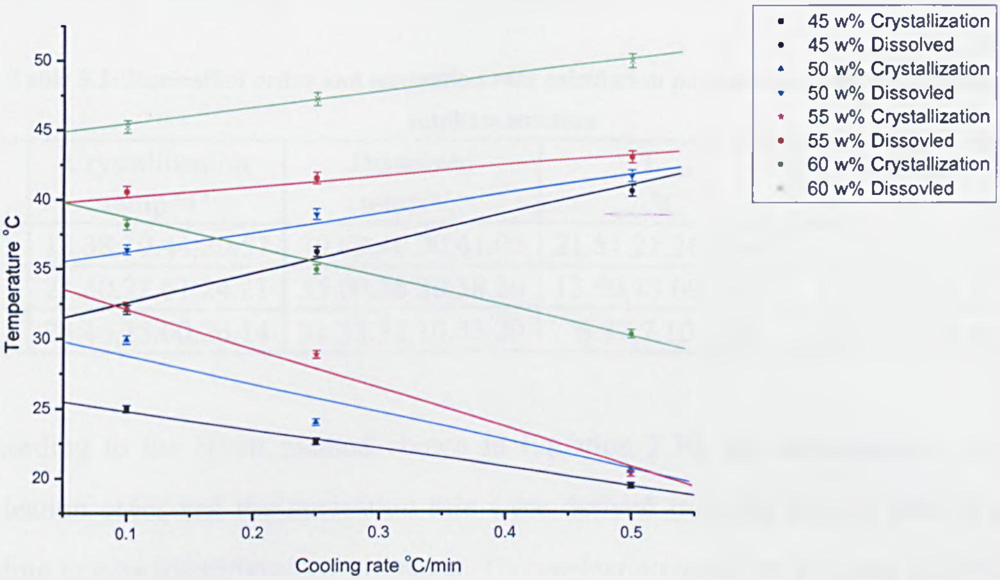

Figure 5.9: Temperature of crystallization and temperature of all crystal dissolved plotted against the cooling rate of copper sulphate with different solute concentrator

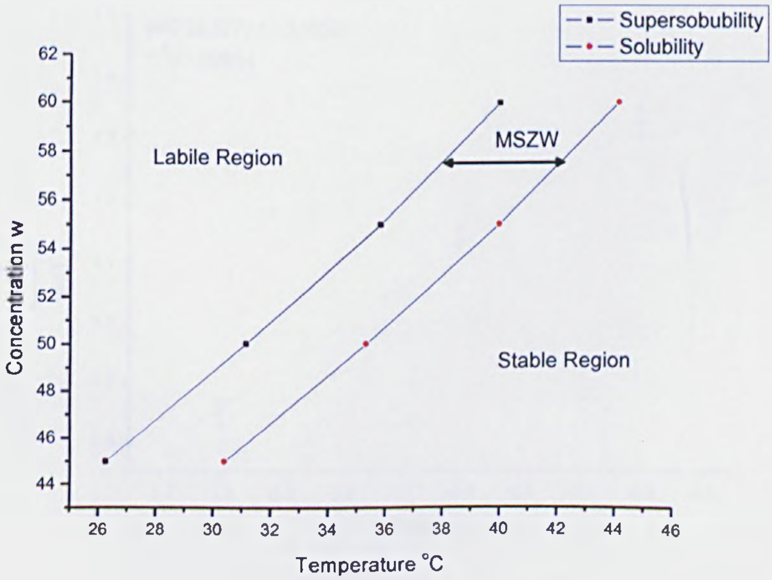

Figure 5.10: MSZW calculation of copper sulphate solution

5.3.3 Nyvlt analysis of MSZW data

Table 5.1: Nucleation order and nucleation rate calculation parameters of 45 w% copper sulphate solution

Cooling rate b °C/min	Crystallization temp °C	Dissolved temp °C	T_{max} °C	log T_{max} °C	log b °C/min
0.50	18.38,19.44,20.57	39.89,40.70,41.05	21.51,21.26,20.48	1.33,1.33,1.31	-0.30103
0.25	21.50,22.61,24.21	35.00,36.30,38.20	13.50,13.69,13.99	1.13,1.14,1.15	-0.60206
0.10	24.46,25.00,26.14	31.33,32.10,33.20	6.87,7.10,7.06	0.83,0.85,0.85	-1

According to the Nyvlt method shown in Equation 2.30, the determination of the nucleation order and the nucleation rate were derived from the plot of MSZW and cooling rate on logarithmic co-ordinates. The nucleation order for this case is 0.68327, which is quite close to the literature data around 0.518 found by Giulietti et al [143]. Compared to another inorganic system ammonium aluminium sulphate, which has the nucleation order of 0.3106 [162], this nucleation order calculated from the conductivity is quite reasonable.

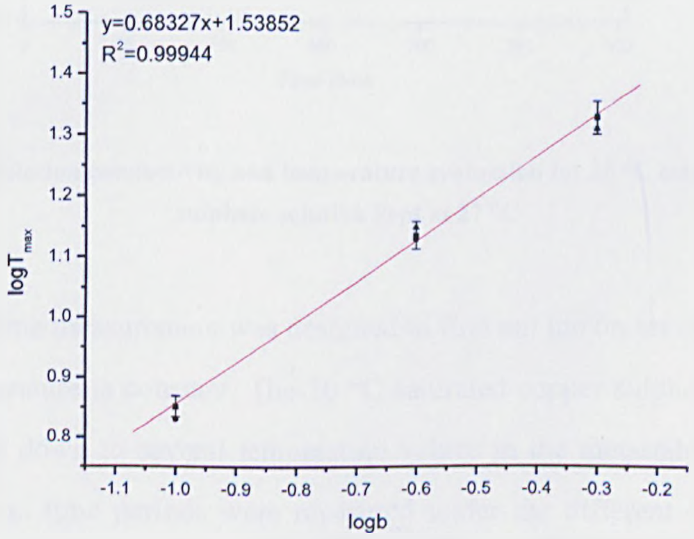

Figure 5.11: Plot logarithm of MSZW value against logarithm of cooling rate value for the nucleation order calculation

5.4 Induction time of copper sulphate pentahydrate

5.4.1 Measurement of induction time

The appearance of the copper sulphate pentahydrate crystal is detected by the drop in the electrical conductivity of the solution without the temperature affecting the conductivity data.

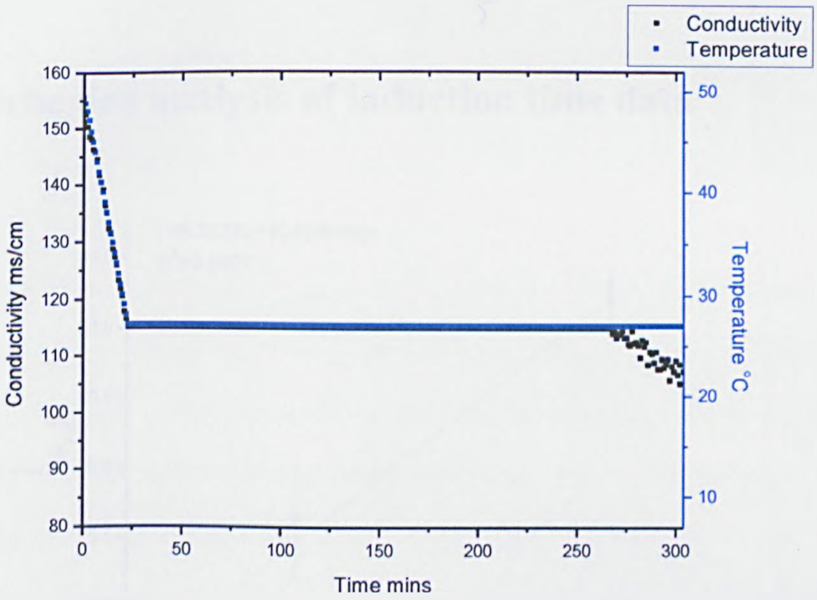

Figure 5.12: Solution conductivity and temperature evaluation for 30 °C saturated copper sulphate solution kept at 27 °C

The induction time measurement was designed to find out the on set of crystallization when the temperature is constant. The 30 °C saturated copper sulphate solution was selected to cool down to several temperature values in the metastable zone (MSZ), and the induction time periods were measured under the different supersaturations generated. The choice of 30 °C saturated solute was because of its common use in the following crystallization experiments, which suits the limitation of the instruments. The solubility value at 30 °C refers to the solubility measurement shown in Figure5.3. The solution was firstly heated up to a high temperature around 50 °C, and kept constant over 1 hour to make sure all the crystals were dissolved in the solution. Thereafter, the solution was fast cooled to the pre-set temperature in the MSZ to generate the supersaturation. The temperature was kept constant until the crystals came out and the time of the constant temperature before crystallization was defined as the induction time and used for the calculation of interfacial tension.

The conductivity evaluation of the solution at a fixed temperature of 27 °C after dissolving all the crystals is presented in Figure 5.12. It is clear to find the drop of the conductivity of the solution when the crystal comes out from the solution.

5.4.2 Arrhenius analysis of induction time data

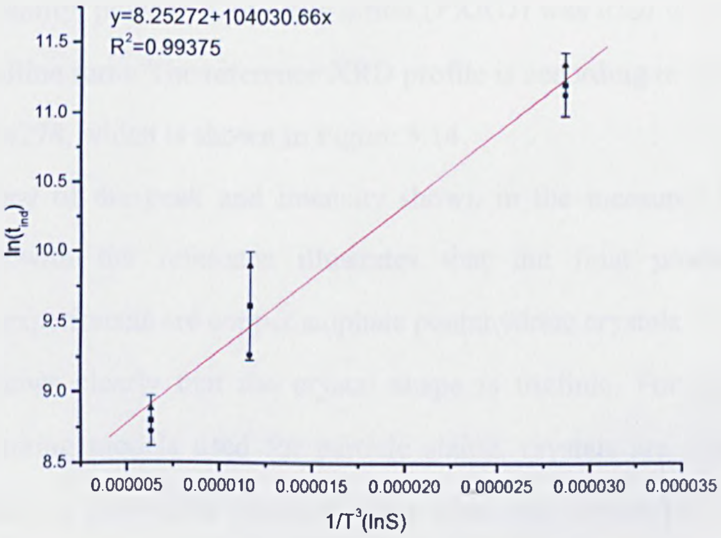

Figure 5.13: Plot of the logarithm of induction time against the logarithm of supersaturation for each pre-set fixed temperature

Table 5.2: Parameters to calculate the interfacial tension of 30 °C saturated copper sulphate solution

Constant temperature T °C	Supersaturation S	$1/T^3(\ln S)^2$	Induction time t_{ind} s	$\ln t_{ind}$
26	1.0800	6.32×10^{-6}	6120,6600, ,7200	8.72,8.79,8.88
27	1.0580	1.17×10^{-5}	10600,15000,20000	9.27,9.62,9.9
28	1.0364	2.87×10^{-5}	68000,73200,84000	11.13,11.20,11.34

The induction times were measured at different supersaturations then plotted against the supersaturation at each fixed temperature shown in Figure 5.13, the slope of the linear fit line was used to calculate the interfacial tension of 30 °C saturated copper sulphate solution according to the Arrhenius equation 2.21 in Chapter 2. The interfacial tension is 7.68×10^{-16} J/m^2, as the molecular volume of copper sulphate pentahydrate crystal is 1.82×10^{-25} m^3/molecular.

5.4.3 Identifying the crystallized copper sulphate pentahydrate crystals

The crystals were collected from the experiments of induction time. In order to prove the crystal's identity, powder X-ray diffraction (PXRD) was used to predict the final products crystalline form. The reference XRD profile is according to the PXRD ICDD cards, 04-00904278, which is shown in Figure 5.14.

High consistency of the peak and intensity shown in the measured PXRD profile (Figure 5.15) with the reference illustrates that the final products after the crystallization experiments are copper sulphate pentahydrate crystals.

Figure 5.16 shows clearly that the crystal shape is triclinic. For the purposes of ultrasonic scattering models used for particle sizing, crystals are considered to be spherical which is a reasonable approximation when the wavelength is much larger than the crystal size.

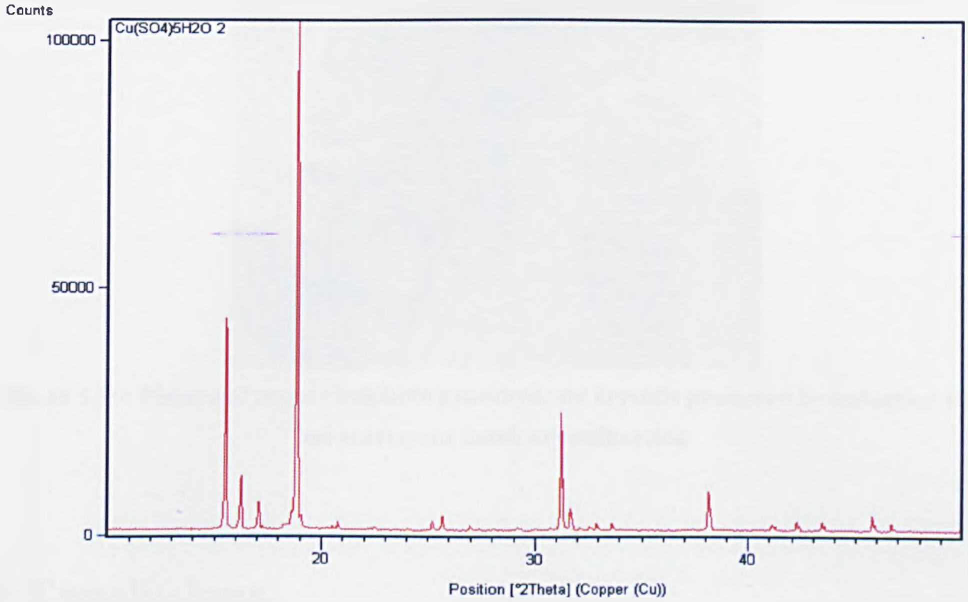

Figure 5.14: Reference PXRD profile with ICDD cards of 04-00904278

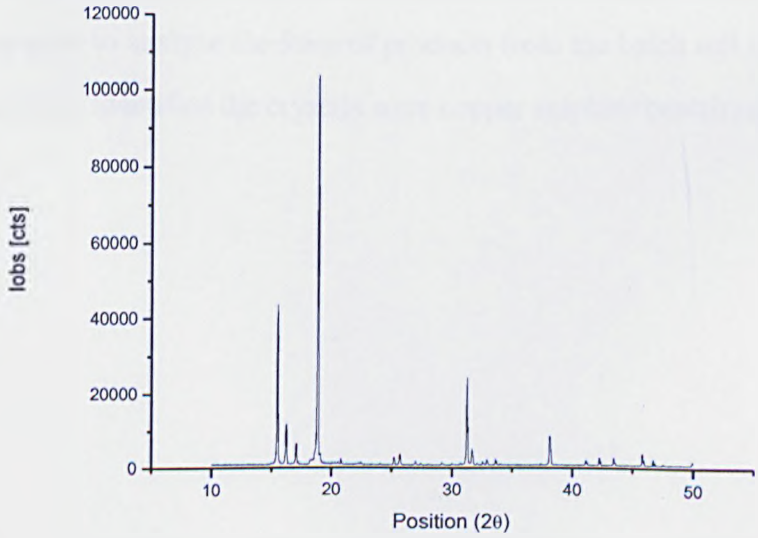

Figure 5.15: XRD measurement of copper sulphate crystal produced by induction time measurement batch crystallization

Figure 5.16: Picture of copper sulphate pentahydrate crystals produced by induction time measurement batch crystallization

5.5 Conclusions

The three fundamental properties of crystallization of copper sulphate pentahydrate system were measured in this chapter. The solubility of the copper sulphate pentahydrate was measured by the gravimetric method depending on the TGA. The MSZW and induction time of the copper sulphate pentahydrate system were both measured by electrical conductivity. The nucleation kinetics parameters were analyzed depending on the measurement of MSZW and induction time. The PXRD technique was used to analyze the form of products from the batch cell crystallization experiments, which identified the crystals were copper sulphate pentahydrate crystals.

Chapter 6 An Examination of the Growth Kinetics of the Copper Sulphate Pentahydrate using Ultrasonic Attenuation Spectroscopy

Summary

This chapter presents the study of the crystallization of copper sulphate pentahydrate in a 20 litre reactor based on ultrasound attenuation spectroscopy. Overall growth rate under different solution supersaturation is extracted.

6.1 Introduction

After reviewing the theoretical description of the relationship between acoustic attenuation with particle size information measured in emulsion and suspension, this chapter introduces the acoustic spectrometer employed in the project. The instrument is an Ultrasizer MSV system developed by Malvern Ltd. The principle of measurement of MSV is described in this chapter and the measurement strategy was manually optimized. The background acoustic properties of copper sulphate pentahydrate were measured and analyzed. A description of the on-line crystallization process particle size analysis is given and the overall crystal growth rate was analyzed from the dynamic perspective.

6.2 Ultrasonic physical description of the copper sulphate pentahydrate system

6.2.1 Ultrasonic physical properties sensitivity analysis of the copper sulphate pentahydrate crystal/solution slurries

The ECAH model which transferred the acoustic spectra into the particle size and concentration involves several physical properties. These values used for properties definitely affected the analysis of the particle information as determined from acoustic measurements and the correct values for these parameters are criteria for the reliable particle analysis result. However, not all the physical parameters play the role of determining the results. The individual physical property sensitivity analysis is completed in this project.

Two copper sulphate pentahydrate crystal samples of different size were selected. Both of the two samples were crystallized in a 1 litre crystallizer, and sieved in the range of 106-125 μm and 20-53 μm, respectively. Solid copper sulphate pentahydrate crystals were suspended in the 30 °C saturated copper sulphate solution, and the suspended volume concentration was fixed at 2 v%. The particle size and volume concentration were analyzed from the acoustic spectra collected using Mougin's copper sulphate pentahydrate physical parameters shown in Table 6.1. Each of the physical parameters listed was individually increased by 10%, and the change in the particle size and suspended particle volume were presented.

Table 6.1: Physical parameters of copper sulphate pentahydrate crystal and copper sulphate solution with a concentration of 24.6 w% (temperature T in °C and frequency f in MHz) from Mougin's data [163]

Physical properties	Copper sulphate pentahydrate crystal	45.7893 w Copper sulphate solution
Density kg.m^{-3}	2.28×10^{3}	1.27×10^{3}
Sound velocity m/s	4.55×10^{3}	1.66×10^{3}
Thermal dilation K^{-1}	1.65×10^{-4}	4.30×10^{-4}
Thermal conductivity J.m^{-1}.s^{-1}.K^{-1}	7.30×10^{-1}	5.72×10^{-1}
Heat capacity J.kg^{-1}.K^{-1}	1.19×10^{3}	3.06×10^{3}
Shear rigidity N.m^{-2}	1.18×10^{10}	
Viscosity N.s.m^{-2}		2.88×10^{-3}
Attenuation dB/inch	$4\times10^{-4}\times f^{2}$	$(1.256\times10^{-1}-2.3\times10^{-3}\times T)f^{1.88}$

Table 6.2: Physical parameter sensitivity analysis of copper sulphate pentahydrate system, based on particles in the size range of 20-53 μm distributed in the saturated copper sulphate solution at 30 °C

Physical properties of solid phase	D50 μm	C v%
Density	23%	33%
Sound velocity	2%	3%
Thermal dilation	0%	0%
Thermal conductivity	0%	0%
Heat capacity	0%	0%
Shear rigidity	-1%	7%
Sound attenuation factor	0%	0%
Physical properties of background continuous phase		
Density	4%	11%
Sound velocity	12%	8%
Thermal dilation	0%	0%
Thermal conductivity	0%	0%
Heat capacity	0%	0%
Viscosity	-4%	5%
Sound attenuation factor	57%	-34%

Table 6.3: Physical parameter sensitivity analysis of copper sulphate pentahydrate system, based on particles in the size range of 106-125 μm distributed in the saturated copper sulphate solution at 30 °C

Physical properties of solid phase	D50 μm	C v%
Density	11%	25%
Sound velocity	6%	9%
Thermal dilation	0%	0%
Thermal conductivity	0%	0%
Heat capacity	0%	0%
Shear rigidity	-1%	3%
Sound attenuation factor	0%	0%
Physical properties of background continuous phase		
Density	5%	7%
Sound velocity	15%	13%
Thermal dilation	0%	0%
Thermal conductivity	0%	0%
Heat capacity	0%	0%
Viscosity	0%	1%
Sound attenuation factor	44%	-82%

Due to the value of the solubility of copper sulphate pentahydrate measured in this project being different from the former work by P. Mough[163], and a different version of the MSV used in the project, some physical parameters of copper sulphate from Mougin's work were not correct for this research. Although the analyzed particle size and concentration are not restricted to the real size and concentration, the sensitivity of these parameters can be defined. As can be seen in Tables 6.2 and 6.3, most of the parametric sensitivity of the solid phase was very low. The only parameter of solid phase which had appreciable influence was the solid density. However, the crystallization process and the acoustic wave had no effect on the solid density, which was stable during the measurement process. The density, sound velocity and sound attenuation coefficient factor of the background continuous phase was highly sensitive to the particle information analysis. The results of the sensitivity analysis of the copper sulphate pentahydrate system are similar to the aqueous glass beads case in Hipp's work[164]. Individually 10% change of the sound velocity in the background solution caused around 10% change in the particle median size, whereas the 10% change of the thermal parameters or shear modules gave almost no change of particle size and particle volume analysis. There is no discussion about the sensitivity of the sound attenuation coefficient factor due the use of high stable medium pure water. In the case of copper sulphate solution, the attenuation coefficient factor played the most important role. The attenuation coefficient factor had high sensitivity for the particle sizing, this was also found for the case of Monosodium glutamate in Mougin's work[163].

The modification of the acoustic attenuation coefficient, the acoustic velocity, and the density of the continuous phase had a significant effect on the particle size and particle volume analysis. Therefore, these properties, and their dependence on temperature and solution concentration were measured, as discussed in more detail below.

6.2.2 Measurement of the physical properties of copper sulphate pentahydrate system

The relationship of acoustic attenuation and sound frequency fit the power law function in solution.

$$\alpha = af^{n} \tag{6.1}$$

where α is the attenuation coefficient, a and n are the attenuation coefficient factor and attenuation coefficient exponent, respectively.

The 30 °C saturated copper sulphate solution refer to solubility data (Figure 5.3) with a concentration of 45.7893 w% was prepared for the crystallization experiments. The solution was heated up to 40 °C and kept at that temperature for over 1 hour to make sure the crystals were all dissolved. Then, the solution was cooled down to 10 °C under different pre-set cooling rates. During the crystallization process, the temperature and the solute concentration were both changed. Compared to the significant effects on the sound attenuation of the solution temperature, the change of the sound attenuation from the solution concentration change can be eliminated. which had similar results with the references [161, 163, 165, 166]. The temperature dependence of the acoustic spectrum of the liquid medium was analyzed in detail. This can be found from the results of factor a and n measured in different concentrations and at different temperatures which listed in Table 6.4. Copper sulphate solutions with different solution concentration were cooling down in their unsaturated temperate range. Fast cooling rate 0.5 °C/min was set for the cooling because it had not effect on the measurement for the unsaturated condition. Because the crystallization process in this project always operated between 40 °C and 20 °C, and the initial solution concentration and final solution concentration are 45 w% and 35 w% refer to the copper sulphate pentahydrate solubility at 30 °C and 20 °C respectively. From the Table 6.3, it is clear to find the attenuation coefficient a has a much bigger change from 30 °C to 20 °C (30 w% solution for example) than the solution concentration change from 45 w% to 30 w% (30 °C for example). Figure 6.1 shows the spectra at different concentrations under 30 °C, which predicts the change of the attenuation has limited variation.

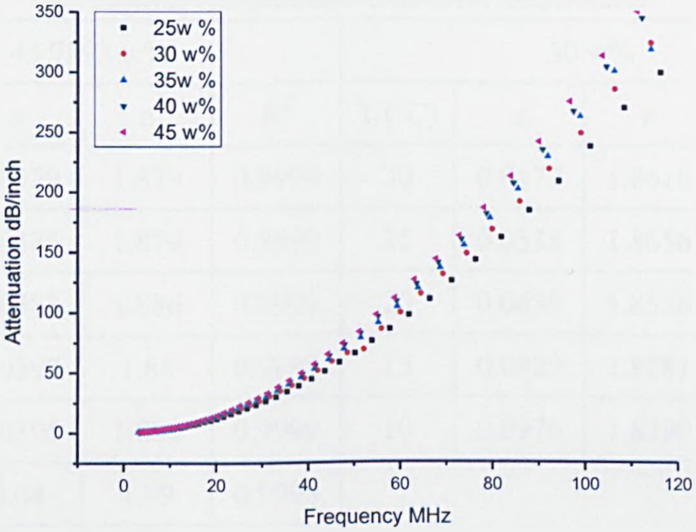

Figure 6.1: Spectra of copper sulphate solution with difference solution concentration under 30°C

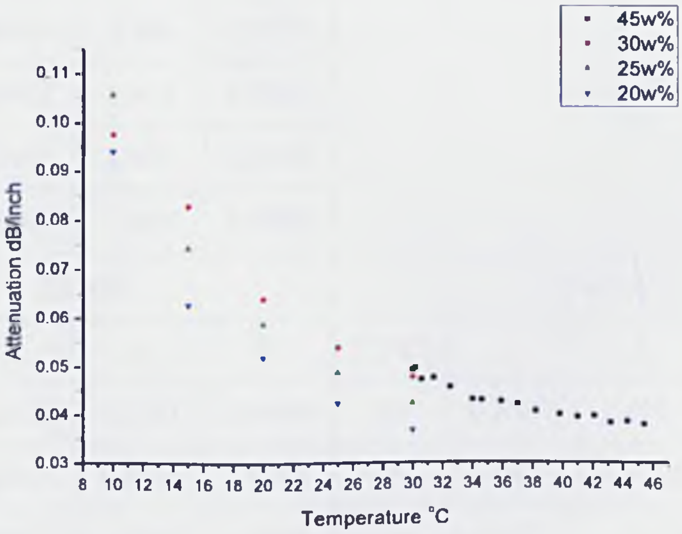

Figure 6.2: Attenuation coefficient factor a changes with the temperature of different concentrations of copper sulphate solution

Table 6.4: Acoustic attenuation coefficient parameter measurement of copper sulphate solution with different concentrations at different temperatures

45.7893 w%				30 w%			
T (°C)	a	n	R^2	T (°C)	a	n	R^2
45.4	0.0379	1.879	0.9999	30	0.0477	1.8616	0.9996
44.3	0.0385	1.879	0.9999	25	0.0538	1.8656	0.9997
43.2	0.0383	1.886	0.9998	20	0.0639	1.8586	0.9999
42.1	0.0397	1.88	0.9998	15	0.0829	1.8281	0.9995
41	0.0395	1.888	0.9999	10	0.0976	1.8299	0.9998
39.8	0.04	1.89	0.9998				
38.2	0.0407	1.893	0.9998				
37	0.0421	1.89	0.9998				
35.9	0.0427	1.892	0.9998				
34.6	0.043	1.898	0.9998				
34	0.0431	1.906	0.9998				
32.5	0.0457	1.894	0.9998				
31.4	0.0476	1.89	0.9998				
30.6	0.0472	1.902	0.9998				
30.2	0.0497	1.891	0.9998				
30	0.0493	1.899	0.9998				
25 w%				20 w%			
T (°C)	a	n	R^2	T (°C)	a	n	R^2
30	0.0422	1.8731	0.9999	30	0.0367	1.8791	0.9999
25	0.0486	1.8724	0.9999	25	0.0423	1.8789	0.9999
20	0.0587	1.8597	0.9999	20	0.052	1.8612	0.9998
15	0.0744	1.8354	0.9996	15	0.0629	1.8505	0.9998
10	0.1056	1.7852	0.9992	10	0.0941	1.7839	0.9991

Table 6.4 shows copper sulphate solution with different concentrations, the measurements condition is only solution without particle, so the measurement

strategies, which mean the transducer passing length and measurement spacing are similar. In order to present the strategies setting under different conditions for the repeatability of the experiments, some measurements strategies under different solution concentration and different temperature were presented below. For instance, 45 w% and 10 w% copper sulphate solution both at 30 °C were compared, in the other hand, the strategies of 10 w% solution were compared under 30 °C and 10 °C. From the data of Table 6.5, it is clear to see that the measurement strategies are quite similar to each other for the copper sulphate solution without particle exists. The solution concentration variation and temperature change would not bring dramatic change on this setting.

Table 6.5 MSV measurement strategies for the copper sulphate solution under different conditions

45 w% at 30 °C	Min Freq MHz	Max Freq MHz		% of Freqs	Position 1 inch	Position 2 inch
Channel 1 Low Freq	3.4	15.1		43	0.1	4
Channel 1 high Freq						
Channel 2 Low Freq	15.6	51.4		35	0.04	0.64
Channel 2 high Freq	53.3	111.4		22	0.03	10
10 w% at 30 °C	Min Freq MHz	Max Freq MHz		% of Freqs	Position 1 inch	Position 2 inch
Channel 1 Low Freq	1	16.5		59	0.05	4
Channel 1 high Freq						
Channel 2 Low Freq	17.3	50		23	0.03	1.1
Channel 2 high Freq	52.5	119.4		18	0.03	0.35
10 w% at 10 °C	Min Freq MHz	Max Freq MHz		% of Freqs	Position 1 inch	Position 2 inch
Channel 1 Low Freq	3.1	16.5		47	0.1	4
Channel 1 high Freq						
Channel 2 Low Freq	17.1	51.2		31	0.04	0.64
Channel 2 high Freq	53.1	114.2		22	0.03	0.11

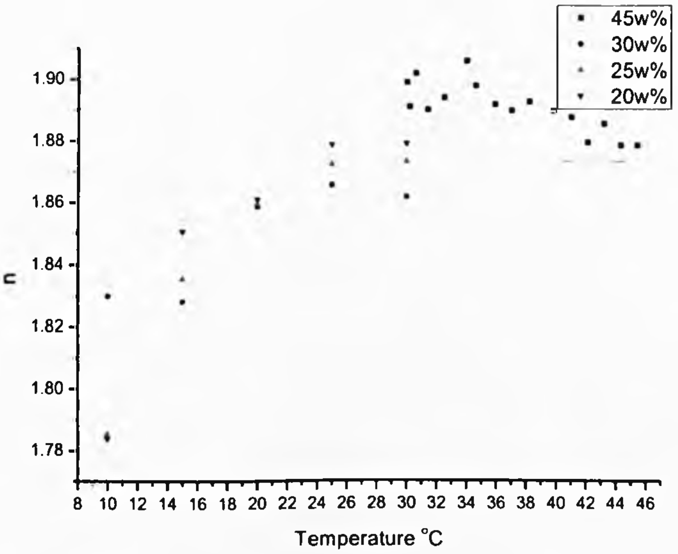

Figure 6.3: Attenuation coefficient factor n changes with the temperature of different concentrations of copper sulphate solution

It is easy to find out the quadratic relationship between the acoustic attenuation coefficient factor a which is depended on the temperature from the Figure 6.2, but the weakness dependence of n and the temperature is also predicted (Figure 6.3). The value of 1.891 for n was used to estimate the n value during the crystallization process, since it is the value relating to the solution concentration of 45w% which is used in the subsequent experiments.

The temperature dependence of the acoustic spectrum of the liquid medium can be described by the equation:

$$\alpha=(4E\text{-}05T^2-0.0041T+0.1305)f^{1.891} \quad (6.2)$$

where α in dB/inch, T in °C and f in MHz

Very precise sound velocity in the pure copper sulphate pentahydrate solution with a concentration of 45.7893 w% at different temperatures was measured using ResoScan. The experimental details are given in Chapter 7.

Table 6.6: Sound velocity in pure copper sulphate pentahydrate solution with a solution concentration of 45.7893 w% at different temperatures

Temperature °C	Sound Velocity m/s
40.00	1621.71
39.02	1621.41
38.01	1620.91
37.02	1620.36
36.03	1619.76
35.00	1619.07
34.01	1618.36
33.02	1617.60
32.04	1616.79
31.00	1615.8704
30.02	1614.9417

The change in the sound velocity was not too dependent on the temperature change, only 0.4 % change in the velocity was detected as the temperature decreased to 10 °C, which was a drop from 40 °C to 30 °C. The value 1614.9417 m/s was used as the sound velocity for the pure saturated copper sulphate solution at 30 °C, i.e. the start point of the crystallization process.

The temperature was dependent on sound velocity in pure solution with a concentration of 45.7893 w% can be explained using the equation below according to the data present in Table 6.6, the R square for the fitting is 0.9999:

$$\upsilon=-0.0299T^2+2.7783T+1558.5 \tag{6.3}$$

where υ is the sound velocity in m/s , and T is the temperature in °C

Extending the temperature to the crystallization process range of 30 °C to 20 °C, the value of the sound velocity can be evaluated at every temperature point. The solution concentration at the end of the crystallization process got close to the solubility of 20°C if the crystals are all crystallized from the solution. The solubility at 20 °C is 35.5369 w%. Compared with the sound velocity of solutions with concentration of 45.7893 w% and 35.5369 w% at selected temperature points in the crystallization process temperature range, the difference is always around 25 m/s, which is a 1.5 % change. The change of the analysed particle size will be under 1% change. During the crystallization process, different process conditions will affect the solution concentration, such as the reactor size, stirrer speed, cooling rate and the materials themselves, etc. The real concentration at each temperature point was not equal to the solubility at that temperature, and the difference between the values is unknown. In order to minimize the error of the sound velocity estimation, the sound velocity value of the saturated concentration at each temperature point is used in the physical matrix for the particle size analysis, which means the temperature dependence for sound velocity is considered.

As the density of the solution will keep changing as the solution concentration changes during the crystallization process, the solution density was measured using the Density Analyzer DSA48 (Anton Paar). The experimental details are presented in Chapter 7. However, the density of solution has no dramatic variation as the temperature and solution concentrations change. The solution density only increased by 0.4% as the temperature decreased to 10 °C. When the solution concentration decreases from 45.7893 w% to 35.5369 w%, the solution density will be decreased by 4.3% at the same temperature. From the effect of solution density on the particle size analysis in the sensitivity analysis, the influence of the variation of the solution density during the crystallization can be ignored. The saturated solution density was used for the size analysis at each temperature point.

Table 6.7: Comparison of the sound velocity of solutions with concentrations of 45.7893 w% and 35.5369 w% at different temperature

Temperature °C	Sound velocity of 45.7893 w% solution m/s	Sound velocity of 35.5369 w% solution m/s
30	1614.93	1590.50
29	1613.92	1589.34
28	1612.85	1588.08
27	1611.71	1586.69
26	1610.52	1585.30
25	1609.27	1583.85
24	1607.95	1582.33
23	1606.58	1580.67
22	1605.15	1579.02
21	1603.65	1577.31
20	1602.10	1575.53

Table 6.8: Physical parameters of copper sulphate pentahydrate crystal and copper sulphate solution with a concentration of 45.7893 w%, frequency f in MHz and temperature T in Celsius

Physical properties	Copper sulphate pentahydrate crystal	45.7893 w% Copper sulphate solution
Density $kg.m^{-3}$	2.28×10^{3}	1.23×10^{3}
Sound velocity m/s	4.55×10^{3}	1.61×10^{3}
Thermal dilation K^{-1}	1.65×10^{-4}	4.30×10^{-4}
Thermal conductivity $J.m^{-1}.s^{-1}.K^{-1}$	7.30×10^{-1}	5.72×10^{-1}
Heat capacity $J.kg^{-1}.K^{-1}$	1.19×10^{3}	3.06×10^{3}
Shear rigidity $N.m^{-2}$	1.18×10^{10}	
Viscosity $N.s.m^{-2}$		2.88×10^{-3}
Attenuation dB/inch	$1.02\times10^{-5}f^{2}$	$(4\times10^{-05}\times T^{2}-0.0041\times T+0.1305)f^{1.891}$

The summary of the physical properties of copper sulphate pentahydrate crystal and copper sulphate solution used for the particle size and volume concentration analysis from the acoustic attenuation spectrum is listed in Table 6.8. The copper sulphate pentahydrate crystal data and the thermal properties of the solution were quoted from the literature [161, 167]. The density, sound velocity, and the acoustic attenuation factor with exponent of copper sulphate solution were measured in this project.

6.2.3 Physical matrix of copper sulphate system analysis and characterization

The accuracy of the new physical parameters of the copper sulphate solution was verified by batch cell attenuation measurements through suspensions of silica particle in 45 w% copper sulphate solutions at 30 °C. Different silica particle volume concentration suspensions were measured. Silica particles were chosen for the validation because of their stable chemical characterization, and non-soluble in the copper sulphate solution. Furthermore, Silica particles have spherical crystal morphology, which is suitable for accurate particle size determination depending on the ECAH model.

The particle size distribution was measured using the Mastersizer 2000 (Malvern Ltd.), and the mean size of the particle was 1.5 μm, shown in Figure 6.4.

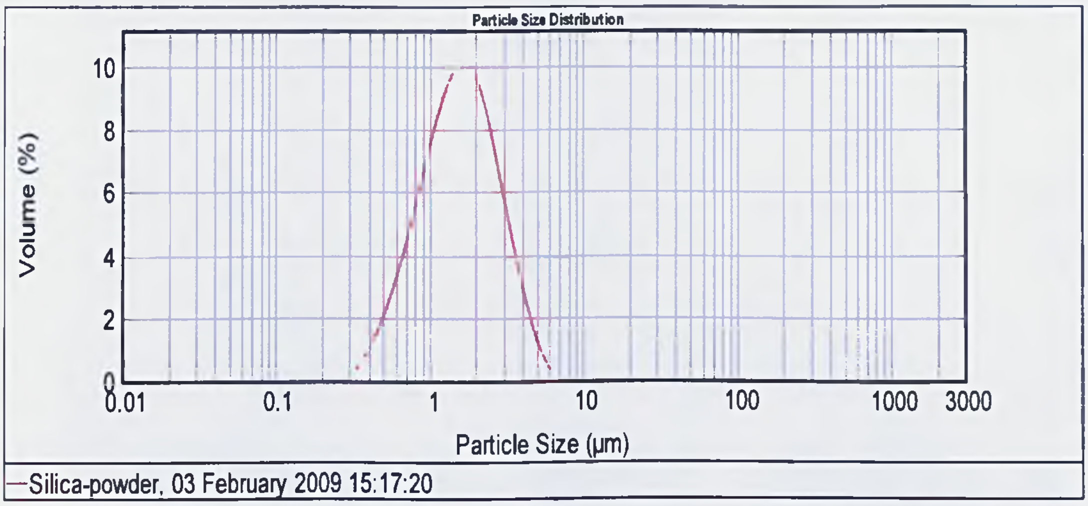

Figure 6.4: Particle size distribution of silica particle measured by Mastersizer 2000

Silica particles are the benchmark material for acoustic spectra study. The physical properties needed for the acoustic measurement are easily found in the literature. The physical matrix used in this project is the one used in Penchev's study [168] shown in Table 6.9.

Table 6.9: Physical matrix of silica particle with water

Physical properties	Silica particle	Water
Density kg.m^{-3}	2.46×10^{3}	1×10^{3}
Sound velocity m/s	5.96×10^{3}	1.49×10^{3}
Thermal dilation K^{-1}	1.56×10^{-6}	2.57×10^{-4}
Thermal conductivity J.m^{-1}.s^{-1}.K^{-1}	1.37	6×10^{-1}
Heat capacity J.kg^{-1}.K^{-1}	7.42×10^{2}	4.18×10^{3}
Shear rigidity N.m^{-2}	3.13×10^{10}	
Viscosity N.s.m^{-2}		2.88×10^{-3}
Attenuation coefficient dB.inch^{-1}.MHz^{-2}	3.75×10^{-5}	5.518×10^{-3}
Attenuation exponent	2	2

The measured attenuation spectra and corresponding particle size distribution obtained from MSV are shown in Figures 6.5 and 6.6, respectively. The particle size distribution is using lognormal distribution in volume, which refer to the description in page 56.

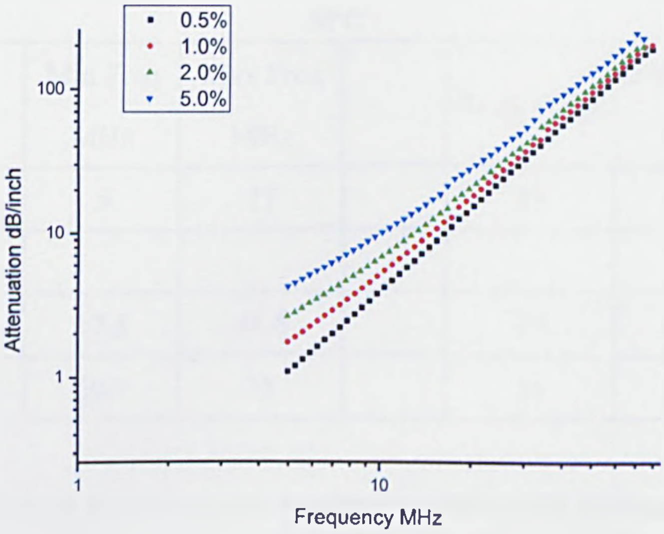

Figure 6.5: Acoustic spectra collection of silica in copper sulphate solution at 30 °C

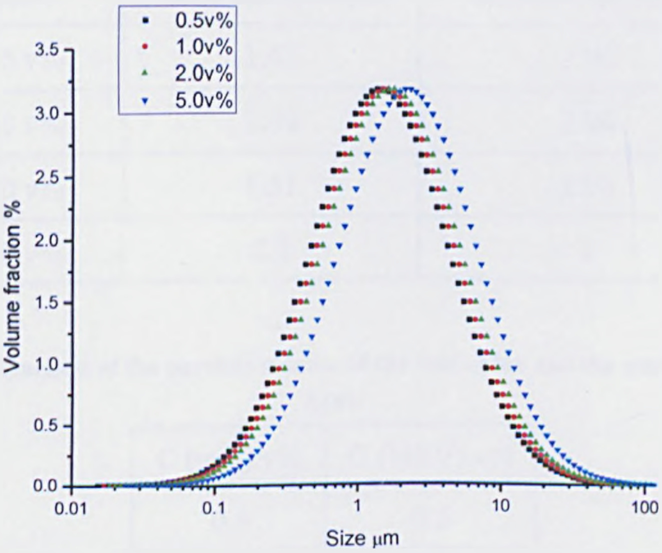

Figure 6.6: Particle size distribution analyzed from the spectra from Figure 6.4

The measurement strategy for the case of 2.0 v% silica in 45 w% copper sulphate solution at 30 ˚C was presented in Table 6.10. The measurement strategies of different suspended silica particle in 45 w% copper sulphate solution at 30 ˚C, only slightly modification on the frequency range on the boundary of the sub-channels would generate good quality spectra.

Table 6.10: MSV measurement strategy of 2.0 v% silica in 45 w% copper sulphate solution at 30˚C

	Min Freq MHz	Max Freq MHz		% of Freqs	Position 1 inch	Position 2 inch
Channel 1 Low Freq	5	17		59	0.1	2.36
Channel 1 high Freq						
Channel 2 Low Freq	17.8	48.6		25	0.04	0.43
Channel 2 high Freq	50.7	75		16	0.03	0.33

Table 6.11: Comparison of Mean size and standard deviation results measured by Mastersizer and MSV

Mastersizer	Mean size D50 µm	Standard deviation
	1.5	1.76
MSV	Mean size D50 µm	Standard deviation
0.5 v%	1.47	2.94
1.0 v%	1.49	2.94
2.0 v%	1.51	2.96
5.0 v%	2.3	3

Table 6.12: Comparison of the particle volume of the real value and the measured data from MSV

C (real) v%	C (MSV) v%
0.5	0.5
1	0.98
2	2
5	4.67

It can be seen that the results of the particle size distribution analyzed from the acoustic spectra have good agreement with the result from the Mastersizer 2000. The mean size of the particle is shown to be around 1.5μm from both instruments (Table 6.11). However, the distribution was a little bit wider from the MSV. That is mainly because the different techniques measured the different properties of the particle and therefore gave a slightly different answer. Comparing the particle size distribution results from MSV under different particle volume concentrations, the size distribution results repeat well under the low concentration. As the particle volume increased to a higher level, the particle mean size also increased slightly. That was attributed to the multiple scattering influences at high particle concentrations. However, the result of suspension with 5 v% concentration is still reasonable, which indicates that the multiple scattering can be ignored and the ECAH model is still valid in this case. Another effect on the particle distribution was from the Heterogeneous nucleation of copper sulphate pentahydrate. During the preparation of the saturated copper sulphate solution at 30 °C, the solution was heated to 40 °C, and kept over 1 hour to make sure the crystals were fully dissolved. Some of the solvent vaporized due to the batch cell being an open operating cell, and the solubility of copper sulphate pentahydrate was high. The solution was under a supersaturated state during the spectra measurement at 30 °C. The existence of the silica particle will act as the crystal seed and introduce the crystallization taking place.

The volume concentration results analyzed from the acoustic spectra are also have good quality (Table 6.12), although consistently lower than the real value. It is mainly caused by the deposition of the silica particle. Most of the deposition happened when the level of suspension changed due to the movement of the transducer. The deposition of the suspended particle on the wall always happened when using the batch cell, which was hard to avoid.

The analysis of silica particles in the copper sulphate solution suspension suggests that the physical matrix of the copper sulphate pentahydrate system used is accurate enough for the measurement. The copper sulphate pentahydrate crystallization process was analyzed depending on this matrix.

6.3 Acoustic attenuation spectra collection during crystallization

6.3.1 High cooling rate and wide cooling temperature range

Crystallization experiments were carried out on aqueous solutions of copper sulphate initially at 45.7893 w% in a 20 L crystallizer which is refer to Section 4.6.1 for experiment setup. Supersaturation was achieved by cooling the solution from 40 °C to 15 °C at a constant cooling rate. The solution was kept at a constant temperature of 15°C until the end of the experiment. The cooling rate was set to 0.3°C/min, 0.4°C/min and 0.5 °C/min.

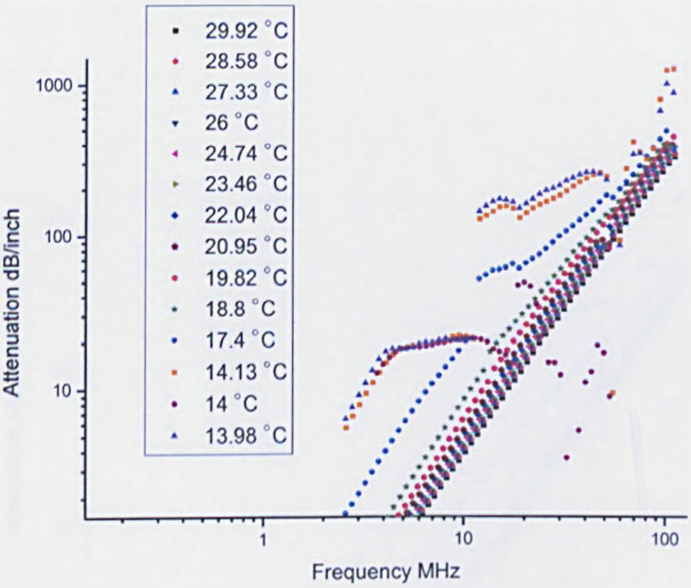

Figure 6.7: Evolution of the acoustic attenuation spectra throughout the crystallization of an aqueous solution of copper sulphate at 45.7893 w% down to 15 °C by cooling at 0.3 °C/min

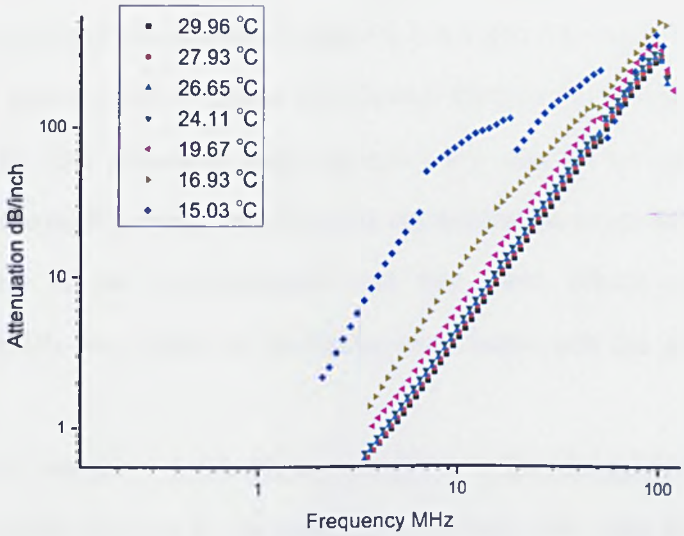

Figure 6.8: Evolution of the acoustic attenuation spectra throughout the crystallization of an aqueous solution of copper sulphate at 45.7893 w% down to 15 °C by cooling at 0.4 °C/min

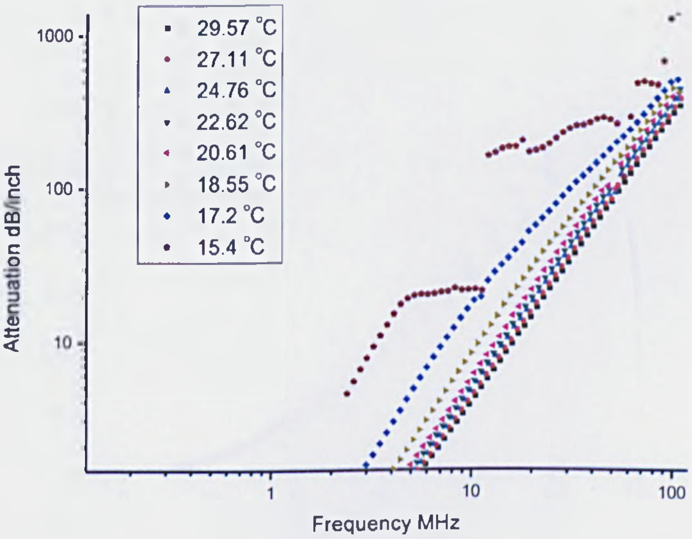

Figure 6.9: Evolution of the acoustic attenuation spectra throughout the crystallization of an aqueous solution of copper sulphate at 45.7893 w% down to 15 °C by cooling at 0.5 °C/min

The evolution of the acoustic attenuation spectra throughout the crystallization at different cooling rates is presented in Figures 6.7, 6.8 and 6.9. Some oscillations were observed in the spectra, which cannot be adjusted through the measurement strategy modification. The data inversion made accuracy low due to the oscillations which were caused by the high cooling rate and wide crystallization temperature range.

The cooling rate of the crystallization had two main effects on the acoustic measurement, which was based on the background liquid and the suspended phase, respectively.

The background solution attenuation increases with decreasing the solution temperature, and the increase of the attenuation is larger for high frequency points. This relationship is presented in Figure 6.10.

In the copper sulphate case, the attenuation of copper sulphate solution with a concentration of 45.7893 w% increased 44.22 dB/inch at 110 MHz as the solution temperature decreased to 5.5 °C.

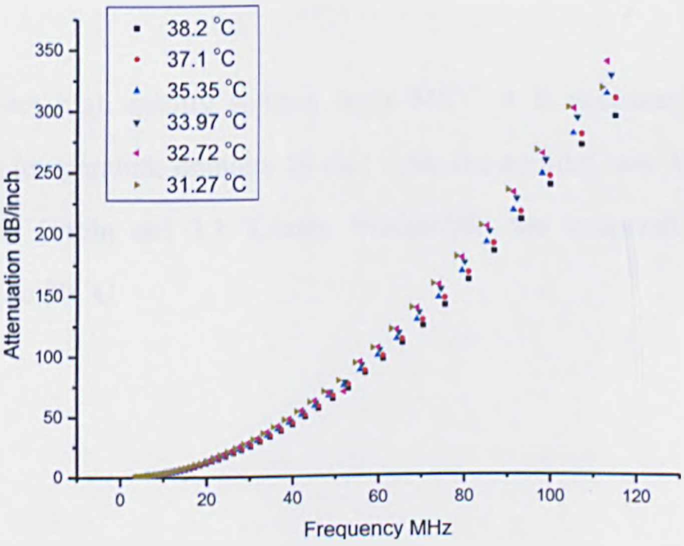

Figure 6.10: Attenuation changing with temperature of copper sulphate solution at a concentration of 45.7893 w%

When a high cooling rate of 0.5 °C/min was used, the solution cooled down to 5.5°C in 11 minutes. 44.22 dB/inch changing was introduced for the background attenuation at a frequency of 110 MHz. The time interval can only be used 2 – 3 times for measurements, as one typical MSV measurement needed around 4 minutes. That means there was 10 – 20 dB/inch changing of the attenuation for each measurement in this case. It is very hard to modify of the measurement strategy as the background changed too fast.

Another effect of cooling rate is on the crystallization dynamic performance. Higher cooling rates generate supersaturation quicker. Larger MSZW is introduced because of the higher supersaturation when the crystallization starts. Higher supersaturation will generate higher nucleation and higher growth rate, which means a dramatic change in the number and the size of the crystals.

A wide crystallization temperature domain is the second issue caused the oscillations of the spectra. The crystals grew along the crystallization, larger temperature domain supply more energy for crystals growth. When the diameter of the crystal is larger than the minimum limit of the transducer position, the acoustic spectrum will fail to collect.

In order to collect high quality spectra from MSV, it is necessary to reduce the cooling rate and temperature domain. In this case, the cooling rate was decreased to 0.1 °C/min, 0.15 °C/min and 0.2 °C/min. Meanwhile, the temperature domain was reduced from 30 to 20 °C.

6.3.2 High quality spectra collection from low cooling rate

New crystallization experiments were set up for the acoustic attenuation measurement. The solution prepared still had a concentration of 45.7892 w%. The solution was heated up to 40 °C, and kept at that temperature over 1 hour to make sure the crystals were entirely dissolved in the solution. Thereafter, the solution was cooled down to 20°C under cooling rate of 0.1 °C/min, 0.15 °C/min and 0.2 °C/min, respectively. The acoustic spectra were collected by MSV during the crystallization process.

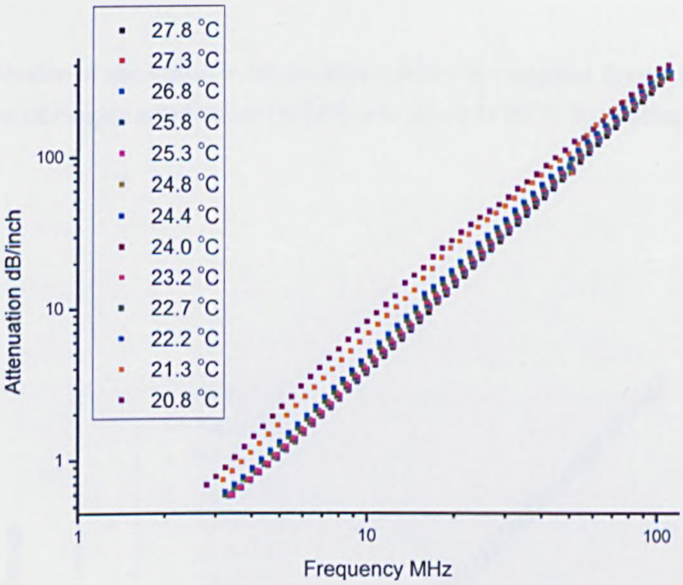

Figure 6.11: Evolution of the acoustic attenuation spectra throughout the crystallization of an aqueous solution of copper sulphate at 45.7893 w% down to 20 °C by cooling at 0.1 °C/min

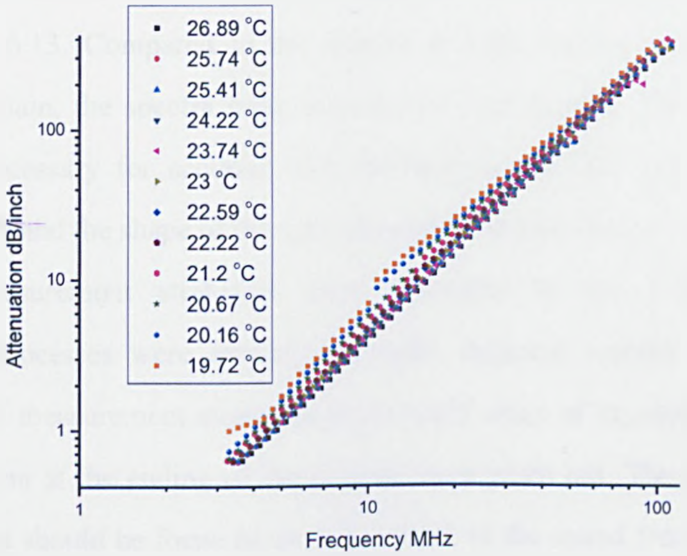

Figure 6.12: Evolution of the acoustic attenuation spectra throughout the crystallization of an aqueous solution of copper sulphate at 45.7893 w% down to 20 °C by cooling at 0.15 °C/min

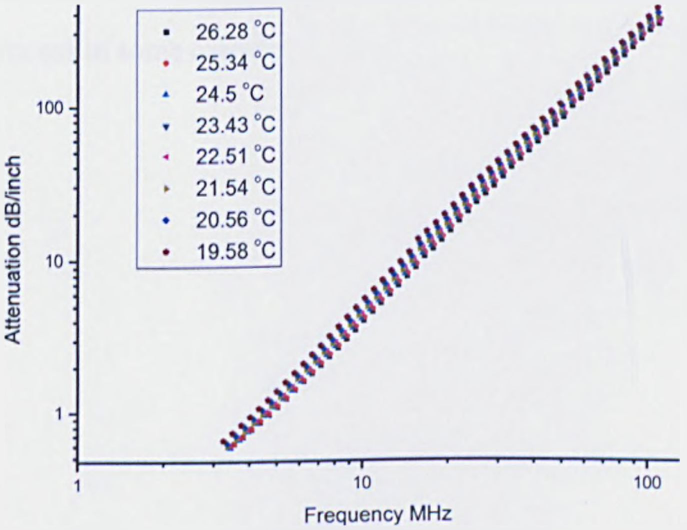

Figure 6.13: Evolution of the acoustic attenuation spectra throughout the crystallization of an aqueous solution of copper sulphate at 45.7893 w% down to 20 °C by cooling at 0.2 °C/min

The spectra collected from the crystallization processes are presented in the Figures 6.11, 6.12 and 6.13. Compared to the spectra at high cooling rates with a wide temperature domain, the spectra were smooth and high quality. These high quality spectra were necessary for accurate size information analysis. The switch of the attenuation value and the shape of the spectra predict the size change of the particles.

The MSV measurement strategies were presented in the Table 6.13. The crystallization processes were carried out under different cooling rate, for each cooling rate, the measurement strategies at the early stage of crystallization and the final measurement at the ending of the process were given out. The modification of the measurement should be focus on the adjustment of the sound frequency selection on the boundary of the sub-channels. This would be influent by the particle size and particle volume suspended in the solution. Different cooling rate would generate different supersaturation level, which will bring the different nucleation and crystal growth phenomenon, and the transducer passing length and passing space should be slightly different. In order to reduce the effect of the particle on the spectra, more sub-channels were used to enhance the accurate of the spectra in the ending of the crystallization process in some cases

Table 6.13: MSV measurement strategies for the crystallization processes under different cooling rates

0.1 cooling rate at 27.3°C	Min Freq MHz	Max Freq MHz		% of Freqs	Position 1 inch	Position 2 inch
Channel 1 Low Freq	3.4	14.8		43	0.1	4
Channel 1 high Freq						
Channel 2 Low Freq	15.3	51.1		35	0.04	0.63
Channel 2 high Freq	53	111.3		22	0.03	0.09
0.1 cooling rate at 20.8°C	Min Freq MHz	Max Freq MHz		% of Freqs	Position 1 inch	Position 2 inch
Channel 1 Low Freq	2.8	12.4		41	0.1	4
Channel 1 high Freq	12.9	16.7		8	0.1	0.38
Channel 2 Low Freq	17.3	52.6		31	0.04	0.27
Channel 2 high Freq	54.6	110.3		20	0.03	0.08
0.15 cooling rate at 26.8°C	Min Freq MHz	Max Freq MHz		% of Freqs	Position 1 inch	Position 2 inch
Channel 1 Low Freq	5	16.2		43	0.05	4
Channel 1 high Freq						
Channel 2 Low Freq	16.7	38.6		31	0.03	1.1
Channel 2 high Freq	39.7	80		26	0.03	0.35
0.15 cooling rate at 19.7°C	Min Freq MHz	Max Freq MHz		% of Freqs	Position 1 inch	Position 2 inch
Channel 1 Low Freq	3.3	9.9		33	0.03	4
Channel 1 high Freq						
Channel 2 Low Freq	10.3	38.1		39	0.04	0.58
Channel 2 high Freq	39.4	100		28	0.03	0.09
0.2 cooling rate at 26.2°C	Min Freq MHz	Max Freq MHz		% of Freqs	Position 1 inch	Position 2 inch
Channel 1 Low Freq	3.4	15.1		43	0.1	4
Channel 1 high Freq						
Channel 2 Low Freq	15.6	51.4		35	0.04	0.62
Channel 2 high Freq	53.3	111.3		22	0.03	0.09
0.2 cooling rate at 19.5°C	Min Freq MHz	Max Freq MHz		% of Freqs	Position 1 inch	Position 2 inch
Channel 1 Low Freq	3.3	9.6		33	0.1	4
Channel 1 high Freq						
Channel 2 Low Freq	9.9	40.4		43	0.04	0.59
Channel 2 high Freq	41.8	90		24	0.03	0.09

6.4 Kinetics analysis during crystallization

Table 6.14: Particle size distribution parameters evolution of copper sulphate crystallization at 0.1°C/min

Time min	T °C	C_v v%	C w%	Solubility w%	Supersaturation	D50 µm	G µm/s
0	27.8	0.22	45.28	43.99	0.0293	9.10	
5	27.3	0.47	44.71	43.54	0.0269	18.30	3.07×10^{-2}
10	26.8	0.66	44.28	43.09	0.0275	31.20	4.30×10^{-2}
15	26.4	0.85	43.85	42.74	0.0259	38.70	2.50×10^{-2}
20	25.8	1.10	43.28	42.25	0.0242	46.00	2.43×10^{-2}
25	25.3	1.37	42.66	41.78	0.0209	50.84	1.61×10^{-2}
30	24.8	1.53	42.30	41.36	0.0226	55.68	1.61×10^{-2}
35	24.4	1.68	41.95	41.02	0.0226	59.31	1.21×10^{-2}
40	24.0	1.90	41.45	40.69	0.0187	61.74	8.10×10^{-3}
46	23.2	2.11	40.97	40.03	0.0235	65.20	9.61×10^{-3}
51	22.7	2.38	40.36	39.63	0.0184	67.40	7.33×10^{-3}
61	22.2	2.80	39.40	39.24	0.0040	69.30	3.17×10^{-3}
71	21.3	3.09	38.74	38.57	0.0043	69.60	5.00×10^{-3}
77	20.8	3.27	38.33	38.13	0.0051	71.20	4.44×10^{-3}

Table 6.15: Particle size distribution parameters evolution of copper sulphate crystallization at 0.15°C/min

Time min	T °C	C_v v%	C w%	Solubility w%	Supersaturation	D50 µm	G µm/s
0	26.8	0.42	44.83	43.17	0.0383	10.28	
6	25.7	0.91	43.71	42.16	0.0366	28.67	5.11×10^{-2}
11	25.4	1.24	42.96	41.88	0.0257	35.36	2.23×10^{-2}
21	24.2	1.67	41.98	40.87	0.0270	48.02	2.11×10^{-2}
25	23.7	1.94	41.36	40.47	0.0219	50.93	1.21×10^{-2}
31	23.0	2.20	40.77	39.87	0.0225	55.35	1.23×10^{-2}
35	22.5	2.38	40.36	39.54	0.0207	57.90	1.06×10^{-2}
38	22.2	2.70	39.63	39.24	0.0098	58.87	5.40×10^{-3}
46	21.2	2.87	39.24	38.44	0.0209	65.11	1.30×10^{-2}
50	20.6	3.23	38.42	38.03	0.0103	66.17	4.40×10^{-3}
53	20.1	3.42	37.99	37.63	0.0093	66.74	3.20×10^{-3}
57	19.7	3.56	37.67	37.30	0.0099	67.97	5.10×10^{-3}

Table 6.16: Particle size distribution parameters evolution of copper sulphate crystallization at 0.2°C/min

Time min	T °C	C_v v%	C w%	Solubility w%	Supersaturation	D50 µm	G µm/s
0	26.2	0.12	45.51	42.63	0.0674	1	
6	25.3	0.96	43.60	41.82	0.0424	30.52	8.20×10^{-2}
12	24.5	1.50	42.36	41.11	0.0305	39.73	2.56×10^{-2}
18	23.4	1.93	41.38	40.22	0.0289	47.65	2.20×10^{-2}
23	22.5	2.20	40.77	39.47	0.0327	57.58	3.31×10^{-2}
29	21.5	2.59	39.88	38.70	0.0303	67.48	2.75×10^{-2}
35	20.5	3.09	38.74	37.94	0.0210	73.24	1.60×10^{-2}
41	19.5	3.49	37.83	37.19	0.0170	75.04	5.00×10^{-3}

The particle size distribution parameters are listed in Tables 6.14, 6.15 and 6.16. The mean particle size D50 and suspended particle volume percentage were analyzed from the spectra using MSV. The solution concentration C is calculated from the suspended particle volume:

$$C = C_0 - \rho_S C_v \tag{6.4}$$

where C is the solution concentration in w%, C_0 is the initial solution concentration in w%, ρ_s is the density of copper sulphate pentahydrate solid in g/cm^3, and C_v is the suspended particle volume percentage.

The supersaturation used here is relative supersaturation, σ, according to Equation 2.11 in Chapter 2.

The overall growth rate was calculated from the change of the D50 and the time.

$$G = \frac{D50_2 - D50_1}{t_2 - t_1} \tag{6.5}$$

where G is the overall growth rate in m/s, D50 is the mean particle size in μm, and t is the time in s

The growth kinetics can be revealed depending on Nyvlt's empirical expressions [142]

$$G = k_g \sigma^g \tag{6.6}$$

where k_g is the growth rate constant and g is the overall growth order

The picture of the final product (copper sulphate pentahydrate crystals) captured by microscopy is shown in Figure 6.14 and the evolution of the crystal size distribution (diameter) at 0.1 °C/min cooling rate is presented in Figure 6.15. Mono-model distribution is selected for the straightforward presentation of the growth of the crystals. The size of the particle estimated from the micrograph shows the good agreement with MSV results. The change of the crystal size along with the time at 0.15 °C/min cooling rate is presented in Figure 6.16. The particle mean size D50 is used to describe the evaluation of the crystal size. The slope of the change decrease with time, which means the growth rate is reduced. The driving force of the growth of the crystals is the supersaturation, which is the difference between the solution concentration and the solubility at the measurement temperature point. The solution concentration change versus solubility with the time for 0.15 cooling crystallization is shown in Figure 6.17. The reduction difference between the solution concentration and the solubility can be observed. High consumption of the supersaturation was caused by the nucleation and crystal growth taking place at the same time especially at the initial stage of the crystallization process. This can also be found in the schematic diagram of the crystallization process in Figure 6.18. From point A to point B, the supersaturation is generated due to the cooling down of the solution. Point B was the starting point of the crystallization process as the supersaturation level is high enough for the homogeneous crystallization to occur. Thereafter, the supersaturation was consumed quickly by the nucleation and the crystal growth. When the solution concentration was close to the solubility, such as at point C, the supersaturation was not high enough to generate new nuclei. The small supersaturation supplies the crystal growth, and eventually the relative supersaturation will keep constant very close to 0.

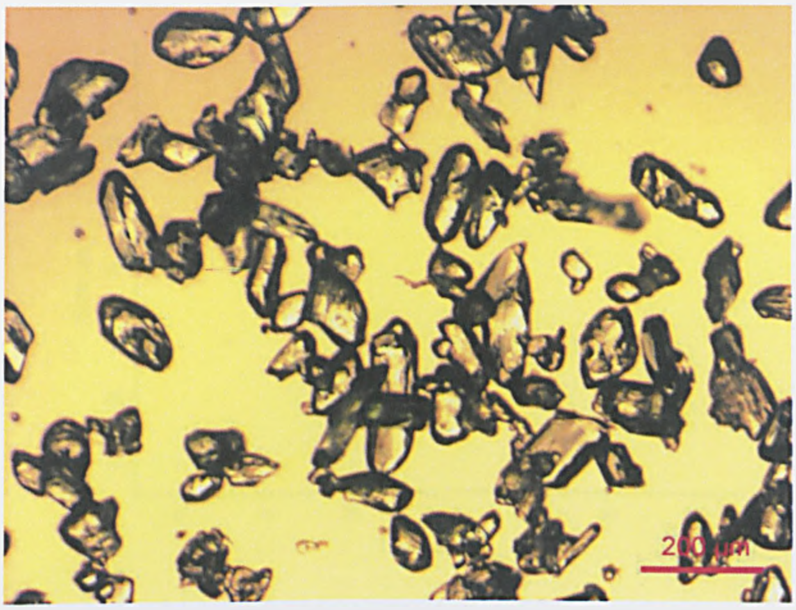

Figure 6.14: Final products of crystallization of an aqueous solution of copper sulphate at 45.7893 w% down to 20 °C by cooling at 0.1 °C/min

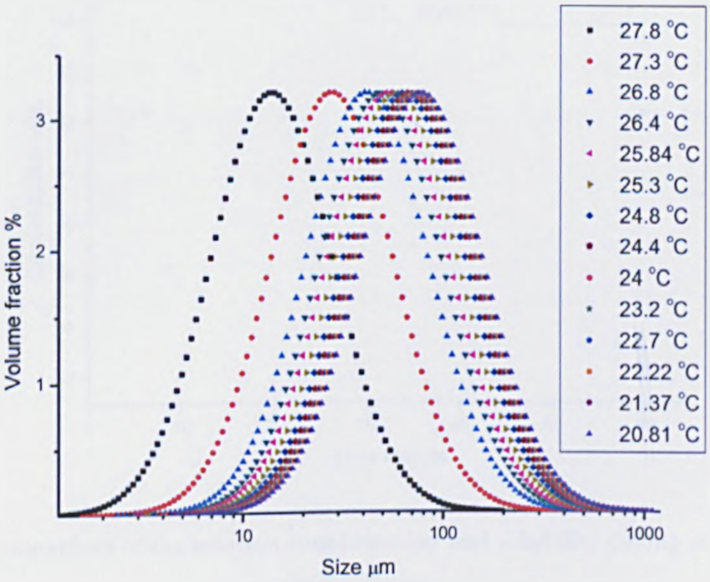

Figure 6.15: Particle size distribution evolution through the crystallization of an aqueous solution of copper sulphate at 45.7893 w% down to 20 °C by cooling at 0.1°C/min

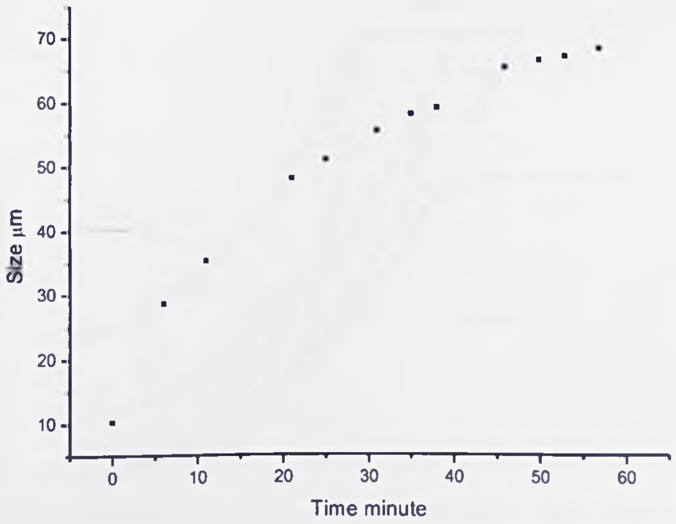

Figure 6.16: Mean particle size evolution during the crystallization at 0.15 °C/min

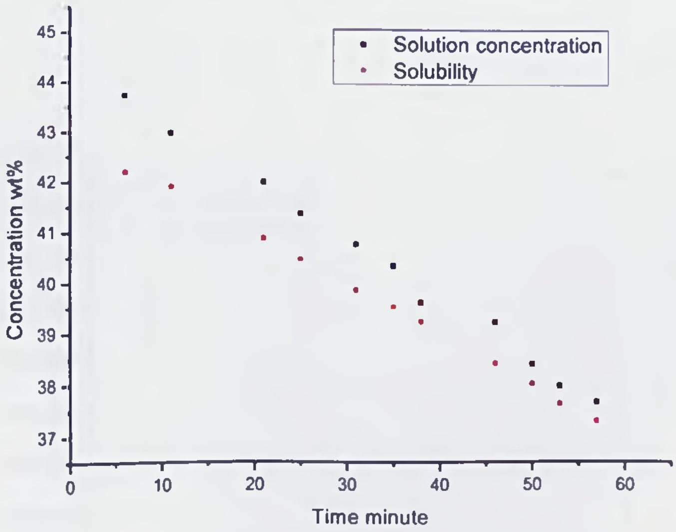

Figure 6.17: Comparison of the solution concentration and solubility during crystallization at 0.15 °C/min

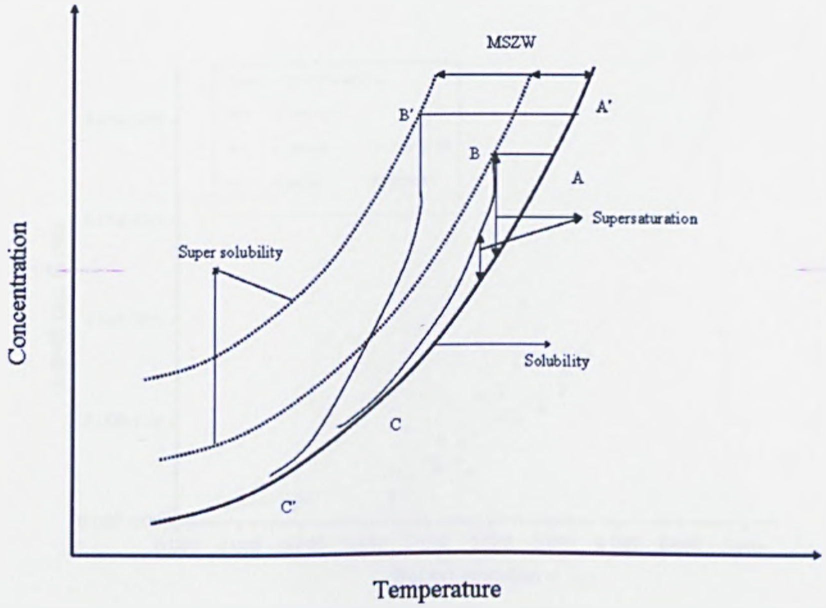

Figure 6.18: Schematic diagram of the crystallization process under different cooling rates

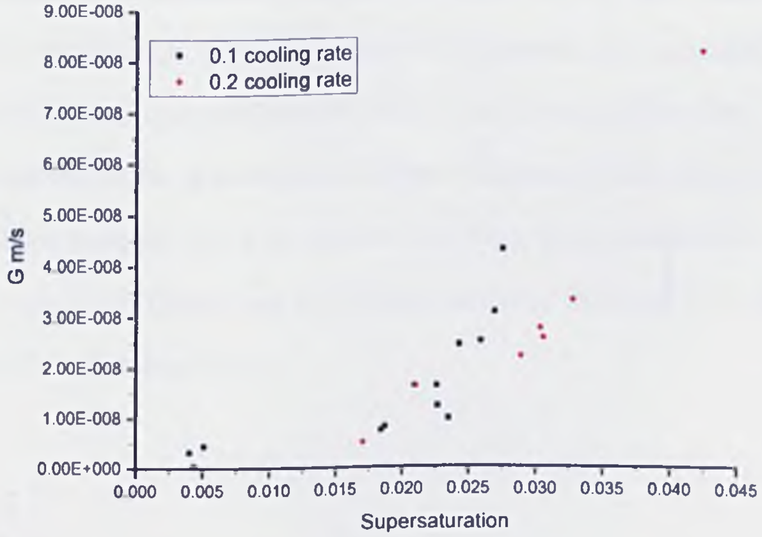

Figure 6.19: Comparison of crystal growth kinetics under different cooling rates of copper sulphate pentahydrate crystallization

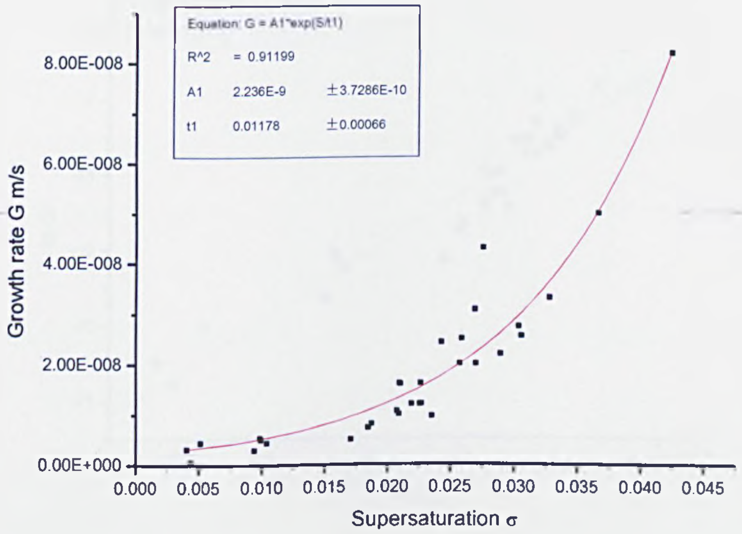

Figure 6.20: Fit of growth rate with supersaturation based on the crystallization experiments at 0.1 °C/min, 0.15 °C/min and 0.2 °C/min

Another phenomenon which can be seen in Figure 6.18 is the metastable zone width which increases as the cooling rate increases. The larger metastable zone width supplies a higher supersaturation level and a wider growth rate exists for the high cooling rate crystallization process. Figure 6.19 presents this explanation from the experiment of 0.1 cooling crystallization and 0.2 cooling crystallization.

The kinetic analysis of the growth rate of copper sulphate pentahydrate crystallization can be calculated from the fit of the growth data from the crystallization experiments under 0.1 °C/min, 0.15 °C/min and 0.2 °C/min presented in Figure 6.19. The R square of the fitting of the function is 0.91

$$G = A_1 \exp\left(\frac{\sigma}{t_1}\right) \tag{6.7}$$

where G is the linear growth rate of copper sulphate pentahydrate in m/s, σ *is the relative supersaturation.* A_1 *and* t_1 *are the growth rate coefficients,* A_1 *is equal to* 2.236×10^{-9} *and* t_1 *is equal to 0.01178, respectively.*

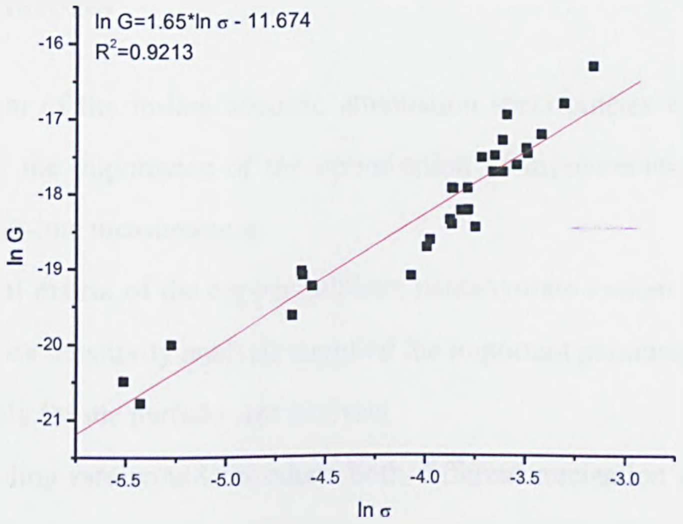

Figure 6.21: Relationship of overall growth rate with relative supersaturation (log-log scale)

The overall crystal growth rates measured under different relative supersaturation values (Figure 6.20) track the growth of copper sulphate pentahydrate crystals. In the low supersaturation region, the crystals grow very slowly. When the supersaturation increases over a critical point, the crystals grow much faster. This phenomenon fits the screw dislocation model well.

If using logarithmic scale for the overall growth rate and relative supersaturation in Figure 6.20, a linear fit could present the crystal growth kinetics shown in Figure 6.21. It is clear to see the overall growth order g (Equation 6.6) of copper sulphate pentahydrate system during the measurement is equal to 1.65. This value, determined by the acoustic spectroscopy, is very close to the reference data which is in the range of 1.2 to 1.8 depending on the various experimental conditions [41, 169-173]

6.5 Conclusions

The measurement of the in-line acoustic attenuation spectrometer was described in this chapter and the importance of the optimisation of measurement condition was emphasized for in-line measurement.

The new physical matrix of the copper sulphate pentahydrate system was set up. The physical properties sensitivity analysis supplied the important parameters needed to be modified carefully for the particle size analysis.

Because the cooling rate would introduce both different nucleation and growth, the particle volume and particle size distribution would be different for these dynamic processes with different cooling rate. The measurement strategies were monitored and modified to create a smooth spectrum according to the quality of last spectrum during measurement. Good spectra through the whole process were collected from the experiments using manually optimized measurement strategy. Good quality spectra determined the precision of the results of the particle size analysis.

The acoustic spectra were analyzed by MSV depending on the ECAH model, and the overall growth kinetics were calculated from the mean particle size and suspended particle volume measurements. The results had good quality and very similar to the reference data on the crystal growth kinetic research of copper sulphate pentahydrate.

Chapter 7 Benchmarking the Ultrasonic Velocity Technique on the Crystallization of Copper Sulphate Pentahydrate

Summary

This chapter presents the measurements of ultrasound velocity in the homogeneous and heterogeneous media. The new model of on-line determination of particle volume concentration based on the sound velocity measurement is developed.

7.1 Introduction

In this chapter, the acoustic velocity measurement was completed using different kinds of acoustic instrument. The accuracy of sound speed measurements from MSV was verified by the ResoScan. The bulk viscosity of the copper sulphate solution and distillated water were calculated based on the Navier-Stokes equation. The sound velocity evolution during the copper sulphate pentahydrate crystallization process was measured using the UVM which predicts the adiabatic compressibility of copper sulphate pentahydrate crystal, and validates the modified Urick equation by using the extermination of the crystal volume in the crystallization system depending on the sound velocity.

7.2 Study of the relationship between solute concentration and sound velocity

7.2.1 Calibration of sound velocity measured by MSV

Besides the sound attenuation, the acoustic spectrometer MSV supplied the sound velocity data simultaneously for each measurement. In order to check the accuracy of the sound velocity from MSV, a series of different experiments, under different conditions were completed. The results were compared with the standard sound velocity instrument ResoScan system. The solute concentration and temperature effects on the sound velocity were both considered, sound velocity was collected at different temperatures and different solute concentrations.

The velocity measurement by MSV is a time-of-flight measurement on a burst of pseudo-continuous ‘single’ frequency signal. A typical velocity spectrum measured by MSV for the saturated copper sulphate solution (45 w%)fixed at 30 °C is presented in Figure 7.1, several frequency points are used to measure the sound velocity. The average value from different frequencies is output as the measured velocity value.

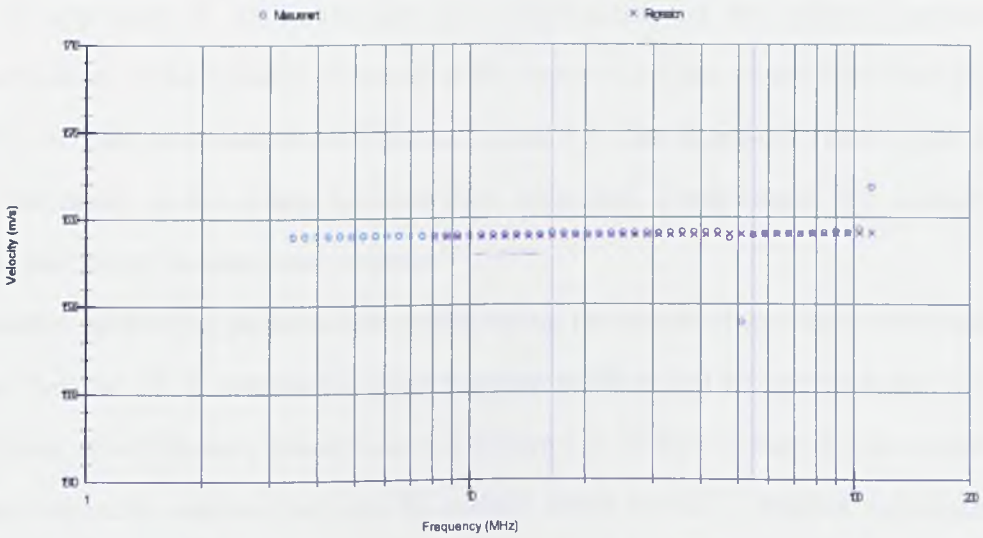

Figure 7.1: The velocity spectrum measured from MSV of 45 w% copper sulphate solution at 30°C

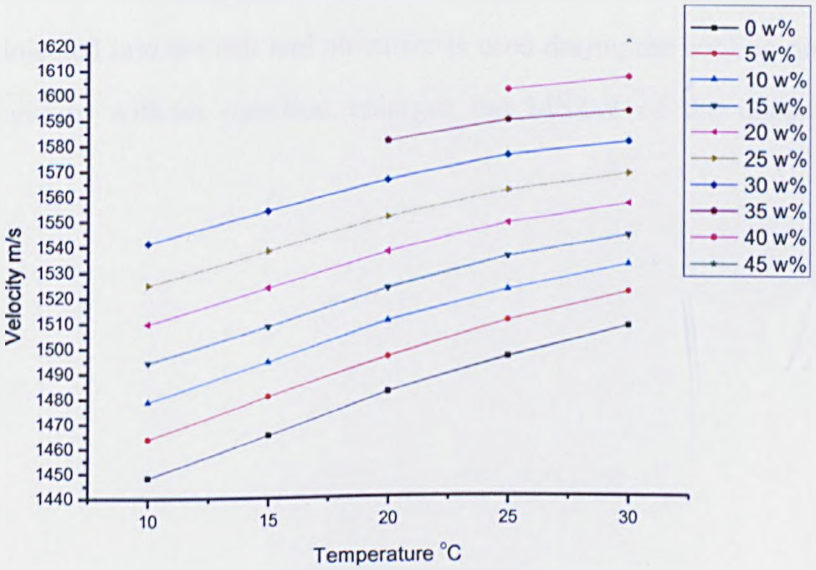

Figure 7.2: Sound velocity measurements under different solute concentrations and different temperatures using MSV

It is important to be aware that the temperature and the solute concentration coefficients of the velocity of sound in the copper sulphate solution are both positive from the data presented in the Figures 7.2 and 7.3. The change of velocity per degree C decreased as the solute concentration increased. Furthermore, the change also deceases as the temperature increases.

Another interesting phenomenon found during the measurement using the ResoScan was that the 30 °C saturated copper sulphate solution can be cooled down to 25 °C without crystallization, this is shown in Figure 7.3. In the practical measurements, the supersaturated solution can even be cooled down to 10 °C without crystallization, which meant the MSZW was larger than 20 °C, which was much higher than the result of 4 to 5 °C measured in a 1 litre crystallizer. The dependence of the sound velocity on the temperature of the super cooling solution can be expressed by a quadratic fitting, and the R square of the fitting is 99.99%, shown in Figure 7.4. The absence of homogeneous crystallization when using the ResoScan was mainly caused by its sealed cell. The cell of the ResoScan is very tiny that is only 0.2 millilitre. The solution is injected into the cell and no stirrer is used during the cooling process. The cooling condition without agitation enlarges the MSZW of the copper sulphate solution.

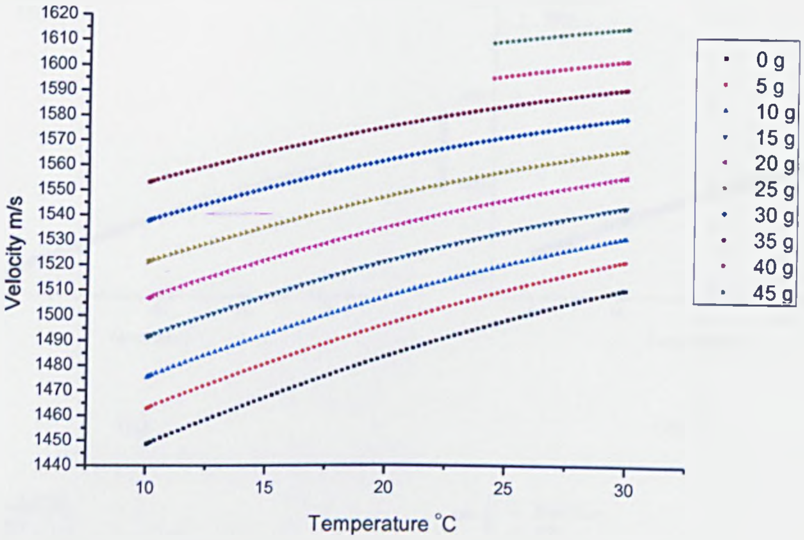

Figure 7.3: Sound velocity measurements under different solute concentrations and different temperatures using ResoScan

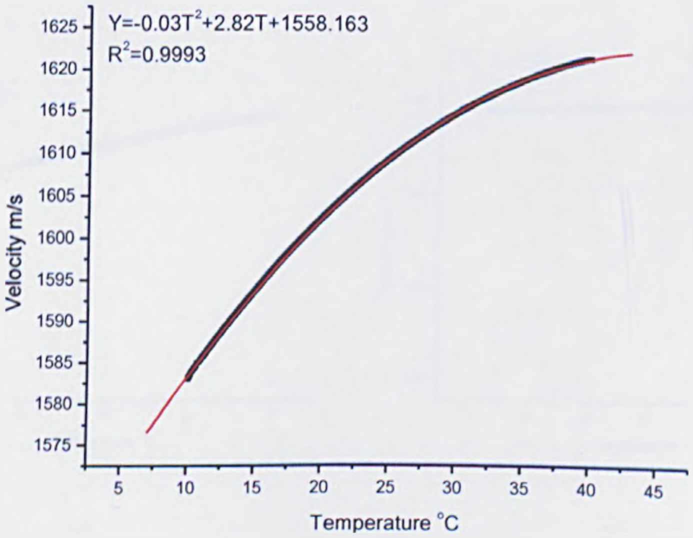

Figure 7.4: Sound velocity measurement of 45 w% copper sulphate solution at temperatures ranging from 30 °C to 10 °C

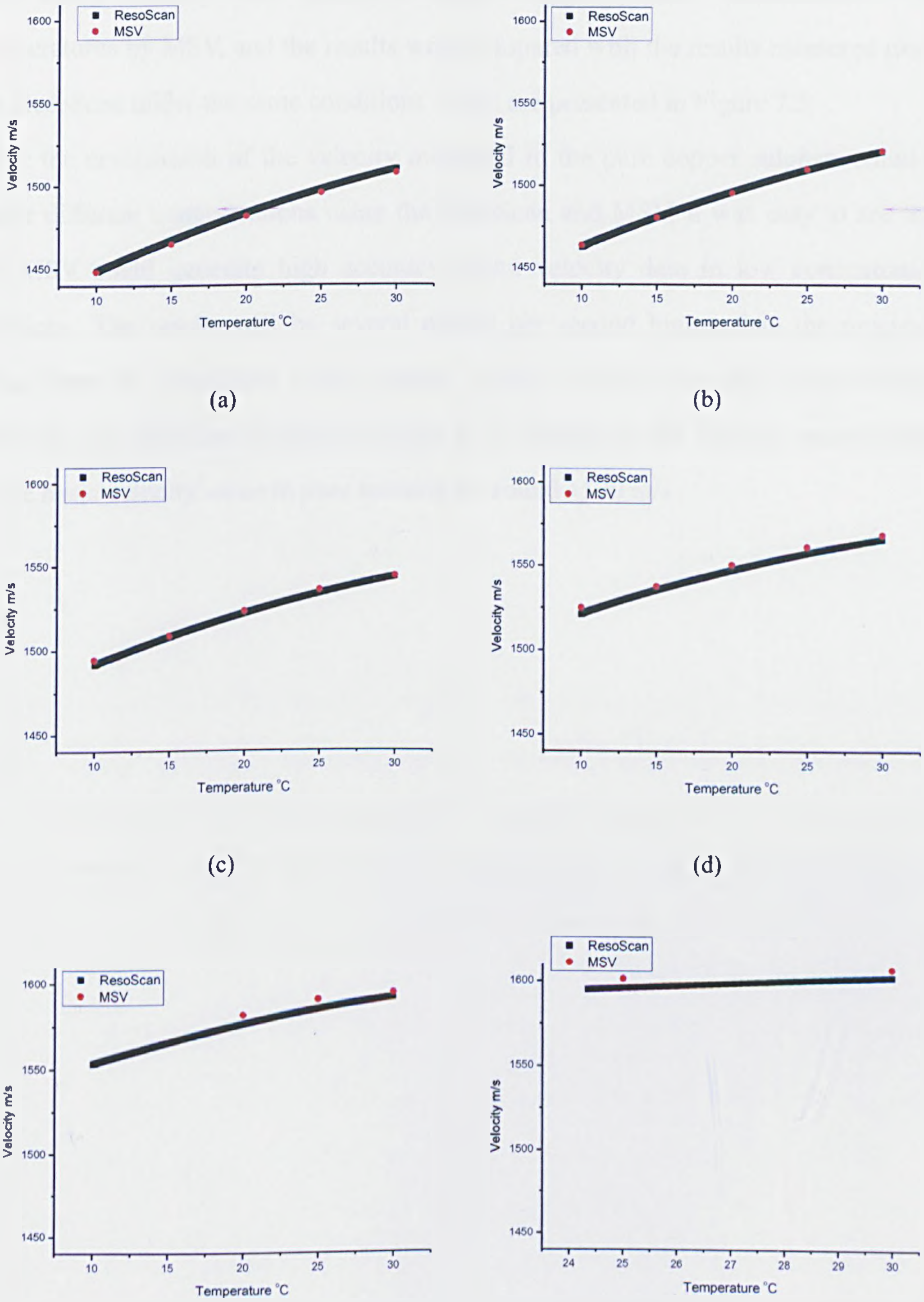

(a) (b)

(c) (d)

(e) (f)

Figure 7.5: Velocity results comparison between the ResoScan and MSV under different solute concentrations(a) is pure water, (b) is 5 w% solution, (c) is 15 w% solution, (d) is 25 w% solution, (e) is 35 w% solution, (f) is 40 w% solution

The sound velocity was measured under different solute concentrations and temperatures by MSV, and the results were compared with the results measured using the ResoScan under the same conditions which are presented in Figure 7.5.

After the comparison of the velocity measured in the pure copper sulphate solution under different concentrations using the ResoScan and MSV, it was easy to see that the MSV could generate high accuracy sound velocity data in low concentration solutions. The results will be several meters per second higher than the precision value from the ResoScan in the copper sulphate solution of high concentration. However, the deviation of several meters is acceptable for the velocity measurement as the basic velocity value in pure solution is around 1500 m/s

7.2.2 Bulk viscosity calculation

The accurate sound velocity measured from MSV in pure copper sulphate solution is very accurate for the calculation of bulk viscosity of the solution. The bulk viscosity is a fundamental parameter in the field of acoustic propagation. It plays an important role in calculating the attenuation of the plane wave propagation through the fluids [174] shown in Equation 3.11. It provides the route to calculate the bulk viscosity by measuring the attenuation and sound speed, assuming the other physical properties of the solution are known. The MSV is validated to offer the sound speed and sound attenuation at the same time, and the bulk viscosity can be calculated by,

$$\mu = \left[\frac{2\alpha \rho \upsilon^3}{\omega^2} - \frac{4\eta}{3} - \frac{(\gamma - 1)\tau}{C_p} \right] \tag{7.1}$$

where μ *is bulk viscosity of the solution,* a *is sound attenuation in the solution,* η *is shear viscosity of the solution,* ω *is angular frequency of the sound,* ρ *is density of the solution,* v *is sound velocity propagation in the solution,* γ *is the ratio of specific heats of solution,* τ *is the thermal conductivity of solution,* C_p *is specific heat of the solution.*

The copper sulphate solution with a concentration of 25 w% was selected to calculate the bulk viscosity. The frequency-dependent attenuation value shown in Figure 7.6 was measured by MSV, and the sound velocity collected simultaneously. The density of the solution was measured using a density and sound analyzer DSA48 (Anton Paar) shown in Figure 7.7, the density at low temperature was extrapolated from the quadratic fitting which had an R square of 98.9 %. The shear viscosity characteristics of aqueous solutions of electrolytes has been investigated by Stokes and Mills [175] and Barry et al. [176]. The estimation of the shear viscosities of solutions was researched by Hu [177].

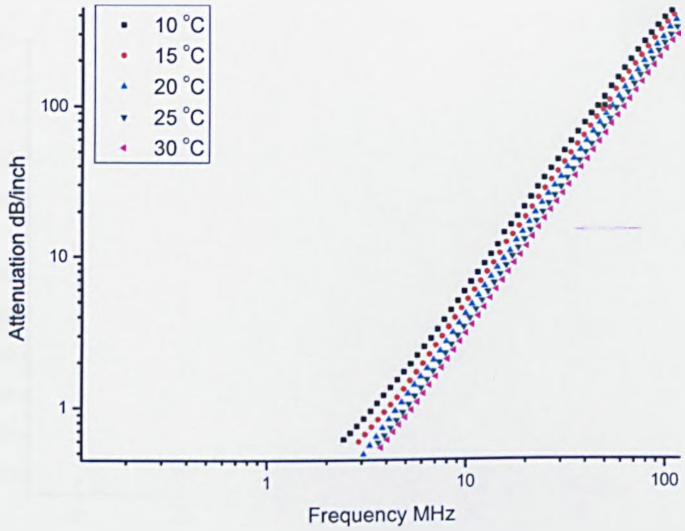

Figure 7.6: Attenuation spectra of copper sulphate solution with 25 w% at different temperatures

The shear viscosity of the solution was quoted from Mougin's previous work[163], and the temperature effect was measured using a rheometer. The thermal conductivity and specific heat of the solution also used the data in Mougin's work. The temperature effect of thermal conductivity and specific heat was eliminated due to the effect being small, and the thermal part $\frac{(\gamma-1)\tau}{C_p}$ for bulk viscosity calculation was quite small compared with the first two terms.

The ratio of specific heats was calculated using Equation 7.2 [75, 178],

$$\gamma = 1 + \frac{T\beta^2 \upsilon^2}{C_p} \tag{7.2}$$

where T is absolute temperature and β is thermal expansion.

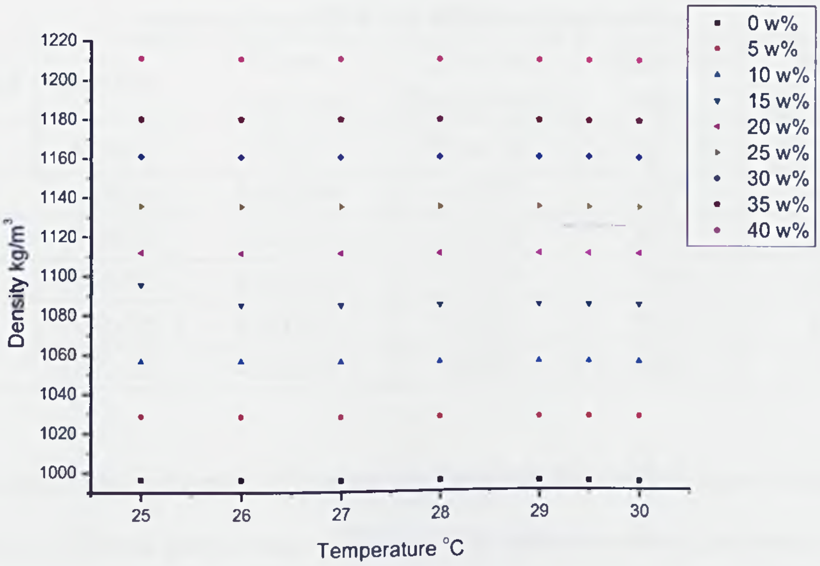

Figure 7.7: Density measurement of copper sulphate solution with different concentrations under different temperatures

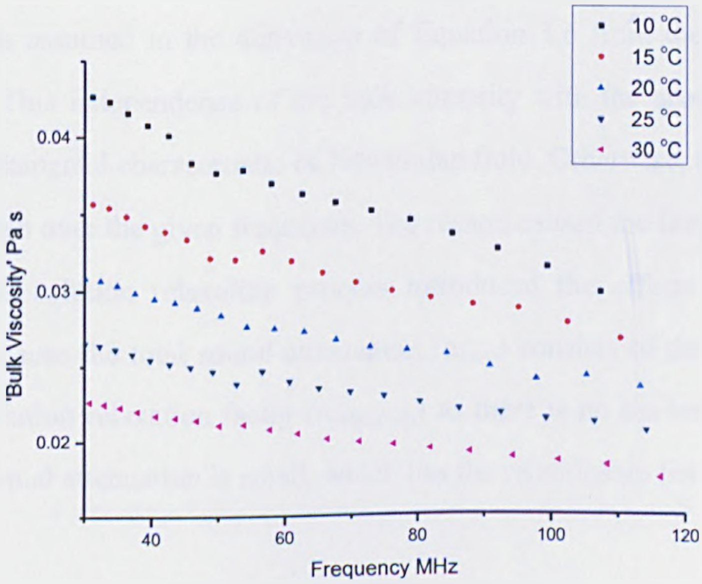

Figure 7.8: Frequency dependent 'bulk viscosity' of copper sulphate solution with a concentration of 25 w% at different temperatures

Table 7.1: Parameters for bulk viscosity calculation of copper sulphate solution with a solute concentration of 25 w% at different temperatures

Temperature	Density	Shear Viscosity	Thermal Conductivity	Specific Heat	Ratio of Specific Heats
°C	kg/m^3	Pa s	W m^{-1} K^{-1}	J kg^{-1} m^{-3}	
10	1114.88	0.00330	0.572	3058	1.0398
15	1108.23	0.00315	0.572	3058	1.0412
20	1098.92	0.00300	0.572	3058	1.0426
25	1086.95	0.00285	0.572	3058	1.0439
30	1072.32	0.00270	0.572	3058	1.0451

The calculated 'bulk viscosity' of copper sulphate solution with a solute concentration of 25 w% at different temperatures (Figure 7.8) showed strong acoustic frequency dependence. The 'bulk viscosity' of the solution decreased as the frequency increased and the changing trend was the same at different temperatures. The variation of the 'bulk viscosity' according to the frequency changing presents that the calculated result is not the real bulk viscosity of the copper sulphate solution. Because a valid application of Equation 3.8 for calculating the bulk viscosity of a particular liquid requires that this bulk viscosity is independent of the ultrasound frequency, since this independence is assumed in the derivation of Equation 3.6 from the Navier-Stokes equation [55]. This independence of the bulk viscosity with the acoustic frequency reveals the fundamental characteristic of Newtonian fluid. Otherwise, the given liquid is non-Newtonian over the given frequency. The reason caused the false measurement was due to the solution relaxation process introduced the effects on the sound attenuation. Because the total sound attenuation (α_{total}) consists of the viscous factor ($\alpha_{viscous}$) and solution relaxation factor ($\alpha_{relaxation}$) as there is no scattering in the pure solvent and thermal attenuation is small, which has the relationship listed below [64]:

$$\alpha_{totoal} = \alpha_{relaxation} + \alpha_{viscous} = a_0 f + a_1 f^2 \tag{7.3}$$

where a_0 and a_1 are the attenuation constant for relaxation attenuation and viscous attenuation, respectively, f is the sound frequency.

The relaxation attenuation can be eliminated from the total attenuation from the regression equation of the attenuation spectra at different temperatures (Figure 7.6). The relationship between the total attenuation and sound frequency can be expressed by a polynomial equation with the order equal to 2, and the intercept was set to be 0, which has the same form as Equation 7.3. The quadratic term presents the contribution from the viscous attenuation, whereas the monomial term comes from the solution relaxation. Thus, the viscous attenuation can be calculated by subtracting the relaxation attenuation from the total attenuation.

After eliminating the relaxation factor, the total sound attenuation is only contributed by the viscous attenuation, and the bulk viscosity results of the copper sulphate pentahydrate with concentration of 25 w% at different temperatures was calculated using Equation 7.1 and shown in Figure 7.9

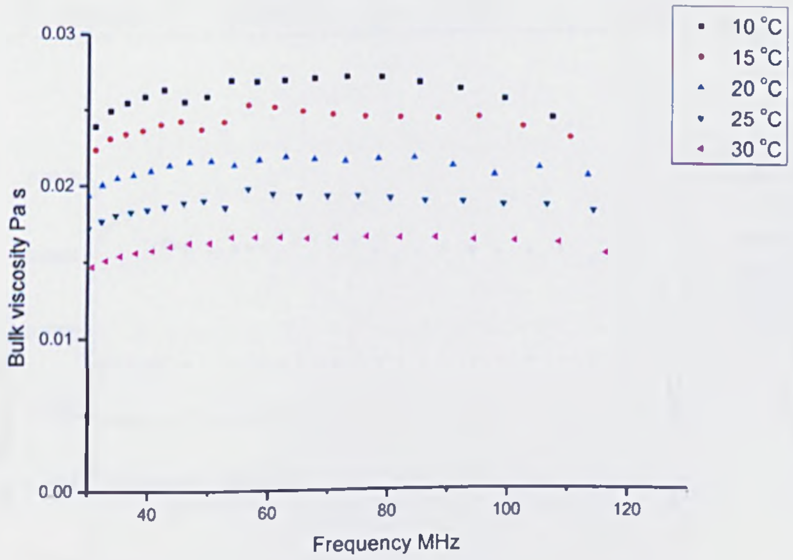

Figure 7.9: Frequency dependent bulk viscosity of copper sulphate solution with concentration 25 w% under different temperature

The bulk viscosity value presented in Figure 7.9 is clearly constant at different sound frequencies, and the quality of the calculation is influenced by the accuracy of the relaxation attenuation calculation.

In order to verify the calculation of bulk viscosity using acoustic attenuation spectroscopy, the classic Newtonian fluid, i.e., the distilled water, was selected to measure the bulk viscosity using the same procedure of copper sulphate solution measurement. The density of water at different temperatures was measured using DSA48 (Anton Paar), the acoustic attenuation and velocity value were measured by MSV simultaneously, the shear viscosity and the thermal parameters of water were taken from the handbook [179]. The parameters are presented in Table 7.2, and the calculated bulk viscosity of water is shown in Figure 7.10.

Table 7.2: Parameters for bulk viscosity calculation of distilled water at different temperatures

Temperature	Density	Shear Viscosity	Thermal Conductivity	Specific Heat	Ratio of Specific Heats
°C	kg/m^3	Pa s	$W\ m^{-1}\ K^{-1}$	$J\ kg^{-1}\ m^{-3}$	
10	999.58	0.00131	0.58	4192.1	1.0094
15	998.63	0.00114	0.59	4187.0	1.0098
20	997.53	0.00103	0.60	4183.1	1.0102
25	996.39	0.00089	0.61	4180.1	1.0105
30	993.86	0.00082	0.62	4179.5	1.0109

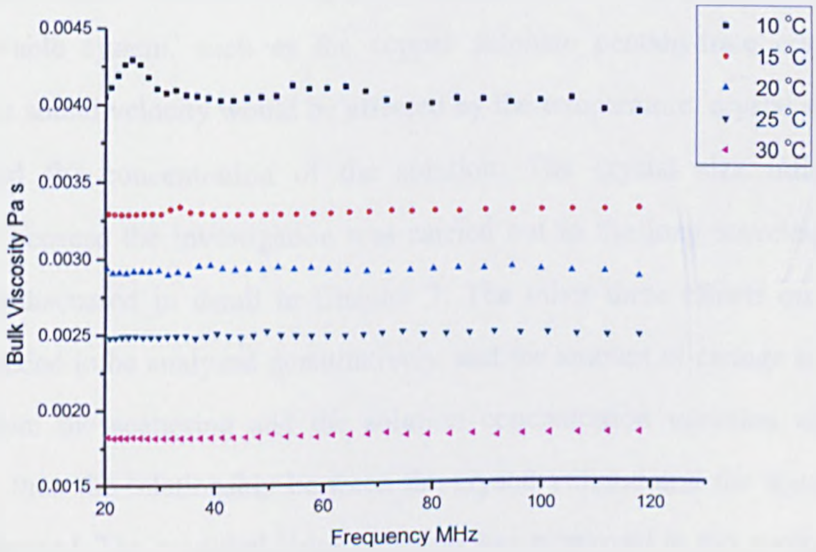

Figure 7.10: Frequency dependent bulk viscosity of distilled water at different temperatures

It is clear to see that the bulk viscosity of water is independent of the acoustic frequency used. The quality of the bulk viscosity result is determined by the quality of the attenuation spectrum. Because the attenuation of the distilled water is quite low, especially in the low frequency range, the quality of the spectrum at low frequencies is hard to control, and the frequencies below 20 MHz was not used in the bulk viscosity calculation. However, the bulk viscosities calculated under different frequencies clearly keep a constant value at different temperatures, and these bulk viscosity values fit the literature data [174, 180, 181].

7.3 Sound velocity measurement in particulate system

The existing scattering models include the solid fat content model and the modified Urick model depending on the sound velocity measurement applied in the particulate system have been developed by Povey et al. Both of these models were mainly employed in the oil in water system, although the solid fat content model was used to investigate the kinetics of crystallization in solid and liquid mineral droplets [117-119]. It is not easy to apply it directly in the dissolvable system due to the solution concentration change during crystallization. For the crystallization process of the dissolvable system, such as the copper sulphate pentahydrate crystallization process, the sound velocity would be affected by the temperature, crystal size, crystal volume and the concentration of the solution. The crystal size influence was eliminated because the investigation was carried out in the long wavelength region which was discussed in detail in Chapter 3. The other three effects on the sound velocity needed to be analyzed quantitatively, and the amount of change in the sound velocity from the scattering and the solution concentration variation needs to be calculated, then the relationship between the crystal volume and the sound velocity can be addressed. The modified Urick equation was employed in this project due to it including the calculation of the effect of scattering on the sound velocity.

7.3.1 Determination of adiabatic compressibility of solid copper sulphate pentahydrate crystal

Before using the modified Urick equation to calculate the compressibility of the solid copper sulphate pentahydrate crystals suspended in the copper sulphate solution during the crystallization, the equation for the copper sulphate system needed to be validated.

The prepared 30 °C saturated copper sulphate solution was heated up to 40 °C in a beaker and the temperature was kept constant for over one hour to make sure the crystals were all dissolved in the solution. After that, the solution was transferred to the UVM and fast cooled down to 28 °C and kept at that constantly. The stirrer speed was fixed at 300 rpm in order that the solution was well agitated and no disturbance introduce to the UVM transducer. The crystals were filtrated out and the mass weighed during the crystallization process. The experiments were repeated multiple times, but stopped at different points. This allowed different amount of copper sulphate pentahydrate crystal comes out from the mother solution. The adiabatic compressibility of the crystal can be calculated by the modified Urick equation (Equitation 3.29). The accuracy of the calculation of the solid compressibility can be validated by comparing the value of the solids which come from different experiments. The sound velocity measurement of the supersaturation copper sulphate solution was demonstrated in Figure 7.11, which the experiment was carried out at 28 °C. The time scale was divided into 4 regions. In cooling region A, the solution was fast cooled down from 40 °C to 28 °C to prepare the supersaturation solution, which is the same method as the induction time measurements experiments stated in Chapter 5. There were no crystals in the solution, which can be verified by comparing the velocity value to the pure solution velocity data shown in Figure 7.4. After region A, the solution temperature was kept constant at 28 °C, and region B was the induction region for this homogenous crystallization process. Region C was the crystallization step, the velocity decreased as the amount of the crystals increased. After all the crystals came out from the solution, the sound velocity was kept constant again. The sound velocity changing in Region C was used to calculate the crystals compressibility depending on the modified Urick model.

It was hard to measure the velocity in the continuous phase after filtration of the crystals from the solution. Because Region C is the crystallization process which is a dynamic process, the amount and size of the crystals changed with time. The crystal weight was stable and could be measured accurately after separating from the solution. However, the solution concentration varied after some disturbance of the temperature during the filtration. The continuous phase velocity in the calculation is then quoted from the relationship between sound velocity and solution concentration of pure solution without temperature effects, as presented in Figure 7.12, as the weight of the crystals was known. For instance, the mass of the flitted crystals was 1.1 g as 60 g water used as the solvent for the experiment carried out at 28 °C, which was quite fit the solubility data shown in Figure 5.4.

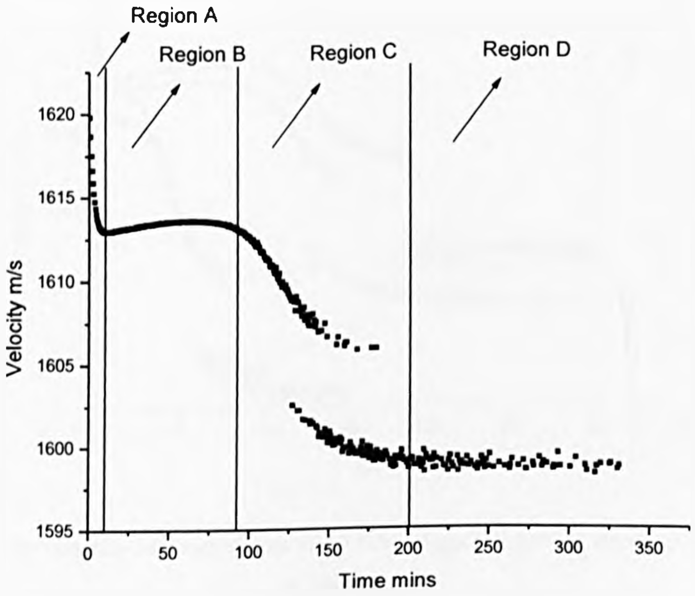

Figure 7.11: Sound velocity measurement of 45 w% copper sulphate solution at a fixed temperature of 28 °C

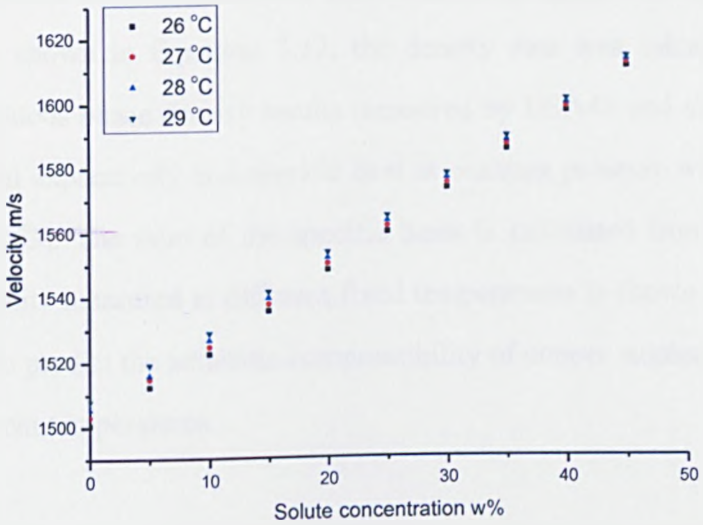

Figure 7.12: Velocity change of copper sulphate solution of different solute concentrations at different temperatures

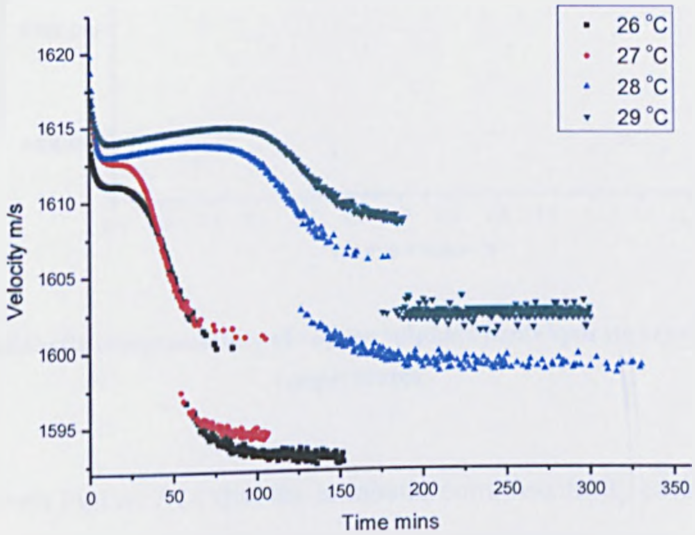

Figure 7.13: Sound velocity measurement of 45 w% copper sulphate solution at different fixed temperature

According to the modified Urick equation presented in Equation 3.29, the adiabatic compressibility was calculated at different crystal volumes relating to the different measured sound velocity for each fixed temperature. The thermal scattering was account for in the calculation which was important for the compressibility results

[182]. The adiabatic compressibility of pure continuous phase was calculated using wood equation shown in Equation 3.12, the density data was calculated from the fitting of continuous phase density results measured by DSA48 and shown in Figure 7.7. The thermal expansively and specific heat at constant pressure was quoted from the literature [163]. The ratio of the specific heats is calculated from Equation 7.2. The sound velocity measured at different fixed temperatures is shown in Figure 7.13, which is used to predict the adiabatic compressibility of copper sulphate pentahydrate crystal at different temperatures.

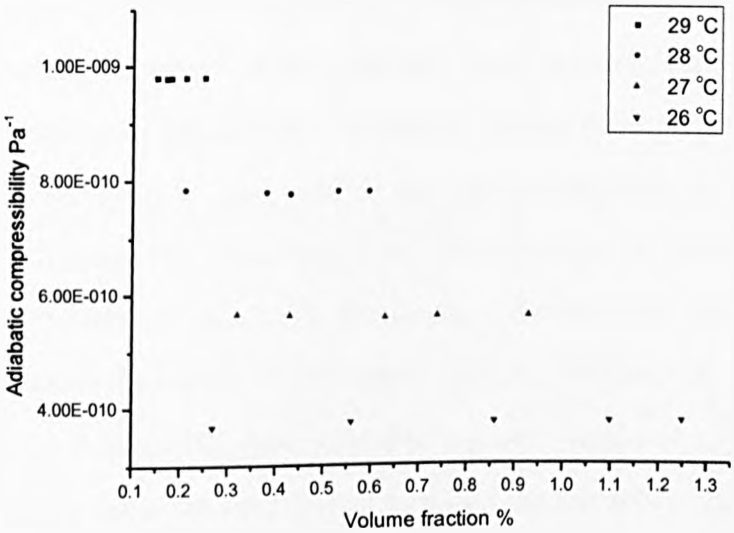

Figure 7.14: Adiabatic compressibility of copper sulphate pentahydrate crystals at different temperatures

It can be seen from Figure 7.14 that the adiabatic compressibility results calculated at different volume fractions of copper sulphate pentahydrate crystal were constant, and the final volume fraction of the crystal fits the solubility data quite well. This validates the modified Urick equation can be used to predict the adiabatic compressibility for the copper sulphate pentahydrate system.

7.3.2 Determination of the volume of crystal depending on the sound velocity measurement

The validation and application of the modified Urick equation on the calculation of the adiabatic compressibility of copper sulphate pentahydrate system means the modified Urick equation can be used to predict the suspended crystal volume. First of all, the scattering coefficients χ and ψ can be calculated after input the particle adiabatic compressibility valve using the equation 3.30 and 3.31 presented in the Chapter 3. The thermal effects were also involved in the calculation, and the thermal parameters were described in the section 7.3.1. After the scattering coefficients were identified, the unknown factors in the modified Urick equation were only solution velocity, continuous phase velocity and the particle volume fraction. The relationship between sound velocity in the pure solvent and solute concentration was shown in Figure 7.12, which means the continuous phase velocity can be calculated if the solute concentration in the solvent was known. For instance, the experiment was carried out at 28 °C, which meant the supersaturated copper sulphate solution with concentration of 45 w% was fixed at 28 °C. Assuming that x grams weight of copper sulphate pentahydrate crystals came out from the solution and the left solute concentration in the solvent should be 45 w% minus x w%. The equation between the sound velocity in the solvent and the crystal weight can be established depending on the data shown in Figure 7.12. On the other hand, the crystal weight can be easily converted into the crystal volume, as the crystal density was known and the solvent density at different solute concentrations were measured by DSA48 shown in Figure 7.7. The relationship between the solvent sound velocity and crystal volume can be built up as a result. As the solution sound velocity was given out by UVM, the crystal volume thus can be calculated using modified Urick equation.

The relationship between the solution sound velocity and crystal volume fraction in this copper sulphate system can be verified by experiment. 10 measured velocity results in the solution for 28 °C shown in Figure 7.11 were selected to calculate the crystal volume fraction and are presented in Figure 7.15.

The modified Urick equation (equation 3.29) can be presented as the following format:

$$\frac{1}{v_{solution}^2}-\frac{1}{v_{solvent}^2}=\frac{\chi}{v_{solvent}^2}\phi+\frac{\psi}{v_{solvent}^2}\phi^2 \qquad (7.4)$$

The linear relationship between the inverse square velocity of sound and crystal volume fraction is suitable for this experimental data shown in Figure 7.15, which predicts that the contributions from the second order in crystal volume fraction which the multiple scattering term is negligible to the velocity change. The modified Urick equation can be derived into a single scattering version for the crystal volume fraction calculation [183]:

$$\frac{1}{v_{solution}^2}-\frac{1}{v_{solvent}^2}=C_{\upsilon}\phi \qquad (7.5)$$

where $C_{\upsilon}=\frac{\chi}{v_{solvent}^2}$ *is the gradient of the straight line fit for the single scattering modified Urick equation.*

According to the scattering model, the gradient C_{υ} is obtained from the velocity measurement relating to the single scattering of the coefficient:

$$C_{\upsilon}=\frac{1}{v_{solvent}^2}\left(\frac{\kappa_{a2}-\kappa_{a1}}{\kappa_{a1}}+\frac{\rho_{a2}-\rho_{a1}}{\rho_{a1}}+Y\right) \qquad (7.6)$$

where Y is the thermal contribution, ρ *and* κ *are density and compressibility, the subscripts 1 and 2 refer to the dispersed and continuous phase, respectively.*

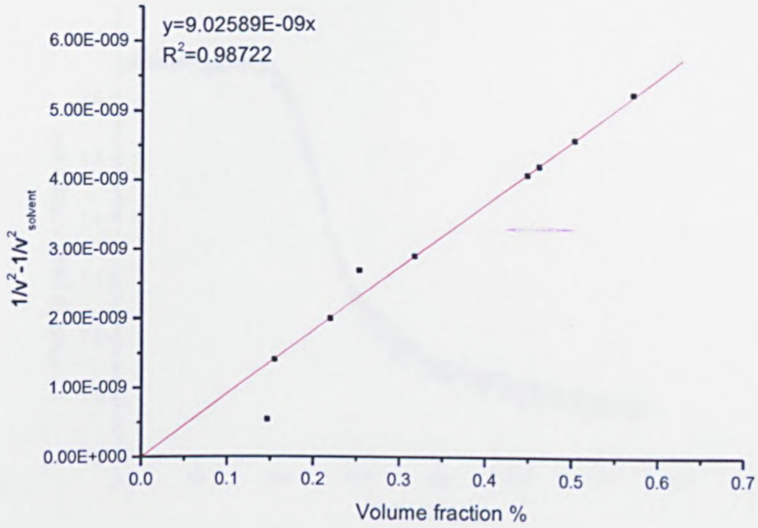

Figure 7.15: Inverse square velocity of sound against crystal volume fraction for 45w% copper sulphate solution at a fixed temperature of 28 °C

The neglect of multiple scattering in this case can be proved by the attenuation data from the attenuation experiments. The UVM could supply the peak to peak voltage value simultaneously when measuring the sound velocity in the solution. The peak to peak voltage can be converted into an attenuation difference value using the equations introduced by Umchid [184] and Bobber [185]

$$a_{solution} - a_{solvent} = \frac{1}{d_{uvm}} \ln \frac{V_{solvent}}{V_{solution}} \tag{7.7}$$

where d_{uvm} *is the distance between the transducers of the UVM which is 3.15 inch,* $V_{solvent}$ *is the peak to peak voltage of solution without crystal, and* $V_{solution}$ *is the measured peak to peak voltage in the solution with crystals.*

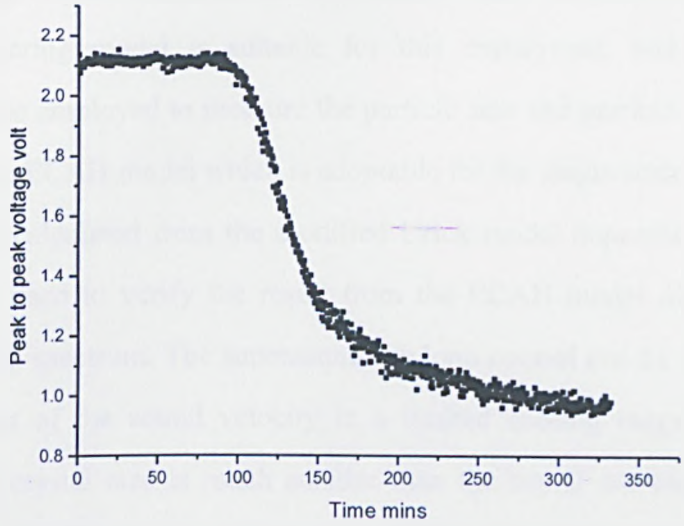

Figure 7.16: Peak to peak voltage measurement of 45 w% copper sulphate solution at a fixed temperature of 28 °C

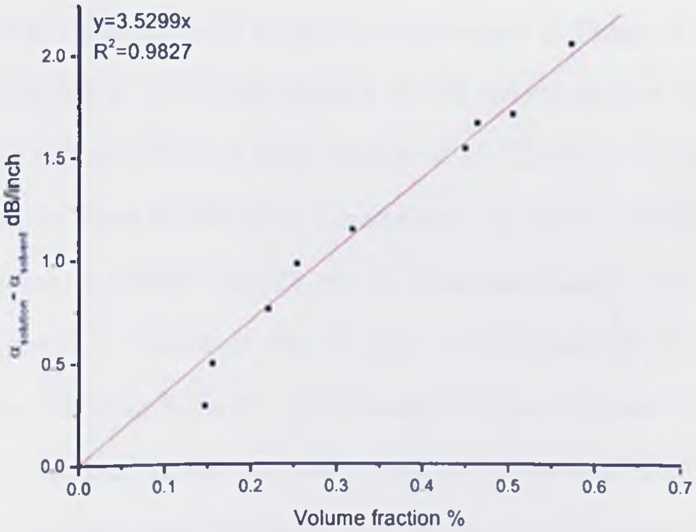

Figure 7.17: Attenuation difference against crystal volume fraction for 45 w% copper sulphate solution fixed at a temperature at 28 °C

The linear change of the attenuation as the crystal volume fraction increased proves the single scattering model is suitable for this experiment, and the MSV and Alphasizer can be employed to measure the particle size and particle volume fraction depending on the ECAH model which is adoptable for the single scattering cases. The volume fraction calculated from the modified Urick model depending on the sound velocity can be used to verify the result from the ECAH model depending on the sound attenuation spectrum. The supersaturation loop control can be realized through the measurement of the sound velocity in a limited cooling range, which should ensure sure the crystal size is much smaller than the sound wavelength. From the crystallization experiments under different cooling rates in Chapter 6, the final crystal size of 45w% copper sulphate solution cooled to 20 °C is under 100 μm which is much smaller than the wavelength of UVM whereas the central frequency of UVM is 2.5 MHz. The selection of the frequency in the measurement using MSV needs to satisfy the limitations of the long wavelength region measurement.

Another interesting detection from the velocity measurement of 45 w% copper sulphate solution at different fixed temperature presented in Figure 7.13, showed that the sound velocity has a little improvement in the induction time period when the fixed temperature of the solution is high, such as at 29 °C and 28 °C, whereas there is no change at the low fixed temperature experiments, i.e., 27 °C and 26 °C. It is clear to find the increase of sound velocity in the induction time of 28 °C experiment presented in Figure 7.11. However, the change was not observed in the attenuation data measured by UVM in Figure 7.16. Because the bandwidth of UVM is narrow, and its frequency is fixed in the very low value, it is not sufficient to indicate no change in the attenuation data. The MSV was employed to measure the attenuation data at different frequency points to check the variation of the attenuation of the solution without crystals existing.

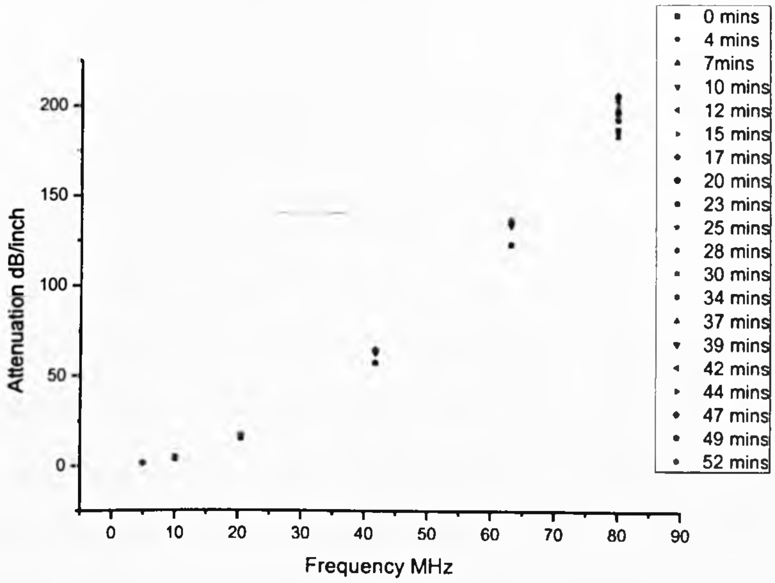

Figure 7.18: Attenuation measurement of 45 w% copper sulphate solution at a fixed temperature of 28 °C

The same experiment was repeated in the MSV batch cell under the same conditions as for the UVM experiments. The copper sulphate solution with concentration of 45w% was prepared, and kept at 28 °C after all the crystals were dissolved at high temperature. The stirrer was turned off to extend the induction time. The sound attenuation spectrum was collected before the crystals came out. The electrical conductivity was used to predict the constant value to make sure there was no nucleation occurring during the measurement of sound attenuation in the induction time. The same measurement strategy was used for the convenience of comparing the results at different frequencies. 6 frequency points at 5 MHz, 10.15 MHz, 20.60 MHz, 41.80 MHz, 63.1736 MHz, and 79.98 MHz were selected to collect the sound attenuation results shown in Figure 7.18.

As indicated by UVM, there is no change in the attenuation at low frequency points. However, it is expected that some increase of attenuation will occur as time goes by (Figure 7.8). The change is bigger as the frequency used is higher. In the absence of scattering effects and solution concentration change, the sound velocity and sound attenuation increase is supposed to be caused by the formation of the molecular cluster, due to the sound technique being very sensitive to the phase transfer of the solution.

As described above, the modified Urick equation is validated for adiabatic compressibility calculation and crystal volume fraction determination during the crystallization process in the copper sulphate system. However, the sound velocity measured by MSV is the average value of the phase velocity at different frequencies. The frequencies selected are based on the measurement strategy. In the particulate system, the phase velocity is dispersed relating to the frequency due to the scattering effect. The velocity dispersion causes the average velocity result to have a large deviation from the real data. On the other hand, the phase velocity in the high frequency is easily destroyed by the scattering because it is out of the limitation of the long wavelength region required. Figure 7.19 presents the velocity spectrum from MSV which was measured at the start of the crystallization. The existence of the crystals clearly affects the accuracy of the velocity result in the high frequency points.

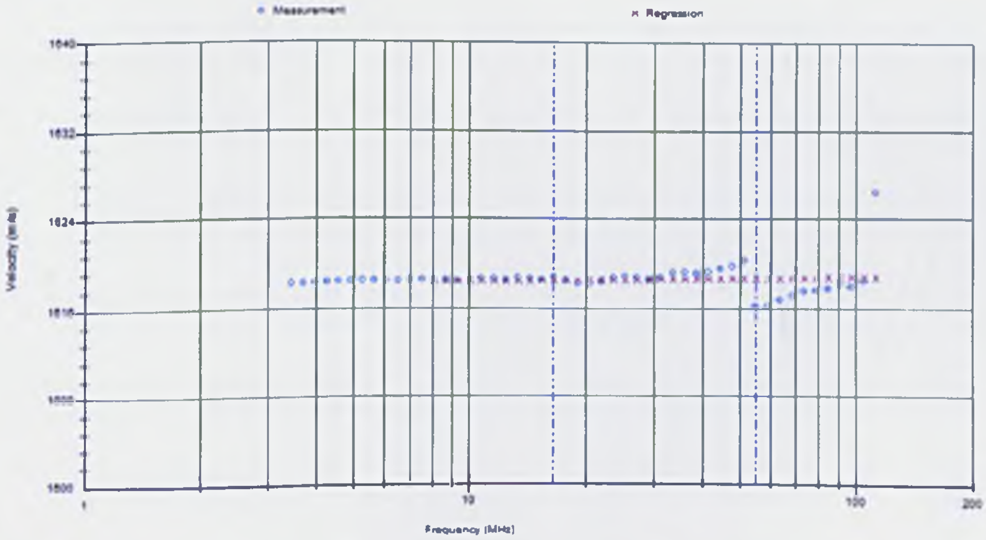

Figure 7.19: The velocity spectrum measured from MSV of 45 w% copper sulphate solution crystallization processes at 28.4 °C

In order to realize the on-line supersaturation control depending on the sound velocity, a new generation of acoustic instrument Alphasizer has been developed, which employed the pulse signal generation system instead of a continuous wave system. The group sound velocity is used to predict the crystal volume fraction as UMV. The instrument calibration work and the build-up of the supersaturation loop control communication system are described in detail in Chapter 8.

7.4 Conclusions

The sound velocity in the pure copper sulphate solution was measured by MSV. The speed in low solute concentrations is accurate as calibrated using the ResoScan. The relaxation effect on the sound attenuation is eliminated for predicting the bulk viscosity of copper sulphate solution for accurate calculation. The bulk viscosity of the pure water is calculated from the velocity and attenuation data from MSV and fits the literature data well which measured using different methods. This presents the advantage of acoustic spectroscopy on the determination of the bulk viscosity of liquids, which offers high precision without requiring knowing many other liquid properties. The application of the modified Urick equation in the crystallization system builds up the theoretical background of using the sound velocity scattering model to predict the crystal volume during the crystallization process. The on line measurement of the supersaturation can be realized depending on this application, and the build up of the supersaturation control system is described in detail in Chapter 8.

Chapter 8 Development of the New Generation Acoustic Instrument for On-line Particle Size Characterization and Closed Loop Control

Summary

A new process acoustic instrument for the on-line particle sizing is described in this chapter. The acoustic spectra are calibrated under different experimental conditions. The new closed supersaturation loop control system was developed.

8.1 Introduction

The particle size distribution and suspended particle volume measurement using MSV depending on the acoustic attenuation spectrum method was introduced in Chapter 6. MSV provides the particle information successfully for the measurement of the copper sulphate pentahydrate system. As described in Chapter 6, the drawback of the MSV for the dynamic crystallization process measurement is its long interval for each measurement. High quality spectra can only be collected at low cooling rates avoiding the dramatic change in acoustic parameters. The time issue limited further development of the acoustic spectrometer on the dynamic system measurement.

A new acoustic spectrum instrument named the Alphasizer developed by Malvern Ltd is designed for solving this problem. New acoustic measurement algorithms, new sensor hardware, new cell design, and a new control system have been developed for the Alphasizer. This new acoustic spectrometer is expected to be faster on data acquisition and is smaller and lighter in design. The new control software can be linked to the standard industry controlling system lab-view, and the automatic measurement function of the Alphasizer provides the possibility of using it in industry. Beside the advantages of the aspect of acoustic attenuation spectrum, the Alphasizer could output the pulsed sound group velocity to the remote control system. Supersaturation loop control can be realized only using the Alphasizer, depending on the modified Urick theory, which was fully described in Chapter 7. The following sections describe the contribution from the author to the Alphasizer developments, which include the calibration work and measurements of the accurate spectra using Alphasizer, the particle size distribution can be obtained, and the communication of the loop control was also set up.

8.2 Comparison of Alphasizer with MSV

The most important difference between the Alphasizer and MSV is the acoustic measurement algorithm. The Alphasizer adopts the bandwidth pulse whereas MSV uses the pseudo continuous frequency sweep. This change shortens the measurement time from 4 minutes using the MSV, to 20 seconds using the Alphasizer. Rapid data acquisition of the Alphasizer makes it suitable for the dynamic system measurement, which is the drawback of the MSV. In order to provide rapid measurement, a narrow frequency range of 5-100 MHz is used instead of 1-150 MHz used in MSV. For the acoustic spectrometer technique, the frequency range of 1-100 MHz is the most popular used in the instrument development. Low attenuations cannot be measured accurately and high attenuations leave undetectable signals on the receiving transducer because of low SNR. The elimination of the low frequencies of 1-5 MHz could reduce the transducer passing length and consequently reduce the cell volume. Single pair transducers designed for the Alphasizer which cover the whole frequency range is aimed at reducing the weight of the instrument.

Only one flow-through cell with a volume of 0.175 litre is fixed in the cell. Compared to the 0.5 litre flow-through cell of the MSV, the reduction of the volume of the cell has several advantages. Small cell size is more suitable for laboratory scale measurement. The total solution volume could be reduced because the requirement of the amount of the sample is reduced. It is easier to realize the specific control for the measurement, such as the high cooling rate requirement of crystallization.

Another modification to the hardware of the Alphasizer is the inlet and outlet positions. The inlet and outlet of the MSV are fixed on the bottom left side and top left side, respectively. The inlet and outlet of the Alphasizer are placed vertically on the bottom and top of the flow-through cell, which is shown in Figure 8.1. This configuration change in the hardware brings hydrodynamic benefits. The dynamic transducer will move into the solution during the measurement, and the existence of the transducer will affect the flow velocity of the solution. If the inlet and outlet are placed horizontally as with the MSV, any movement of the transducer would cause more serious effects on the flow velocity compared to the vertical position under the same flow rate of the pump supplied. The mixture grade of the solution is determined by the flow velocity due to no stirrer being positioned in the cell. Low flow velocity would reduce the homogeneity of the solution, and some particles will settle on the bottom of the cell, especially in the space under the moving transducer.

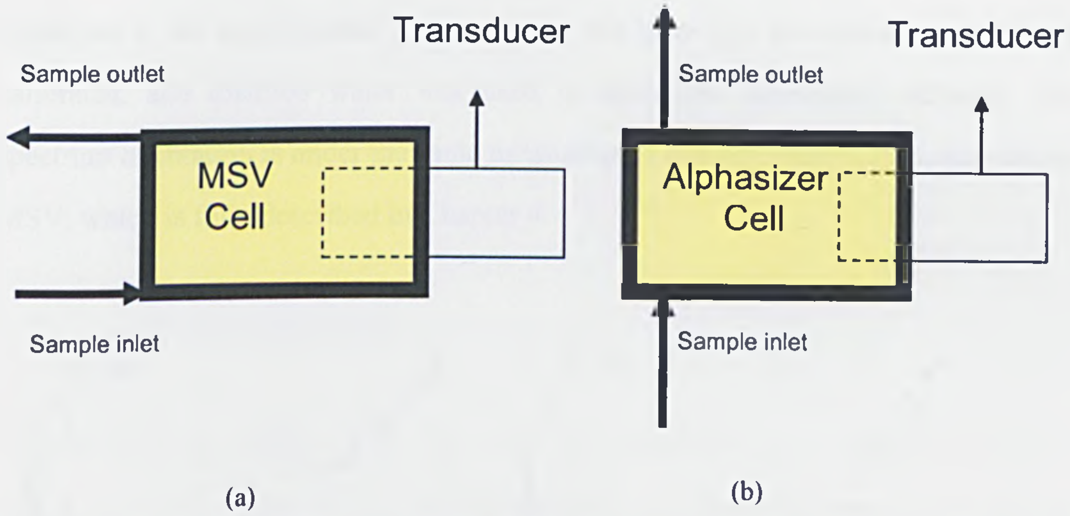

Figure 8.1: Schematic diagram of the MSV flow-through cell (a) and the Alphasizer flow-through cell (b)

The weight reduction of the Alphasizer is more convenient for transportation in the laboratory when the Alphasizer is required to link to the different experiment systems. Ensuring the transmitting transducer and receiving transducer are parallel to each other determines the accuracy of the instrument. The MSV always lost its calibration during transportation due to it being hard to move.

The improvement in the software of the Alphasizer is that it can be directly connected to a remote computer and output the sound velocity and analyzed particle size information. This function allows the Alphasizer to monitor the solution supersaturation, and the application will be presented in the following section 8.4.

8.3 Calibration of acoustic attenuation spectra and particle size analysis

8.3.1 Alphasizer water spectra modification

The Alphasizer is a new prototype instrument from Malvern Ltd. Before being employed in the experimental measurement, this prototype instrument needed to be calibrated, and distilled water was used to make the benchmark calibrate. The spectrum calibration is under the same measurement strategy modification rules as the MSV, which is fully described in Chapter 4.

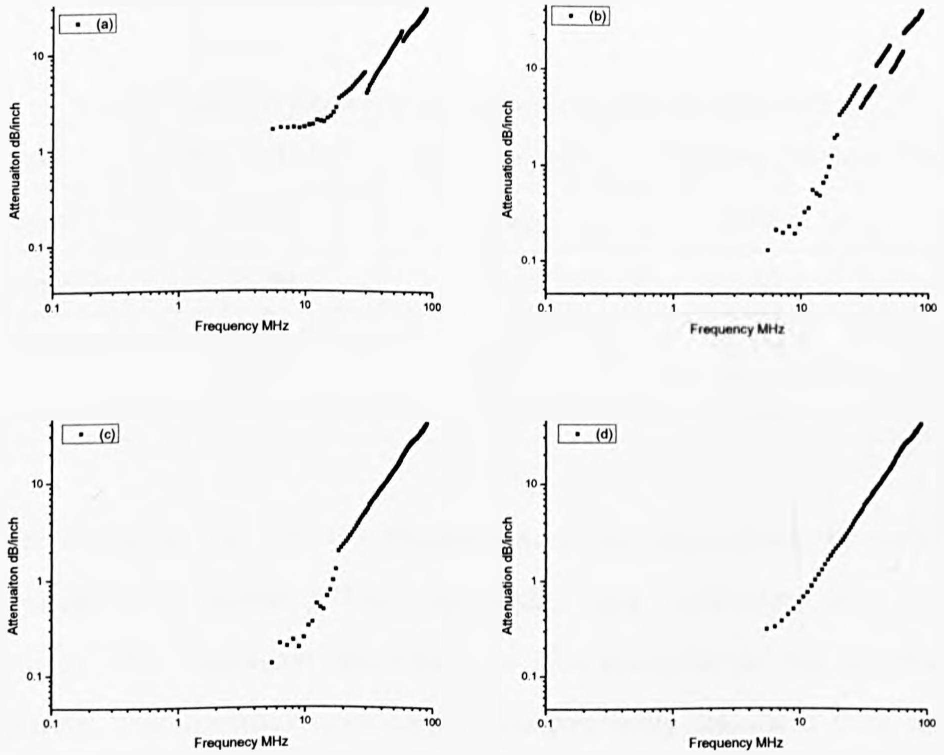

Figure 8.2: Modification of spectra by changing the measurement strategy in water at 25 °C. From a random spectrum (a) to a good quality spectrum (d)

Because of the acoustic generation method, the bandwidth, even the hardware is different from the MSV. The optimisation measurement strategy for the MSV cannot be applied to the Alphasizer. For the same sample conditions, the strategy parameters are totally different for the MSV and Alphasizer. In order to find the optimal strategy, the frequency bandwidth is divided into several sub-channels. The spacing between the transducers and the frequency bandwidth can be chosen manually. The modification of the transducers' spacing can be realized by setting the initial and end position of the transmitting transducer before it moves. The spectrum of water modified from a random spectrum to a smooth spectrum is presented in Figure 8.2. The Alphasizer measurement strategy for water under 25 °C is presented in Table 8.1, and the water strategies under different temperature is quite similar and only need slightly modification at the transducer moving space.

Table 8.1: Alphasizer measurement strategy for water at 25 °C

channel no.	Min Freq MHz	Max Freq MHz	Position 1 inch	Position 2 inch
Channel 1	5.51	30.324	1.96	0.08
Channel 2	32.04	55.99	1.49	0.08
Channel 3	56.85	81.67	1.18	0.08
Channel 4	82.53	90.23	0.94	0.08

After collecting the smooth spectrum from the Alphasizer, the spectrum was compared to the spectrum from the 'golden mark' instrument MSV to prove its accuracy. The Alphasizer spectrum was also compared to the theoretical water spectrum. The theoretical spectrum is mathematically calculated from the acoustic physical parameters. The sound attenuation can be presented by a single polynomial in frequency of the form f^2, which present the relationship of sound attenuation and sound frequency in pure water [102].

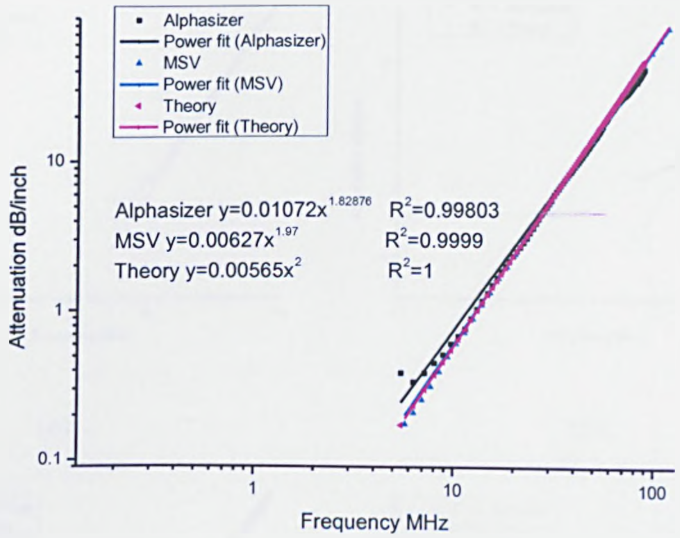

Figure 8.3: Comparison of spectra measured by the Alphasizer, MSV and theory data of pure water at 20 °C

From the comparison of the spectra presented in Figure 8.3, the manually modified spectrum from the Alphasizer was smooth and good quality. The attenuation value fits the theory data at most of the frequency points in the spectrum, which is the standard for the Alphasizer calibration work. Comparing the power trend line of these three results, the MSV still provides a better result which is closer to the theoretical data. Because the power value in the power fitting curve presented in Figure 8.3 should be equal to 2 for the pure solution without any scattering from particle or relaxation process happen. However, for single attenuation spectrum measurement under the same conditions, the MSV needed around 4 minutes to complete the measurement due to its complicated measurement method, although this provides very high precision attenuation data for MSV. The drawback of the long time consumption cannot avoid the dynamic process measurement. The pulse acoustic generation system of the Alphasizer simplifies the measurement process and shortens the measurement time, and the accuracy is good after careful calibration.

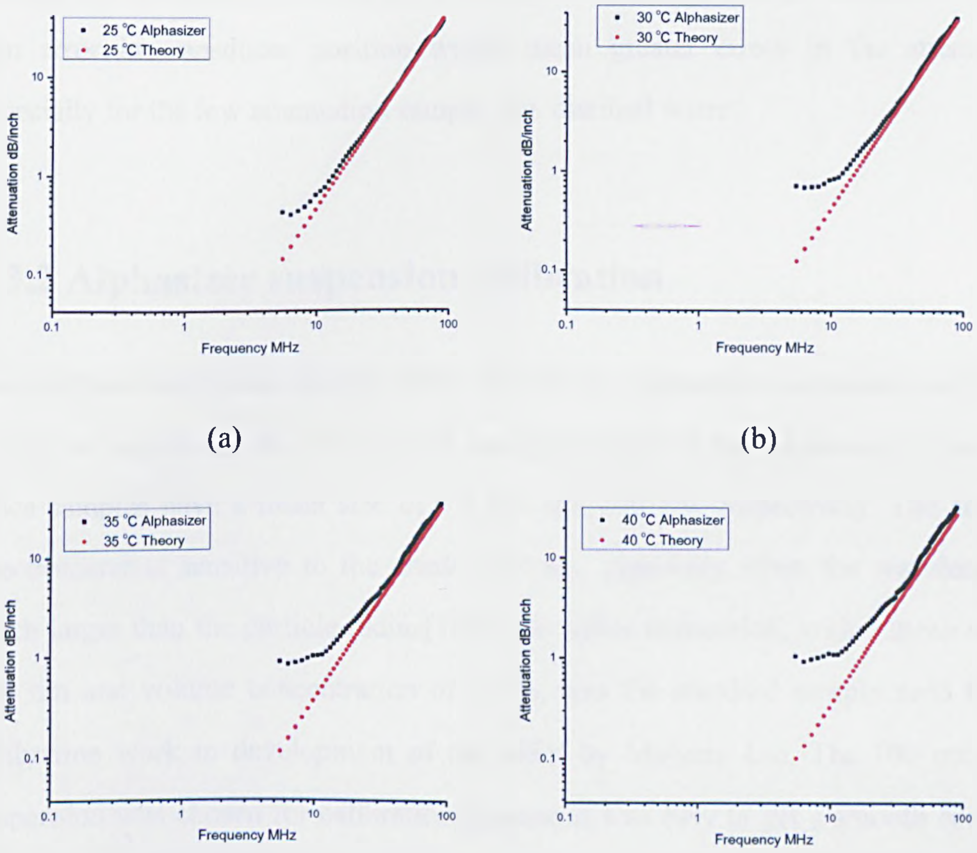

(a) (b)

(c) (d)

Figure 8.4: Comparison of the spectrum measured by the Alphasizer and theory spectrum measured in distilled water at different temperatures, (a) 25 °C, (b) 30 °C, (c) 35 °C, and (d) 40 °C

Figure 8.4 presents the spectra from the Alphasizer measured in distilled water at different temperatures and compared to the theory for water spectra. It is easy to see that the spectrum fits the theoretical spectrum well at low temperatures, as the temperature increases, the accuracy of the Alphasizer goes down. The log-log scale is used in Figure 8.4, the proportional difference from the theoretical data at low frequency is larger than the high frequency, which means the low frequency data has less accuracy. The attenuation is very low at low frequency, which means it is not easy to detect the signal. Therefore, long distances between the transducers are needed for low frequency measurement. The transducer needs to be moved to the far end to provide the longest transducer spacing, around 50 mm, to measure the attenuation of water at low frequency. However, the preliminary test from Imran in his MSc project showed the transducer position has 1 mm error in the 50 mm position[186]. This 1 mm error in transducer position would mean greater errors in the attenuation, especially for the low attenuation sample, e.g. distilled water.

8.3.2 Alphasizer suspension calibration

Two different size silica samples were used for the Alphasizer suspension calibration aiming to implement the particle size analysis ability of the Alphasizer. These two silica samples have a mean size of 1.5 μm and 100 nm, respectively. The acoustic spectrometer is sensitive to the small particles, especially when the wavelength is much larger than the particle radius[187]. The silica suspension, with a mean size of 200 nm and volume concentration of 2 v%, was the standard sample used for the calibration work in development of the MSV by Malvern Ltd. The 100 nm silica suspension was chosen for calibration because it was easy to get a smooth spectrum and then get the particle size distribution plus suspended particle volume. Another silica sample with mean size 1.5 μm was the standard sample commonly used in the laboratory, which was used in the characterization of the MSV as described in Chapter 6. The sample was also analyzed using the other size technique such as the Mastersizer 2000, the particle size distribution and the characteristics of the sample were defined in Chapter 6. It is more straightforward to find an accurate measurement strategy and get smooth spectrum when using familiar samples.

The accuracy of the spectrum measured using the Alphasizer was validated by comparing the results to the spectrum measured using the MSV and simulation data. The simulation function was installed in the MSV and Alphasizer, which can simulate an attenuation by using the assumed particle size information plus the scattering physical parameters [7]. Theses parameters are basically used to derive a particle size distribution from an acoustic attenuation spectrum. During simulation, this process is reversed and an acoustic attenuation spectrum is derived from a particle size distribution. The simulation function provides a expect spectrum prior to measuring the sample in the chamber, and the measurement strategy of the Alphasizer can be modified after comparing the measured spectrum with simulated spectrum. The simulation spectrum also investigates the sensitivity of the measurement to measurement noise and changes in the particle size distribution, concentration and temperature, etc. To make the simulation as realistic as possible, the effect of the measurement electronics and the transducers are included in the simulation. The dynamic range or signal to noise limitations of the measurement system are simulated and the operator may apply random measurement noise.

Acoustic attenuation spectra were collected by modifying the measurement strategy manually using the Alphasizer under different measurement conditions. The measurement temperature was set from 20 ˚C to 50 ˚C, the spectra were collected by MSV and Alphasizer every 5 ˚C, and compared to the simulated spectra. Six suspended particle volume concentrations of 0.1 v%, 0.5 v%, 1.0 v%, 2.0 v%, 5.0 v% and 10.0 v% were used to investigate the spectrum evolution at different concentrations. The physical property of silica powder and pure water is quoted from Dr. Penchev's work [168].

The measurement strategy setting for the particulate system, the spectrum in the low frequency region needs to be eliminated due to the noise, and the transducer moving required modification for different case. The basic Alphasizer measurement strategy for particulate system is presented in the Table 8.2, different particle size, different particle volume and different temperature condition needs little modification on the sub-channel frequency selection and transducer spacing

Table 8.2: Alphasizer measurement strategy for 1.5 μm silica suspension with concentration of 0.5v% at 25 ˚C

channel no.	Min Freq MHz	Max Freq MHz	Position 1 inch	Position 2 inch
Channel 1	10.64	30.324	1.96	0.08
Channel 2	32.04	55.99	1.65	0.08
Channel 3	56.85	81.67	0.98	0.08
Channel 4	82.53	90.23	0.47	0.08

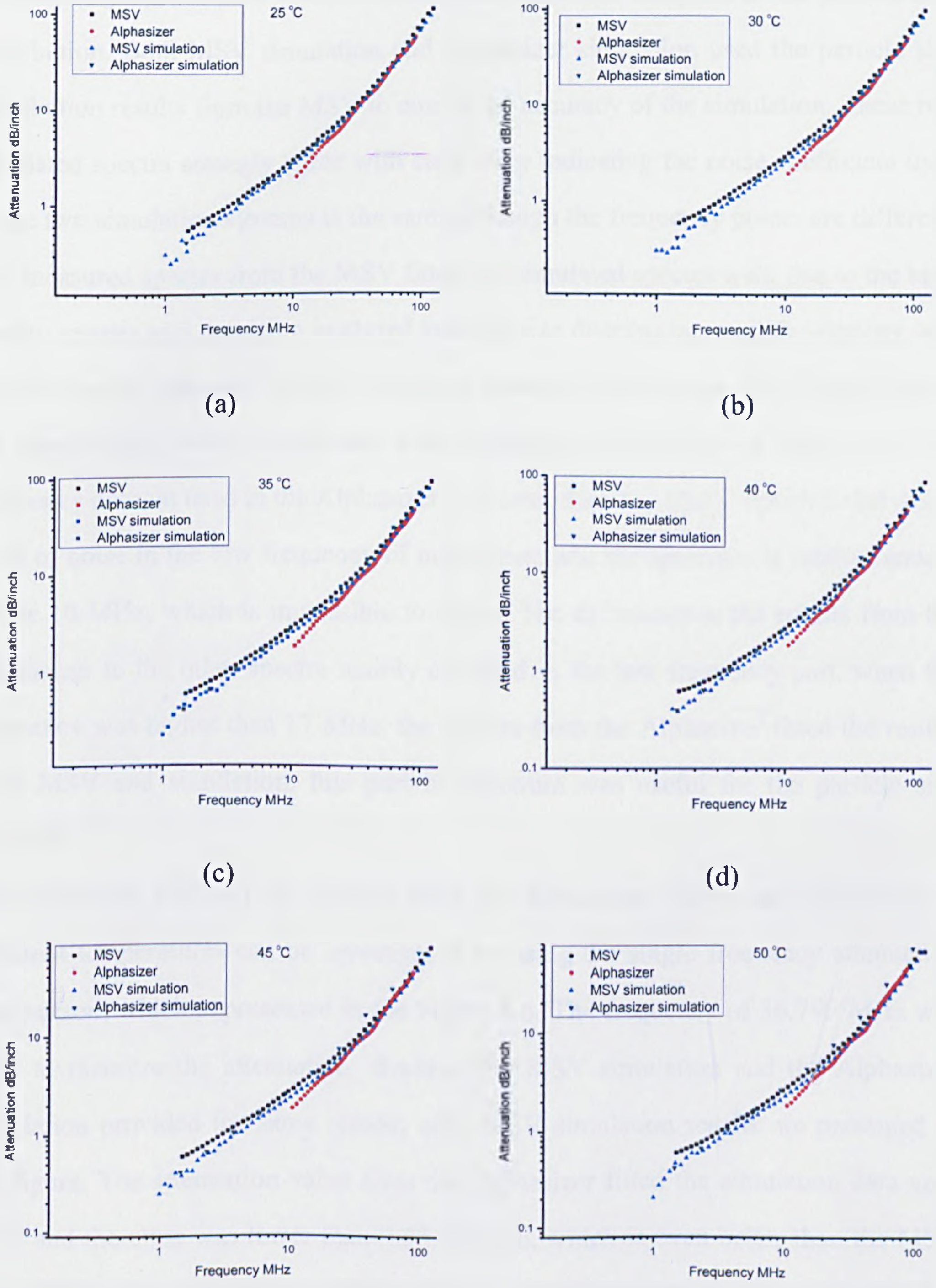

(a) (b)

(c) (d)

(e) (f)

Figure 8.5: Comparison of spectra measured using the Alphasizer, MSV and simulation results of 0.5 v% silica suspension with a mean size of 1.5 µm under different Temperature(a) is 25 °C, (b) is 30 °C, (c) is 35 °C, (d) is 40 °C, (e) is 45 °C and (f) is 50 °C

The spectra of the silica sample with a particle mean size of 1.5 µm was firstly measured by MSV under different conditions, and then analyzed to the particle size distribution. Both MSV simulation and Alphasizer simulation used the particle size distribution results from the MSV to ensure the accuracy of the simulation. These two simulated spectra strongly agree with each other indicating the noise coefficient used in the two simulation systems is the same although the frequency points are different. The measured spectra from the MSV fitted the simulated spectra well, due to the high quality spectra and precision analyzed particle size distribution, and the strategy was recorded as the reference for the Alphasizer strategy modification. The comparison of the spectra from MSV, Alphasizer and simulation is illustrated in Figure 8.5. The frequency domain used in the Alphasizer is shorter than the others, which is due to the level of noise in the low frequency of instrument, and the spectrum is totally random below 10 MHz, which is impossible to adjust. The difference in the results from the Alphasizer to the other spectra mainly occurred in the low frequency part, when the frequency was higher than 17 MHz, the spectra from the Alphasizer fitted the results from MSV and simulation, this part of spectrum was useful for the particle size analysis.

The difference between the spectra from the Alphasizer, MSV, and simulation at different temperatures can be investigated by using the single frequency attenuation comparison, which is presented in the Figure 8.6. The frequency of 36.799 MHz was used to measure the attenuation. Because the MSV simulation and the Alphasizer simulation provided the same results, only MSV simulation results are presented in the figure. The attenuation value from the Alphasizer fitted the simulation data very well, and the error was lower than 0.25 dB/inch, which is even better than the MSV data. The temperature change had no effect on the error between the Alphasizer and simulation results, which mean the Alphasizer could provide stable attenuation data at high temperatures.

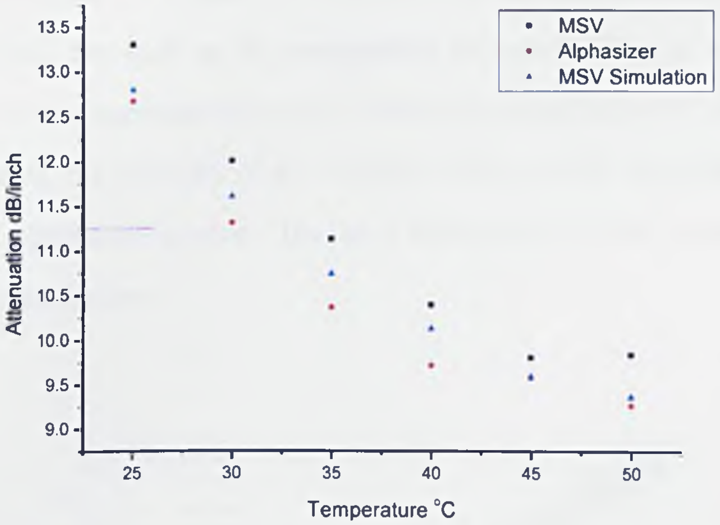

Figure 8.6: Comparison of attenuation from the MSV, Alphasizer and simulation at single frequency, 36.799 MHz at different temperatures for 0.5 v% silica suspension with a mean particle size of 1.5 μm

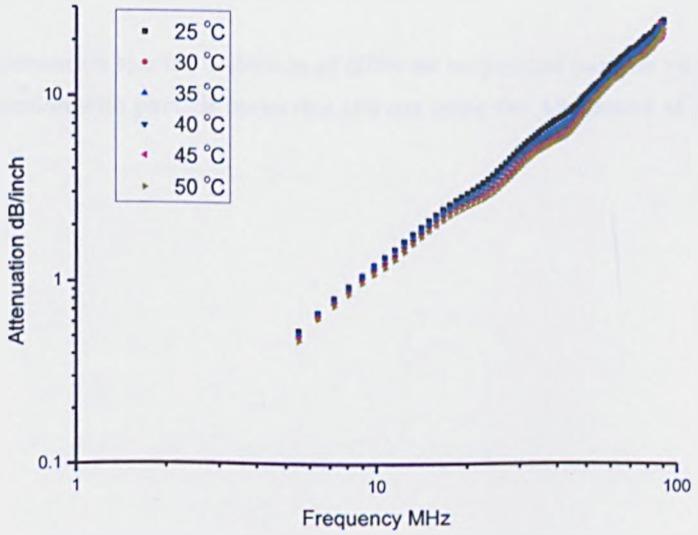

Figure 8.7: Spectra measured by the Alphasizer at different temperatures for 1.0 v% silica suspension with a mean particle size of 1.5 μm

The spectra presented in Figure 8.7 illustrate that the acoustic attenuation of the suspension would decrease as the temperature increased. This is because of the decreasing of the background attenuation. When the temperature of the background solution increases, the viscosity of the solution will decrease, which will reduce the effect of the viscous absorption. The total attenuation of the suspension would decrease as a consequence.

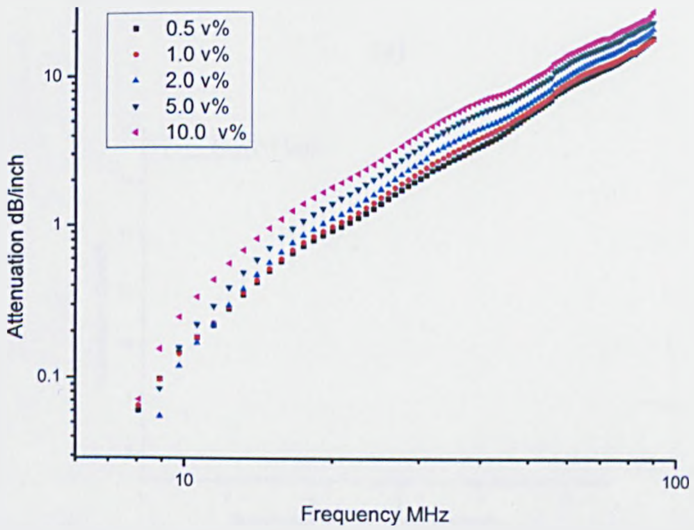

Figure 8.8: Attenuation spectra collection of different suspended particle volumes for silica suspension with particle mean size 100 nm using the Alphasizer at 25 °C

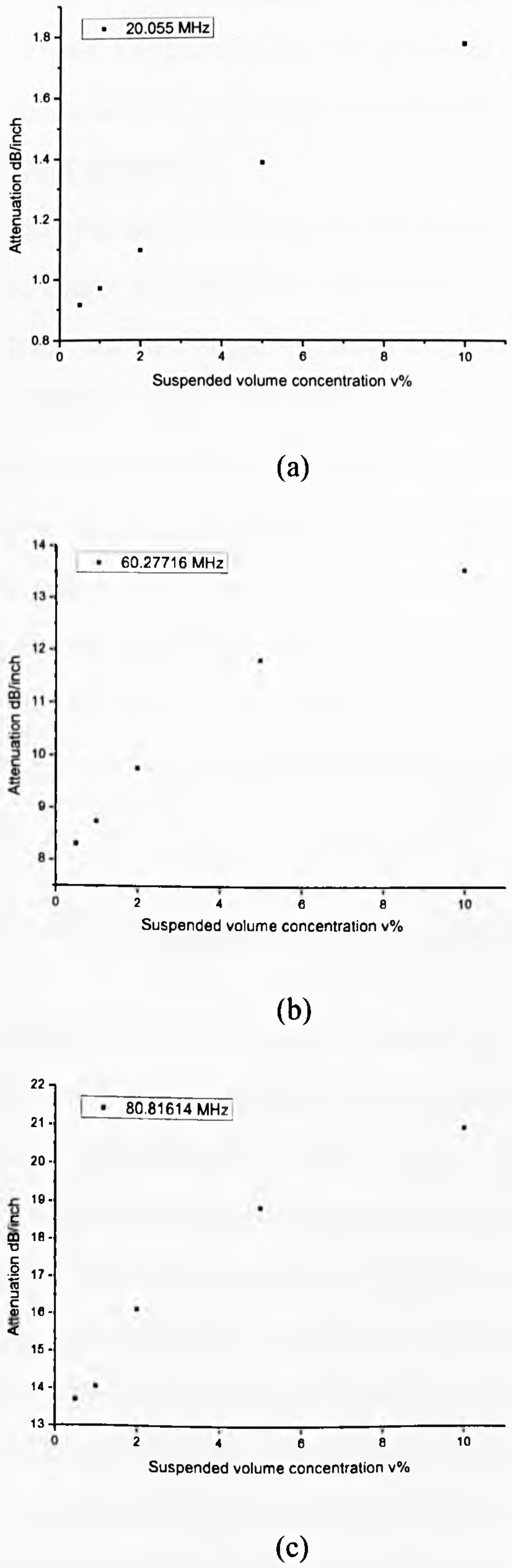

Figure 8.9: Attenuation of specific single frequency tests of different suspended particle volume concentrations for silica suspension with a particle mean size of 100 nm using the Alphasizer at 25 °C

The spectra were collected for the 100 nm silica suspension under different suspended volume concentrations, Figure 8.8 illustrates the attenuation of the solution increasing as the particle volume increases. It is easy to understand that more suspended particles bring more attenuation from scattering.

The relationship of attenuation and suspended volume concentration for three single frequencies is plotted in Figure 8.9, the sound attenuation is linear change with the suspended particle volume for the single frequency test. This linear relationship indicates there are no multiple scattering effects, and the ECAH model is valid for this case. For the high single frequency test, i.e. the 80.81614 MHz test, the data is not so good as the results show a low frequency of 20.055 MHz. This is mainly because the spacing between the transducer is very tiny for the high frequency measurement, and the spacing limited the flow rate of the solution through the cell, which induced some particles to settle and this affected the test results. The sound noise at the high end frequency is another influence on the accuracy of the attenuation data.

8.3.3 Particle size distribution analysis using the Alphasizer

After modification of the measurement strategy and comparison with the results from MSV and simulation data, attenuation spectra with good quality were collected using the Alphasizer. However, the attenuation spectra are still unable to analyze the particle size. This was caused by the incorrect physical matrix or incorrect attenuation spectra. The silica particle is the standard sample for the acoustic spectrometer development, and its physical parameters are validated by research. The incapability of particle size analysis comes from the sound noise in the high frequency near the threshold and the error existed in the low frequency part, which can be seen in the comparison with the spectrum from MSV and simulation data shown in Figure 8.5.

The frequency range was then reduced and the most accurate part of the spectrum was kept for the analysis. Meanwhile, the spacing between the transducers was reduced to half of the original value for each sub-channel in order to improve data acquisition ability and avoid the sound noise of the instrument.

The spectra collected for the 2.0 v% silica suspension with a particle mean size of 1.5μm at different temperatures are presented in Figure 8.10. Compared to the spectra collected for the solution with concentration of 1.0 v% shown in Figure 8.8, the frequency domain was reduced to 17-40 MHz from 5-100 MHz. The measurement strategy for 2 v% silica suspension at 25 °C was demonstrated in Table 8.3. Different particle size, different particle volume and different temperature condition needs little modification on the sub-channel frequency selection and transducer spacing. The spectra in this frequency domain are precision to analyze the particle size distribution and the volume concentration.

Table 8.3: Modified Alphasizer measurement strategy using short frequency range for 2 v% silica suspension with particle mean size 1.5 μm at 25 °C

channel no.	Min Freq MHz	Max Freq MHz	Position 1 inch	Position 2 inch
Channel 1	17	32	0.98	0.08
Channel 2	32.04	40	0.47	0.08

The analyzed size distribution is presented in Figure 8.11 and the size distribution parameters and measured volume concentration are listed in Table 8.4. The particle size distribution measured by Mastersizer was presented in Chapter 6. The particle mean size and volume concentration analyzed using the Alphasizer was very accurate and close to the real value. High temperature measurement conditions had some influence on the width of the size distribution.

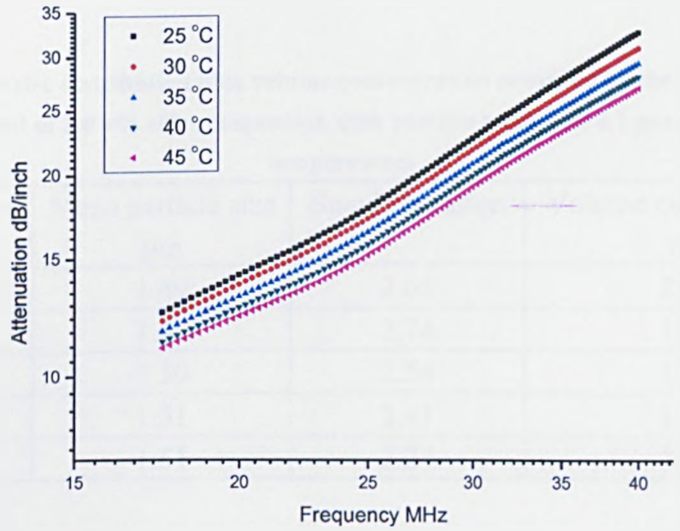

Figure 8.10: Modified spectra using a short frequency range measurement of 2 v% silica suspension with particle mean size 1.5 µm at different temperatures

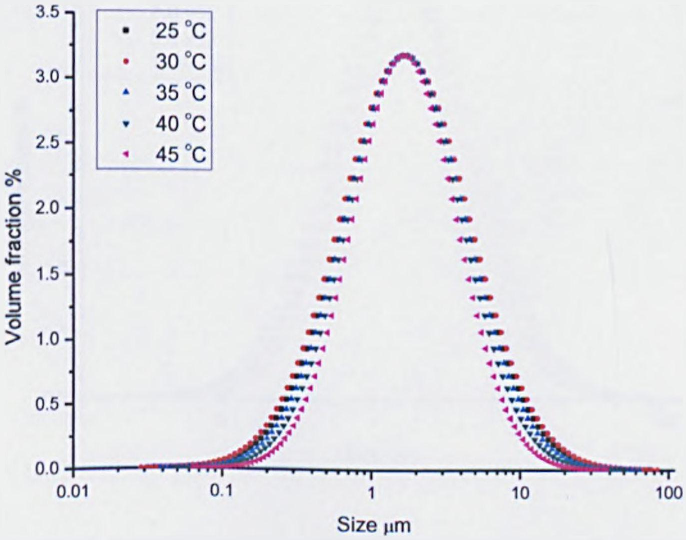

Figure 8.11: Particle size distribution of 2.0 v% silica suspension with particle mean size 1.5µm at different temperatures

Table 8.4: Particle size distribution plus volume concentration provided by the Alphasizer for the measurement of 2.0 v% silica suspension with particle mean size 1.5 μm at different temperatures

Temperature °C	Mean particle size μm	Stand deviation	Volume concentration v%
25	1.49	2.65	2.02
30	1.48	2.74	1.91
35	1.50	2.54	1.91
40	1.51	2.41	1.89
45	1.51	2.24	1.92

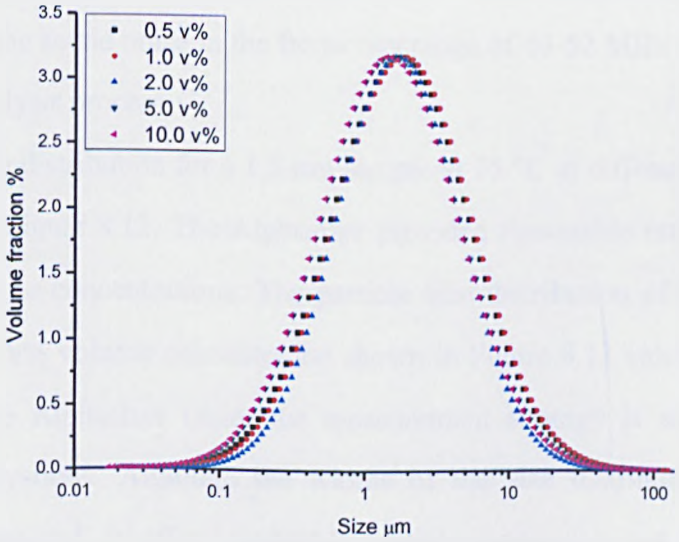

Figure 8.12: Particle size distribution of silica suspension with particle mean size 1.5μm under different volume concentrations at 25 °C

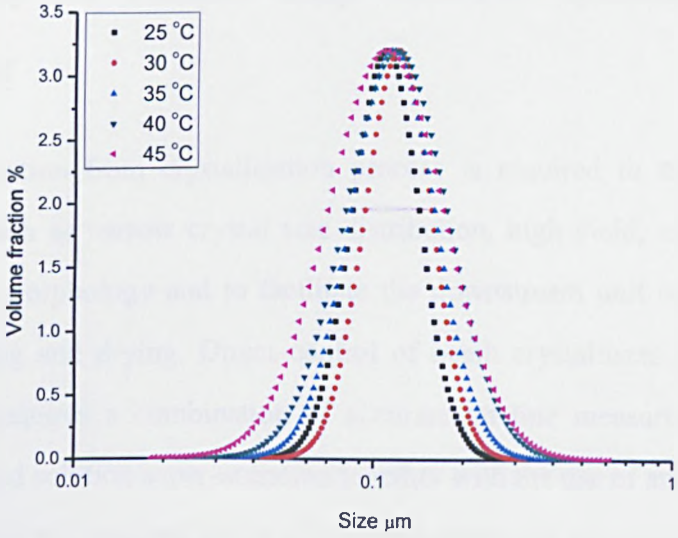

Figure 8.13: Particle size distribution of 10.0 v% silica suspension with particle mean size 100nm at different temperatures

To allow for getting high accurate particle size distribution results, the measurement frequency domain is commonly extended to 17-52 MHz depending on the sample characters, i.e. the sound noise in the frequency range of 40-52 MHz does not ruin the particle size analysis process.

The particle size distribution for a 1.5 µm sample at 25 °C at different concentrations is illustrated in Figure 8.12. The Alphasizer provided reasonable results for the high suspended volume concentrations. The particle size distribution of a 100 nm silica sample with 10 v% volume concentration shown in Figure 8.13 validated the spectra collected by the Alphasizer under the measurement strategy is accurate for high volume concentrations. Although the widths of the size distribution shift as the temperature increased, it offers creditable particle mean size and particle volume concentration.

8.4 Set up of closed loop control system base on Alphasizer

The solid formation from crystallisation process is required to meet the specific requirements such as narrow crystal size distribution, high yield, crystal purity and desired crystal morphology and to facilitate the downstream unit operation such as filtration, milling and drying. Direct control of batch crystallisers to meet product specifications requires a combination of accurate on line measurements of solute concentration and solution supersaturation together with the use of appropriate control models to sustain the required levels of supersaturation for the following nucleation and crystal growth processes.

In this section, the supersaturation was monitored by Alphasizer, because the Alphasizer could supply the sound velocity value, and the crystal volume concentration can be determined by the sound velocity value depending on the acoustic scattering model developed in Chapter 7 Equation 7.4. The crystal volume concentration can be easily converted into the solution concentration calculated by the Equation 6.4, and the supersaturation can be consequently calculated from the solution concentration using Equation 2.10.

8.4.1 Loop control system construction

The closed loop system consisted of the 20 litre reactor, WinISO control software, MatLab and the Alphasizer. The WinISO software was the temperature controlling system and was connected to the other hardware of the system. The communication between WinISO and MatLab was completed by the WinISO toolbox developed by the University of Newcastle. The toolbox allowed the MatLab to read the measurement value from the WinISO and send the feedback data back to the WinISO. The connection between the MatLab and Alphasizer was dependent on the TCP-IP protocol (Ethernet) and the Alphasizer remote control Active X package. A Proportional-Integral (PI) control algorithm is applied in the MatLab which realizes the loop control. The PI controlled MatLab program was modified from the program used for AIR FTIR, which is described in the following section. The C_0 and C* in the Figure 8.14 and 8.15 are the initial solution concentration and equilibrium solution concentration at the measured temperature, respectively.

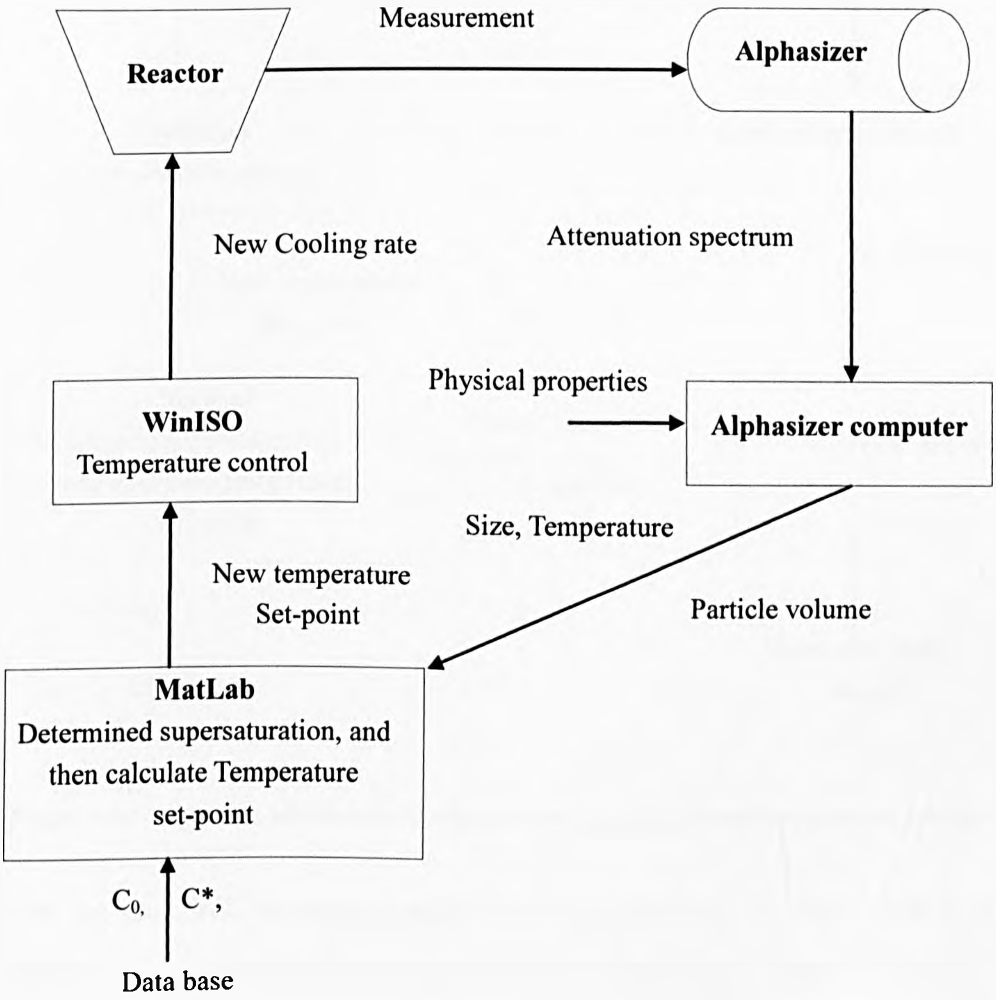

Figure 8.14: Schematic structure of the loop control system depending on sound attenuation data

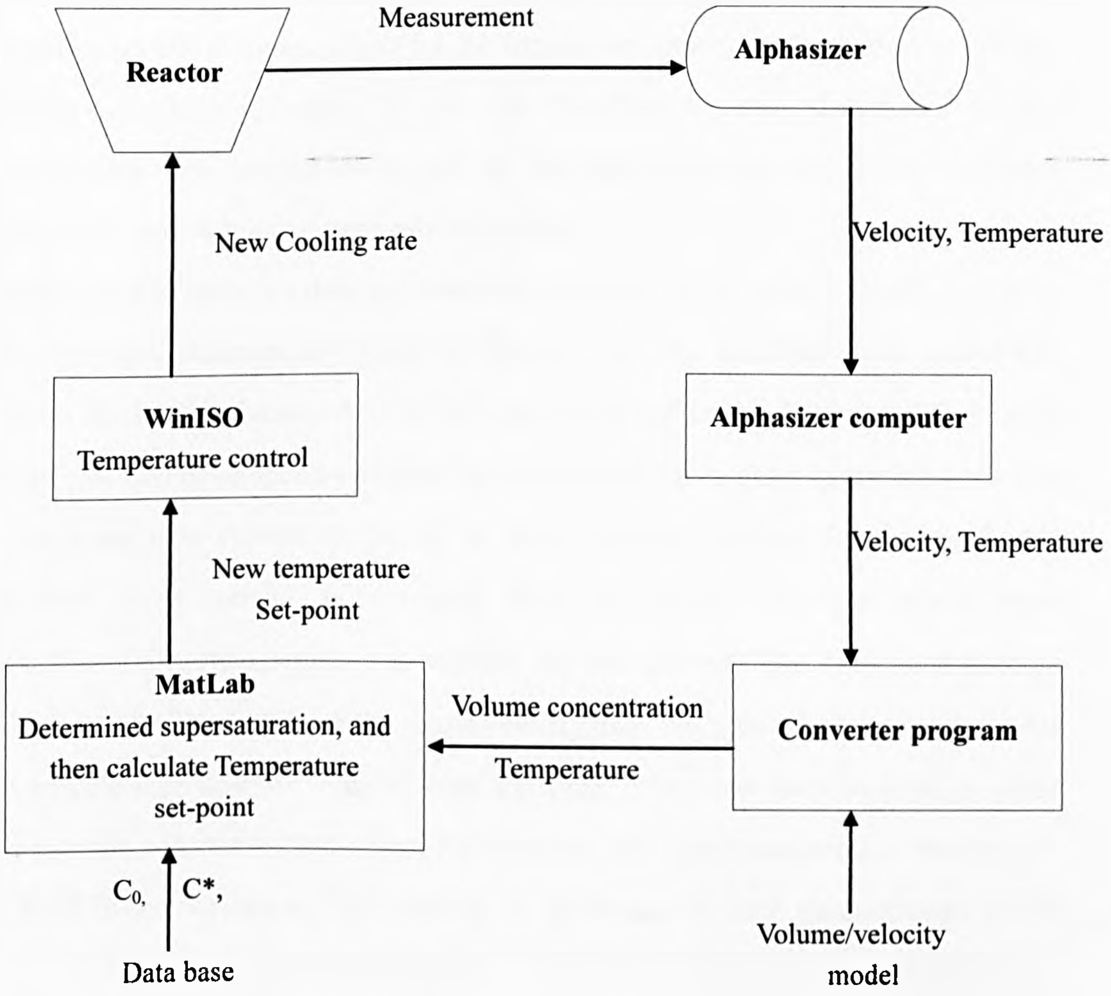

Figure 8.15: Schematic structure of the loop control system depending on sound velocity data

There are two different mathematical models controlling the loop control systems depending on the acoustic information from the Alphasizer. As shown in Figure 8.14, the Alphasizer could output sound attenuation data to the Alphasizer control computer, then the attenuation spectra could be analyzed into the particle size distribution and suspended particle volume using the ECAH model, the particle volume is collected by MatLab for the supersaturation calculation. The solute concentration can be obtained by initial solute concentration minus the weight of the crystallized crystal. The supersaturation can be derived from the solute concentration directly depending on Equation 2.10. It is apparently to see that the solution supersaturation can be monitored by measuring the suspended particle volume from the solution. However, the particle volume from the ECAH model needs the accuracy spectrum, which should be collected automatically by the Alphasizer. However, the automatic optimal strategy searching function is not yet installed in the Alphasizer, so the supersaturation monitoring can be realized after the Alphasizer further developed that installed the automatic data acquisition function.

Another way to calculate the supersaturation is based on the sound velocity data from the Alphasizer schematically shown in Figure 8.15. The modified Urick model was applied for the calculation which is fully described in Chapter 7. The modified Urick model was first developed by Pinfield et al.[10], and was applied on the measurement of the suspended volume in the oil in water emulsion system. In Chapter 7, this modified Urick model is extended into the copper sulphate pentahydrate crystallization system which was suitable for this project. The suspended particle volume can be obtained from the sound velocity data. No need for entire spectrum for the particle size analysis, only a short spectrum in the low frequency range could generate the accurate velocity data. Furthermore, the short measurement strategy can be fixed in the Alphasizer. The strategy is repeatable for each measurement, which could realize the automatic measurement. The particle volume calculated from the sound velocity data is more straightforward and accurate compared with the ECAH model. From Figure 8.15, it is easy to find that after the supersaturation was calculated from the particle volume concentration obtained from the sound velocity data, the MatLab turn to calculate the new temperature set point. The new temperature set point can determine the cooling rate of the cooling system, which modify the crystal nucleation and crystal growth rate, thus maintain the desired supersaturation level.

8.4.2 Supersaturation control algorithm

The conventional PI control algorithm was appointed in the supersaturation control system. This PI control algorithm was originally used in the previous project CBBII, which realized the supersaturation control depending on the ATR FTIR spectroscopy. The control code in MatLab was developed by Dr Layla Ozkan from University of Newcastle. In this project, the ultrasound velocity technique was used instead of the ATR FTIR spectra, and the MatLab code was modified by the Author to change the ATR FTIR interface into the Alphasizer interface in MatLab. The crystallization process code was changed to suit the copper sulphate pentahydrate crystallization process in this project.

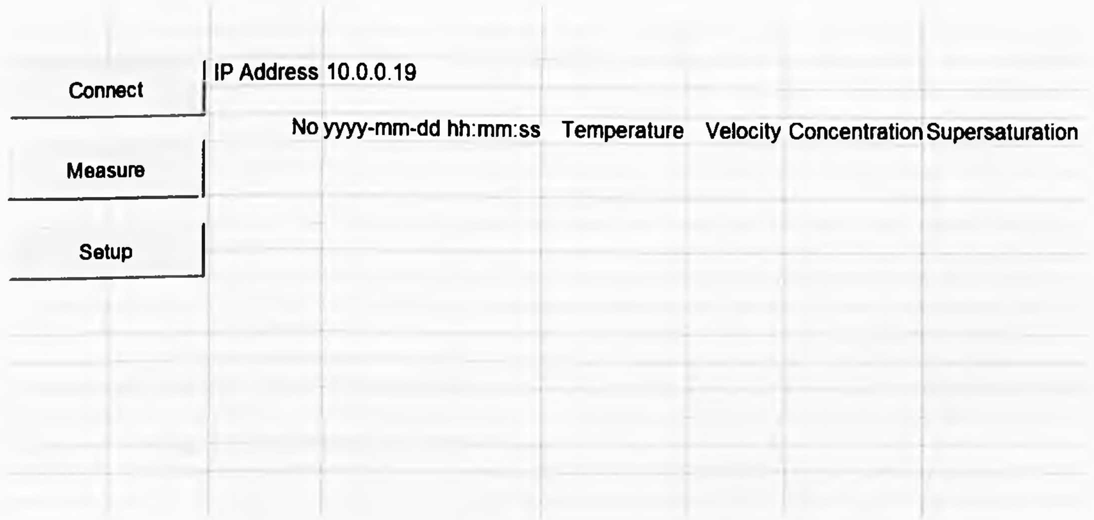

IP Address 10.0.0.19

No	yyyy-mm-dd hh:mm:ss	Temperature	Velocity	Concentration	Supersaturation

Figure 8.16: Interface of loop control system installed in MatLab

The data acquisition from the Alphasizer was described above and the interface of the loop control system is presented in Figure 8.16. The temperature data and sound velocity data were measured and transmitted to the controlling system. The control program then calculated the suspended solid crystal volume concentration, which can be converted into the current solute concentration. Combining the solute concentration and the solubility of copper sulphate pentahydrate at the current temperature, the supersaturation value can be calculated and shown in the interface.

The PI control on the supersaturation was realized by controlling the reactor cooling rate, which was determined from the sum of the cooling rates calculated from the proportional part and integral part.

$$dTdt = dTdt_{old} + dTdt\_P + dTdt\_I \tag{8.1}$$

where dTdt is the new cooling rate, $dTdt_{old}$ *is the old cooling rate, dTdt_P is the calculated correction of the cooling rate from the proportional part, and dTdt_I is the calculated correction of the cooling rate from the integral part.*

The correction of the cooling rate is proportional to the integral of the supersaturation error and determined by the error the supersaturation S_e. The supersaturation error is the difference between the supersaturation set point S_{sp} and the current supersaturation S:

$$S_e = S_{sp} - S \tag{8.2}$$

The output of the proportional part of the cooling rate correction is related to the supersaturation error during the controlling:

$$dTdt\_P = K_c(S_{e(end)} - S_{e(end-1)}) \tag{8.3}$$

where K_c *is the controller gain.*

The output from the integral part is proportional to the supersaturation error:

$$dTdt\_I = \frac{K_c}{\tau_I} S_{e(end)} \tag{8.4}$$

where τ_I *is the integral time constant.*

The controlling parameters include the process gain K_p, process dead time Θ, and the process time constant τ_c which are determined by the size of the reactor and the controlling environment. The values of these parameters were calculated and optimized by Dr. Khan during his PhD project [188]. The parameters for the 20 L reactor used in this project have the values of K_p= -1.2, Θ= 14, and τ_c= 10.5. The integral time constant τ_I= 0.6(Θ + τ_c), and the control gain K_c= 0.6/ K_p. However, these controlling parameters are not exactly accurate due to the different responding dynamics between the Alphasizer system and ATR-FTIR system. In the future, more experiments should be carried out to modify these controlling parameters in the future.

After the thousand times calibration work on the Alphasizer to find the optimal measurement strategy, the transducer of the Alphasizer was forced to change the moving distance at each experiment, the transducer was out of alignment eventually. Due to the Alphasizer being a prototype instrument which is not the commercial one, the realignment work was time consuming. The time is out of the time scale of this PhD project. Consequently, the repeats of the loop controlling work under correct solubility of copper sulphate pentahydrate need to be completed by new researchers.

Before successfully establish the Alphasizer closed loop supersaturation control system, the sound velocity measurement should be calibrated, and the results calculated from the sound velocity measurement can also be compared to the results from the sound attenuation data. The accuracy between this two methodology can be identified in the future.

8.5 Conclusions

The third generation acoustic spectroscopy Alphasizer was introduced in this chapter. The instrument was calibrated under different experimental conditions. The particle size plus particle volume concentration can be analyzed by the Alphasizer using the ECAH model depending on the acoustic attenuation spectrum. On the other hand, the supersaturation loop control system for the Alphasizer was built. The controlling model was based on the relation of crystal volume concentration and the pulsed sound group velocity which was described in Chapter 7. The communication system, the controlling model and the controlling algorithm were provided to build up the loop control system. The controlling experiments can be modified after the Alphasizer well aligned in the future.

Chapter 9 Conclusions and Future Work

Summary

This chapter gives an overview of the conclusions from the thesis and some suggestions for the direction of future research.

9.1 Conclusions

This project clearly illustrates the utilisation of ultrasonic techniques for the monitoring and measurement of the crystallization process. Both the ultrasonic attenuation and ultrasonic velocity techniques were used to predict the crystal size distribution, crystal volume concentration and the solution concentration during the dynamic crystallization process.

The fundamental characterization on the copper sulphate pentahydrate crystal was carried out and described in Chapter 5. The parameters measured include the solubility, MSZW, and the induction time, which help to predict the kinetics analysis of the material. The study of the morphology of the copper sulphate pentahydrate crystal using material studio showed the triclinic result of the material which validated the system as suitable for the acoustic analysis model, i.e., ECAH model.

It was seen in the study of the crystallization of copper sulphate that ultrasonic attenuation could measure the crystal size distribution and dispersed crystal volume concentration through the process in Chapter 6. In this study, the physical parameters for the size evaluation were identified before the measurements. The sensitivity of these physical parameters on the size evaluation was analyzed and each important parameter was measured precisely. The accuracy of the physical matrix of the copper sulphate solution was validated using the silica particles, which was the standard calibration sample for the acoustic measurements. The attenuation spectra were manually collected during the process, and the procedure for strategy optimization followed the method described in Chapter 4. The effect of the cooling rate is analyzed in this study and the suitable cooling rate and cooling range was selected considering the measurement interval requirements of MSV. The results of crystal size and crystal volume concentration monitoring throughout the process were converted into the information for growth rate. The relationship between the growth rates under different cooling rates with relative supersaturation interprets the growth mechanism of the copper sulphate pentahydrate system. On the other hand, the final crystal size in the study was around 70μm, which is still in the LWR as the low sound frequency (e.g.

1MHz) used for the measurement. In the LWR, the supersaturation can be monitored by the acoustic velocity depending on the new model developed in Chapter 7.

Studies of the acoustic velocity in Chapter 7 were divided into two parts, which included the sound velocity measurement in the pure copper sulphate solution and the particulate system, i.e., sound velocity measurement during the crystallization process. The measurements in the pure solution were carried out for the different solute concentrations under different temperatures. The sound velocity results were measured using MSV and calibrated using the ResoScan, which predicted that MSV could supply the reasonable velocity result under a limited concentration solution. The classic sound attenuation equation was employed to calculate the bulk viscosity of the Newtonian fluid only dependent on MSV, as MSV could measure the sound attenuation and sound velocity simultaneously for the limited concentration solution. In the measurement of the particulate system, the quasi induction time measurements were carried out, the adiabatic compressibility was calculated using the modified Urick equation. The modified Urick equation was first developed for the particle volume prediction in the non-solvent oil-in-water system. However, unlike the non-solvent system, the solution concentration would change along with the crystal coming out from the solution during the copper sulphate pentahydrate crystallization process. A new modified Urick equation was developed in Chapter 7 to predict the crystal volume during crystallization, which included the issue of the change in solvent concentration.

In order to counteract the drawback of the time consuming MSV for the dynamic system measurements, a new acoustic attenuation spectrometer, i.e. the Alphasizer was developed by Malvern Ltd. A number of improvements over the MSV make it more suitable for process measurement and control. The in-line sensor hardware, measurement algorithm, control software and flow-cell geometry was redesigned for the requirements of simple control and faster data acquisition. The acoustic attenuation spectra were calibrated under different conditions and shown in Chapter 8. Two silica samples of different sizes were measured under different suspended particle volumes and different temperatures. The measured spectra were compared with the results from the MSV under the same experimental conditions and simulation results. The spectra from the Alphasizer were adjusted by manually changing the measurement strategy until the results matched the MSV data. The analyzed particle size distributions based on the spectra were compared with the particle size distribution measured using the Mastersizer 2000 and the real volume concentration (known), the upper limit of the concentration was analyzed for the instrument. Due to the employment of the pulsed generation system, the group velocity can be used to determine the particle volume concentration during crystallization depending on the new model developed in Chapter 7. The supersaturation of the solution thus can be in-line calculated by the Alphasizer during the dynamic process. A new closed supersaturation loop control system was set up based on the Alphasizer, and the Proportional-Integral control algorithm was applied for the control system. The controlling structure is presented in Chapter 8 and the communication between the instruments was successfully built up.

9.2 Future work

As discussed in the conclusions, the communication of the loop control system has been successfully established, and the control programme has also been developed. However, the calibration work on the acoustic velocity of the Alphasizer is out the timescale of this project. The sound velocity calibration work can be carried out using the ResoScan and the UVM, which is similar to the calibration work on the MSV. After sound velocity calibration, the Alphasizer can be used to in-line measure the solution concentration, supersaturation, and particle volume concentration. The supersaturation loop control can be realized based on the control model presented in Chapter 7. Meanwhile the particle volume plus particle size can be analyzed from the sound attenuation results depending on the ECAH model. Because the multiple scattering system and low quality spectrum would damage the volume concentration analysis using the ECAH model, the use of acoustic velocity is more straightforward to analyze the particle volume during the crystallization process. However, the sound velocity model is of limited use in the LWR, which means the crystal size should be under the specific size according to the sound frequency used. The crystallization process includes the cooling rate and temperature range which should be redesigned to make sure the final crystals are the size in the LWR after the crystals grew.

Compared to the sound velocity prediction model, it is compulsory to calibrate the attenuation spectrum for the copper sulphate pentahydrate system due to the quality of the spectrum determining the accuracy of the analyzed volume result. Furthermore, the spectrum is different for each material based on its characteristics, the measurement strategies should be different from the ones used for the silica sample.

The applicability of the acoustic spectroscopy for solid concentration measurement and consequent estimation of the solution supersaturation was clearly demonstrated using the MSV system. This realized the possibility for applying the acoustic spectroscopy technique for the control of crystallization as the ultimate purpose of in-situ measurement only depending on this technique. After the measurement strategy of the Alphasizer was fully calibrated on the crystallization material (e.g. copper sulphate pentahydrate), it is more rapid to monitor the crystallization process due to its short measurement interval for each measurement. The kinetic analysis could predict more details on the nucleation and crystal growth steps. Combined with the growth analysis of the selected crystal face, more information can be revealed on the crystal growth mechanism.

For the deep colour solution copper sulphate, it was not possible to use the turbidity probe to predict the on set of crystallization due to the low level of light transmittance, even in the pure solution. The electrolytic conductivity probe was employed instead of the turbidity probe and successfully predicted the MSZW and induction time of the copper sulphate pentahydrate. However, the conductivity value would be disturbed by the agitation in the reactor. The conductivity probe can be used for on-line measurement if a suitable conductivity device was designed for the reactor. Along with the conductivity measurement, it is easier to define the crystallization set point but not only to observe the shape changing of the acoustic attenuation spectrum.

Reference

1. Fujiwara, M., et al., *First-principles and Direct Design Approaches for the Control of Pharmaceutical Crystallization.* Journal of Process Control, 2005. **15**(5): p. 493-504.
2. Yu, Z.Q., et al., *Recent Advances in Crystallization Control: An Industrial Perspective.* Chemical Engineering Research and Design, 2007. **85**(7): p. 893-905.
3. Heimer, S. and D. Tezak, *Structure of Polydispersed Colloids Characterised by Light Scattering and Electron Microscopy.* Advances in Colloid and Interface Science, 2002. **98**(1): p. 23.
4. Barrett, P. and B. Glennon, *Characterizing the Metastable Zone Width and Solubility Curve Using Lasentec FBRM and PVM.* chemical Engineering Research and Design, 2002. **7**: p. 799.
5. Borissova, A., et al., *In Situ Measurement of Solution Concentration during the Batch Cooling Crystallization of l-Glutamic Acid using ATR-FTIR Spectroscopy Coupled with Chemometrics.* Crystal Growth & Design, 2008. **9**(2): p. 692-706.
6. Li, R.F., X.Z. Wang, and S.B. Abebe, *Monitoring Batch Cooling Crystallization Using NIR: Development of Calibration Models Using Genetic Algorithm and PLS.* Particle & Particle Systems Characterization, 2008. **25**(4): p. 314-327.
7. Mougin, P., D. Wilkinson, and K.J. Roberts, *In Situ Measurement of Particle Size during the Crystallization of l-Glutamic Acid under Two Polymorphic Forms: Influence of Crystal Habit on Ultrasonic Attenuation Measurements.* Crystal Growth & Design, 2002. **2**(3): p. 227-234.
8. McClements, D.J., *Ultrasonic Characterisation of Emulsions and Suspensions.* Advances in Colloid and Interface Science, 1991. **37**(1-2): p. 33-72.
9. Challis, R.E., et al., *Ultrasound Techniques for Characterizing Coloidal Dispersions.* Reports on Progress in Physics, 2005. **68**: p. 1541-1637.
10. Pinfield, V.J., M.J.W. Povey, and E. Dickinson, *The Application of Modified Forms of the Urick Equation to The Interpretation of Ultrasound Velocity in Scattering Systems.* Ultrasonics, 1995. **33**(3): p. 243-251.
11. McClements, D.J. and M.J.W. Povey, *Ultrasonic Velocity as A Probe of Emulsions and Suspensions.* Advances in Colloid and Interface Science, 1987. **27**(3-4): p. 285-316.
12. Epstein, P.S. and R.R. Carhart, *The Absorption of Sound in Suspensions and Emulsions. * I. Water Fog in Air.* the Journal of the Acoustical Society of America, 1953. **25**(3): p. 553-565.
13. Ahuja, A.S., *Effect of Particle Viscosity on Propagation of Sound in Suspensions and Emulsions.* The Journal of the Acoustical Society of America, 1972. **51**(1B): p. 182-191.
14. Malvern Instrument Ltd, *Ultrasizer Manual.* 2002.

15. Giacovazzo, M., H. Artioli, and G. Viterbo, *Fundamentals of Crystallography*, ed. U. Press. 2002, Oxford.
16. Bravais, M.A., *Etudes Cristallographiques*. Academie des Sciences, 1866.
17. Mullin, J.W., *Crystallization 4th Edition*, ed. Butterworth-Heinemann. 2001, Oxford.
18. Bernstein, J., *Polymorphism in Molecular Crystals*, ed. C. Press. 2002.
19. Kitamura, M., *Controlling Factor of Polymorphism in Crystallization Process* Jounal of Grystal Growth, 2002. **237-239**: p. 2205-2214.
20. Beiny, D.H. and J.W. Mullin, *Solubilities of Higher Normal Alkanes in m-xylene*. Journal Name: J. Chem. Eng. Data; (United States); Journal Volume: 32:1, 1987: p. Medium: X; Size: Pages: 9-10.
21. Thomson, W., *On the Equilibrium of Vapour at A Curved Surface of Liquid*. Philosophical Magazine, 1871. **42**: p. 448-452.
22. Gibbs, J.W., *The Collected Work of J Willard Gibbs*. 1948, New York: Longmann Green.
23. Ostwald, W., *Über die Vermeintliche Isomerie des Roten und Gelben Quecksilberoxyds und die Oberflächenspannung Fester Körper*. Zeitschrift für physikalische Chemie, 1900. **34**: p. 495-503.
24. Freundlich, H., *Capillary and Colloid Chemistry*. Journal of the Society of Chemical Industry, 1926. **45**(44): p. 797-798.
25. Ostwald, W., *Studien über die Bildung und Umwandlung fester Körper*. Zeitschrift für physikalische Chemie, 1897. **22**: p. 289-330.
26. Miers, H.A. and F. Isaac, *Refractive Indices of Crystallyzing Solutions*. Journal of the Chemical Society, 1906. **89**: p. 413-454.
27. Miers, H.A. and F. Isaac, *The Spontaneous Crystallization of Binary Mixtures*. Proceedings of the Royal Society, 1907. **A79**: p. 322-351.
28. Nyvlt, J., *Industrial Crystallisation from Solutions*, ed. Butterworth-Heinemann. 1971, London.
29. Nyvlt, J., *Kinetics of Nucleation in Solutions*. Journal of Crystal Growth, 1968. **3-4**: p. 377-383.
30. Ni, X. and A. Liao, *Effects of Mixing, Seeding, Material of Baffles and Final Temperature on Solution Crystallization of L-glutamic Acid in an Oscillatory Baffled Crystallizer*. Chemical Engineering Journal, 2010. **156**(1): p. 226-233.
31. Nyvlt, J., et al., *Metastable Zone-width of Some Aqueous Solutions*. Journal of Crystal Growth, 1970. **6**(2): p. 151-162.
32. Gron, H., *On-line Monitoring and Control of Supersaturation in Batch Crystallisers for Oranic Fine Chemical Products Using ATR FTIR Spectroscopy*, in *Department of Mechanical and Chemical Engineering*. 2001, Heriot-Watt University: Edinburgh.
33. Nielsen, A.E., *Kinetics of Precipitation*, ed. P. Press. 1964, New York.
34. Gibbs, J.W., *Thermodynamics*, ed. Y.U. Press. 1934, New Haven.
35. Volmer, M., *Kinetic der Phasenbilding*, ed. Steinkoff. 1939, Dresden.
36. Becker, R. and W. Doring, *Kinetische Behandlung der Keimbildung in ubersattigen Dampfen*. Annalen der Physik, 1935. **24**: p. 719-752.

37. Myerson, A.S., *Handbook of Industrial Crystallization*, ed. Butterworth-Heinemann. 1993.
38. Kashchiev, D., *Nucleation: Basic Theory with Applications*, ed. Butterworth-Heinemann. 2000, Oxford.
39. Volmer, M., *Kinetic der Phasenbildung*, ed. Steinkoff. 1939, Leipzig.
40. Ting, H.H. and W.L. McCabe, *Supersaturation and Crystal Formation in Seeded Solutions of MgSO4.* Industrial & Engineering Chemistry Research, 1934. **26**(1201-1207).
41. McCabe, W.L. and R.P. Stevens, *Rate of Growth of Crystals in Aqueous Solution.* Chemical Engineering Progress, 1951. **47**(168-174).
42. Garside, J. and R.J. Davey, *Secondary Contact Nucleation: Kinetics, Growth and Scale-up.* chemical Engineering Communications, 1980. **4**: p. 393-424.
43. Garside, J., *Industrial Crystallization from Solution.* Chemical Engineering Science, 1985. **40**: p. 3-26.
44. Nyvlt, J., et al., *The Kinetics of Industrial Crystallization*, A. Press, Editor. 1985: Prague.
45. Strickland-Constable, R.F., *Kinetics and Mechanism of Crystallization*, ed. a. Press. 1968, London.
46. Nyvlt, J., *Induction Period of Nucleation and Metastable Zone Width* Collections of the Czechoslovak Chemical Communications, 1983. **48**: p. 1977-1983.
47. Kossel, W., *Zur Energetik von Oberflachenvorgangen.* Annalen der Physik, 1934. **21**(457-480).
48. O'Hara, M. and R.C. Reidd, *Modelling Crystal Growth Rates from Solution.* Englewood Cliffs, ed. Prentice-Hall. 1973.
49. Eerden, V.d., J.P. Bennema, and T.A. Cherepanova, *Survey of Monte Carlo Simulations of Crystal Surfaces and Crystal Growth.* Progress in Crystal Growth and Characterization, 1978. **1**: p. 219-264.
50. Burton, W.K., N. Cabrera, and F.C. Frank, *The Growth of Crystals and the Equilibrium Structure of Their Surfaces.* Philosophical Transactions, 1951. **A243**: p. 299-358.
51. Chernov, A.A., *The Spiral Growth of Crystals.* Soviet Physiccs Uspekhi, 1961. **4**: p. 116-148.
52. David, J. and N. Cheeke, *Fundamentals and Applications of Ultrasonic Waves* ed. C. Series. 2002.
53. Morse, P.M. and K.U. Ingard, *Theoretical Acoustics*, ed. P.U. Press. 1986, New Jersey.
54. Kinsler, L.E., et al., *Fundamentals of Acoustics, 4th Edition*, ed. Wiley. 2000, New York.
55. Temkin, S., *Elements of Acoustics*, ed. J.W.a. Sons. 2001, USA.
56. Trevena, D.H., *Ultrasonic Waves in Liquids.* Contemporary Physics, 1969. **10**(6): p. 601-614.
57. Stokes, G.G., *On the Theories of the Internal friction of Fluids in Motion, and of the Equilibrium and Motion of Elastic Solids.* Transactions of the

Cambridge Philosophical Society, 1849. **8**.

58. Lamb, H., *Hydrohynamics 6th Edition*, ed. D. Publications. 1945, New York.
59. Vigoureux, P., *Ultrasonics*, ed. L. Chapman&Hall Ltd. 1950.
60. Andreae, J.H., E.L. Heasell, and J. Lamb, *Ultrasonic Relaxation and the Vibrational Specific Heat of Carbon Disulphide* Proceedings of the Physical Society. Section B, 1956. **69**(6): p. 625-632.
61. Neppiras, E.A., *W.P. Mason,Editors, ,Physical Acoustics ,Principles and Methods Vol. 1 (1964) Academic Press,New York Part B. 376pp.* Ultrasonics, 1965. **3**(3): p. 157.
62. Hall, L., *The Origin of Ultrasonic Absorption in Water.* Physical Review, 1948. **73**(7): p. 775-781.
63. Asher, R.C., *Ultrasonic Sensors for Chemical and Process Plant*, ed. T. Francis. 1997.
64. Kaatze, U. and R. Behrends, *Hydrogen Bond Fluctuations and Dispersive Interactions of Alcohol/alkane Mixtures. An Ultrasonic Relaxation Study.* Chemical Physics Letters, 2011. **510**(1-3): p. 67-72.
65. Sato, T., A. Chiba, and R. Nozaki, *Dielectric Relaxation Mechanism and Dynamical Structures of the Alcohol/water Mixtures.* Journal of Molecular Liquids, 2002. **101**(1-3): p. 99-111.
66. Strutt, J.W.L.R., *Theory of Sound*, ed. Macmillan. 1877, London.
67. Wood , A.B., *A Textbook of Sound*, ed. B.a. Sons. 1941, London.
68. Wood , A.B., *A Textbook of Sound, 3rd Edition*, ed. B.a. Sons. 1964, London.
69. Nomura, H., F. Kawaizumi, and T. Iida, *Partial Specific Compressibility and its Relation to Solvation of Solute Based on Measurements of Suspension System.* Bulletin of the Chemical Society of Japan, 1987. **60**: p. 25-30.
70. Povey, M.J.W. and T.J. Mason, *Ultrasound in Food Processing*, ed. B.A. Professional. 1998, London.
71. Dukhin, A.S. and P.J. Goetz, *Ultrasound for Characterizing Colloids: Particle Sizing, Zeta Potential, Rheology*, ed. Elsevier. 2002.
72. Kocis, S. and Z. Figura, *Ultrasonic Measurements and Technologies*, ed. C. Hall. 1996.
73. Elmore, W.C. and M.A. Heald, *Physics of Waves*, ed. D. Publications. 1985, New York.
74. Waterman, P.C. and R. Truell, *Multiple Scattering of Waves.* Journal of mathematical physics, 1961. **2**(4): p. 512-537.
75. McClements, D.J. and M.J.W. Povey, *Scattering of Ultrasound by Emulsions.* Journal of Physics D: Applied Physics, 1989. **22**: p. 38-47.
76. Miles, C.A., D. Shore, and K.R. Langley, *Attenuation of Ultrasound in Milks and Creams.* Ultrasonics, 1990. **28**(6): p. 394-400.
77. Anson, L.W. and R.C. Chivers, *Thermal Effects in the Attenuation of Ultrasound in Dilute Suspensions for Low Values of Acoustic Radius.* Ultrasonics, 1990. **28**(1): p. 16-26.
78. Kytomaa, H.K., *Theory of Sound Propagation in Suspensions: A Guide to Particle Size and Concentration Characterization.* Powder Technology, 1995.

82(1): p. 115-121.

79. Dukhin, A.S., P.J. Goetz, and C.W. Hamlet, *Acoustic Spectroscopy for Concentrated Polydisperse Colloids With Low-density Contrast* Langmuir, 1996. **12**: p. 4998-5003.
80. McClements, D.J., *Ultrasonic Measurements in Particle Size Analysis*, in *Encyclopedia of Analytical Chemistry*. 2006, John Wiley & Sons, Ltd.
81. Wang, Y. and M.J.W. Povey, *A Simple and Rapid Method for the Determination of Particle Size in Emulsions from Ultrasound Data.* Colloids and Surfaces B: Biointerfaces, 1999. **12**(3-6): p. 417-427.
82. McClements, D.J., *Principles of Ultrasonic Droplet Size Determination.* Langmuir, 1996. **12**: p. 3454-3461.
83. Tebbutt, J.S. and R.E. Challis, *Ultrasonic Wave Propagation in Colloidal Suspensions and Emulsions: A Comparison of Four Models.* Ultrasonics, 1996. **34**(2-5): p. 363-368.
84. Gomez Alvarez-Arenas, T.E., L. Elvira Segura, and E. Riera Franco de Sarabia, *Characterization of Suspensions of Particles in Water by an Ultrasonic Resonant Cell.* Ultrasonics, 2002. **39**(10): p. 715-727.
85. Challis, R.E., J.S. Tebbutt, and A.K. Holmes, *Equivalence Between Three Scattering Formulations for Ultrasonic Wave Propagation in Particulate Mixtures.* Journal of Physics D: Applied Physics, 1998. **31**: p. 3481-3497.
86. Hipp, A.K., G. Storti, and M. Morbidelli, *On multiple-particle Effects in the Acoustic Characterization of Colloidal Dispersoins.* Journal of Physics D: Applied Physics, 1999. **32**(5): p. 568.
87. Sewell, C.J.T., *The Extinction of Sound in a Viscous Atmosphere by Small Obstacles of Cylindrical and Spherical Form.* Philosophical Transactions of the Royal Society of London, 1911. **210**: p. 239-270.
88. Hartmann, G.K. and A.B. Focke, *Absorption of Supersonic Waves in Water and in Aqueous Suspensions.* Physical Review, 1940. **57**(3): p. 221-225.
89. Ulrick, R.J., *The Absorption of Sound in Suspensions of Irregular Particles.* The Journal of the Acoustical Society of America, 1948. **20**(3): p. 283-289.
90. Ulrick, R.J. and W.S. Ament, *The Propagaton of Sound in Composite Media.* The Journal of the Acoustical Society of America, 1949. **21**(2): p. 115-119.
91. Ament, W.S., *Sound Propagation in Gross Mixtures.* The Journal of the Acoustical Society of America, 1953. **25**(4): p. 638-641.
92. Allegra, J.R. and S.A. Hawley, *Attenuation of Sound in Suspensions and Emulsions: Theory and Experiments.* The Journal of the Acoustical Society of America, 1971. **51**(5): p. 1545-1564.
93. Lloyd, P. and M.V. Berry, *Wave Propagation through An Assembly of Spheres IV. Relations between Different Multiple Scattering Theories.* Proceedings of the Physical Society, 1967. **91**: p. 678-688.
94. Twersky, V., *Acoustic Bulk Parameters in Distributions of Pair - Correlated Scatterers.* 1978, 1978. **64**(6): p. 1710-1719.
95. Javanaud, C. and A. Thomas, *Multiple Scattering using the Foldy-Twersky Integral Equation.* Ultrasonics, 1988. **26**(6): p. 341-343.

96. Harker, A.H. and J.A.G. Temple, *Velocity and Attenuation of Ultrasound in Suspensions of Particles in Fluids.* Journal of Physics D: Applied Physics, 1987. **21**: p. 1576-1588.
97. Harker, A.H., et al., *Ultrasonic Propagation in Slurries.* Ultrasonics, 1991. **29**(6): p. 427-438.
98. Austin, J.C., et al., *Ultrasonic Wave Propagation in Colloid Suspensions and Emulsions: Recent Experimental Results.* Ultrasonics, 1996. **34**: p. 369-374.
99. Babick, F., et al., *Ultrasonic Spectrometry for Particle Size Analysis in Dense Submicron Suspensions.* Particle & Particle Systems Characterization, 1998. **15**(5): p. 230-236.
100. Hipp, A.K., G. Storti, and M. Morbidelli, *Acoustic Characterization of Concentrated. Suspensions and Emulsions. 1. Model Analysis.* Langmuir, 2002. **18**: p. 391-404.
101. Spelt, P.D.M., et al., *Determination of Particle Size Distributions from Acoustic Wave Propagation Measurements.* Physics of Fluids, 1999. **11**(5): p. 1065-1080.
102. Povey, M.J.W., *Ultrasonic Techniques for Fluids*, ed. A. Press. 1997, London.
103. McClements, D.J. and J.N. Coupland, *Theory of Droplet Size Distribution in Emulsions Using Ultrasonic Spectroscopy.* Colloids and Surfaces A: Physicochemical and Engineering Aspects, 1996. **117**: p. 161-170.
104. Meyer, S., et al., *A Comparative Study of Ultrasound and Laser Light Diffraction Techniques for Particle Size Determination in Dairy Beverages.* Measurement Science and Technology, 2006. **17**(2): p. 289-297.
105. Kuster, G.T. and M.N. Toksoz, *Velocity and Attenuation of Seimic Waves in Two-phase Media: Part I. Theoretical Formulations.* Geophysics, 1974. **39**(5): p. 587-606.
106. Kuster, G.T. and M.N. Toksoz, *Velocity and Attenuation of Seismic Waves in Two- phase Media: Part II. Experimental Results.* Geophysics, 1974. **39**(5): p. 607-618.
107. Johnson, D.L. and T.J. Plona, *Acoustic Slow Waves and the Consolidation Transition.* The Journal of the Acoustical Society of America, 1982. **72**(2): p. 556-565.
108. Pinfield, V., *Studies of Creaming, Flocculation and Crystallization in Emulsions: Computer Modelling and Analysis of Ultrasound Propagation.* , in *Food Science.* 1996, University of Leeds: Leeds.
109. Dickinson, E., D.J. McClements, and M.J.W. Povey, *Ultrasonic Investigation of the Particle Size Dependence of Crystallization in n-hexadecane-in-water Emulsions.* Journal of Colloid and Interface Science, 1991. **142**(1): p. 103-110.
110. McClements, D.J., M.J.W. Povey, and E. Dickinson, *Absorption and Velocity Dispersion due to Crystallization and Melting of Emulsion Droplets.* Ultrasonics, 1993. **31**(6): p. 433-437.
111. Miles, C.A., G.A.J. Fursey, and R.C.D. Jones, *Ultrasonic Estimation of Solid/liquid Ratios in Fats, Oils and Adipose Tissue.* Journal of the science of food and agriculture, 1985. **36**(3): p. 215-228.

112. McClements, D.J., *The Use of Ultrasonics for Characterising Fats and Emulsions*, in *Food Science Department*. 1988, University of Leeds: Leeds.
113. Julian McClements, D., E. Dickinson, and M. J.W. Povey, *Crystallization in Hydrocarbon-in-water Emulsions Containing a Mixture of Solid and Liquid Droplets.* Chemical Physics Letters, 1990. **172**(6): p. 449-452.
114. McClements, D.J., et al., *Effect of Emulsifier Type on the Crystallization Kinetics of Oil-in-Water Emulsions Containing a Mixture of Solid and Liquid Droplets.* Journal of Colloid and Interface Science, 1993. **160**(2): p. 293-297.
115. McClements, D.J. and M.J.W. Povey, *Ultrasonic Analysis of Edible Fats and Oils.* Ultrasonics, 1992. **30**(6): p. 383-388.
116. Dickinson, E., et al., *Crystallization in Oil-in-water Emulsions Containing Liquid and Solid Droplets.* Colloids and Surfaces A: Physicochemical and Engineering Aspects, 1993. **81**(0): p. 273-279.
117. Hindle, S., M.J.W. Povey, and K. Smith, *Kinetics of Crystallization in n-Hexadecane and Cocoa Butter Oil-in-Water Emulsions Accounting for Droplet Collision-Mediated Nucleation.* Journal of Colloid and Interface Science, 2000. **232**(2): p. 370-380.
118. Hindle, S.A., M.J.W. Povey, and K.W. Smith, *Characterizing Cocoa Butter Seed Crystals by the Oil-in-water Emulsion Crystallization Method.* Journal of the American Oil Chemists' Society, 2002. **79**(10): p. 993-1002.
119. Dickinson, E., J. Ma, and M.J.W. Povey, *Crystallization Kinetics in Oil-in-water Emulsions Containing A Mixture of Solid and Liquid Droplets.* Journal of the Chemical Society, Faraday Transactions, 1996. **92**(7).
120. TF Instruments Ltd, *ResoScan Manual.* 1990.
121. Liu, L., *Application of Ultrasound Spectroscopy for Nanoparticle Sizing in High Concentration Suspensions: A Factor Analysis on the Effects of Concentration and Frequency.* Chemical Engineering Science, 2009. **64**(23): p. 5036-5042.
122. Povey, M.J.W., *Acoustic Methods for Particle Characterisation.* Kona, 2006. **24**: p. 126-133.
123. Novak, J., *What Is Conductivity and How Is IT Measured, A Technical Handbook for Industry*, in *Hach Company*. 2003.
124. Coulson, J. and J. Richardson, *Chemical Engineering: Fluid Flow, Heat Transfer and Mass Transfer vol.1.* 6 Edition, ed. Butterworth-Heinemann. 1999.
125. Jillavenkatesa, A., S.J. Dapkunas, and L.H. Lum, *Particle Size Characterization*, ed. N.I.o.S.a. Technology. 2001.
126. Xu, R., *Particle Characterization: Light Scattering Methods*, ed. K.A. Publishers. 2001.
127. Ruf, A., J. Worlitschek, and M. Mazzotti, *Modeling and Experimental Analysis of PSD Measurements through FBRM.* Particle & Particle Systems Characterization, 2000. **17**(4): p. 167-179.
128. Kerker, M., *The scattering of Light and other electromagnetic radiation*, ed. a. Press. 1969, New York.

129. Hulst, H.C.v.d., *Light Scattering by Small Particles*, ed. Wiley. 1957, New York.
130. Malvern Instrument Ltd, *MAN 0247*, in *MasterSizer Operator Manua*. 2007.
131. Kittel, C., *Introduction to Solid State Physics, 7th edition*, ed. J.W. Sons. 1996.
132. Cullity, B.D., *Elements of X-ray Diffraction*, ed. Addison-Wesley. 1959.
133. Bergström, C.A.S., et al., *Experimental and Computational Screening Models for Prediction of Aqueous Drug Solubility.* Pharmaceutical Research, 2002. **19**(2): p. 182-188.
134. Chen, X.-Q. and S. Venkatesh, *Miniature Device for Aqueous and Non-aqueous Solubility Measurements During Drug Discovery.* Pharmaceutical Research, 2004. **21**(10): p. 1758-1761.
135. Glomme, A., J. März, and J.B. Dressman, *Comparison of a Miniaturized Shake-flask Solubility Method with Automated Potentiometric Acid/base Titrations and Calculated Solubilities.* Journal of Pharmaceutical Sciences, 2005. **94**(1): p. 1-16.
136. Yi, Y., et al., *Development of a Small-Scale Automated Solubility Measurement Apparatus.* Industrial & Engineering Chemistry Research, 2005. **44**(15): p. 5427-5433.
137. Harris, A.D. and L.H. Kalbus, *Decomposition of Copper(II) Sulfate Pentahydrate: A Sequential Gravimetric Analysis.* Journal of Chemical Education, 1979. **56**(6): p. 417.
138. Saig, A., et al., *A Continuous Polymorphic Transition of Coordinating Water Molecules in CuSO4 5H2O.* Journal of Physics and Chemistry of Solids, 2003. **64**(4): p. 701-706.
139. Oki, H., E. Kyuno, and R. Tsuchiya, *Some Thermal Properties of Deuterated Copper(II) Sulphate Pentahydrate.* Bulletin of the Chemical Society of Japan, 1970. **43**: p. 3263-3264.
140. Sohnel, O. and P. Novotny, *Densities of Aqueous Solutions of Inorganic Substances*, ed. Elsevier. 1985, Amsterdam.
141. Mullin.J.W, *Crystallization 4th Edition*, ed. Butterworth-Heinemann. 2001, Oxford.
142. Garside, J., A. Mersmann, and J. Nyvlt, *Measurement of Crystral Growth and Nucleation Rates (second edition)*, ed. I.o.C.E. (IChemE). 2002.
143. Giulietti, M., et al., *Crystallization of Copper Sulphate.* Crystal Research and Technology, 1995. **30**: p. 177-183.
144. Jiang, H.Y., *Crystllization Research of Copper Sulphate Pentahydrate.* 2007, Tianjing University Tianjing.
145. Gerson, A.R., K.J. Roberts, and J.N. Sherwood, *An Instrument for the Examination of Nucleation from Solution and Its Application to the Study of Precipitation from Diesel Fuels and Solutions of n-alkanes.* Powder Technology, 1991. **65**(1-3): p. 243-249.
146. Boyd, S., et al., *Solubility, Metastable Zone Width Measurement and Crystal Growth of the 1:1 Benzoic Acid/isonicotinamide Cocrystal in Solutions of Variable Stoichiometry.* Journal of Pharmaceutical Sciences, 2010. **99**(9): p.

3779-3786.

147. Fey, G.T.-K., W.-K. Liu, and Y.-C. Chang, *Temperature and Concentration Effects on the Conductivity of LiAlCl4/SOCl2 Electrolyte Solutions.* Journal of Power Sources, 2001. **97-98**(0): p. 602-605.
148. de Diego, A., J.M. Madariaga, and E. Chapela, *Empirical Model of General Application to Fit (k, c, T) Experimental Data from Concentrated Aqueous Electrolyte Solutions.* Electrochimica Acta, 1997. **42**(9): p. 1449-1456.
149. de Diego, A., et al., *Application of the Electrical Conductivity of Concentrated Electrolyte Solutions to Industrial Process Control and Design: from Experimental Measurement towards Prediction through Modelling.* TrAC Trends in Analytical Chemistry, 2001. **20**(2): p. 65-78.
150. Kralchevsky, P.A., et al., *Method for Analysis of the Composition of Acid Soaps by Electrolytic Conductivity Measurements.* Journal of Colloid and Interface Science, 2008. **327**(1): p. 169-179.
151. Halden, K., A.A.P. De Alwis, and P.J. Fryer, *Changes in the Electrical Conductivity of Foods during Ohmic Heating.* International Journal of Food Science & Technology, 1990. **25**(1): p. 9-25.
152. Assiry, A.M., et al., *Electrical Conductivity of Seawater during Ohmic Heating.* Desalination, 2010. **260**(1-3): p. 9-17.
153. Mehla, P.S., S.K. Chakarvarti, and N. Singh, *On the Variation of Electrical Conductivity with Temperature and Concentration of Some Etchants Used in Electrolytically Controlled Etching of Nuclear Track Filters.* International Journal of Radiation Applications and Instrumentation. Part D. Nuclear Tracks and Radiation Measurements, 1988. **15**(1-4): p. 305-307.
154. Málek, J., J. Klikorka, and L. Tichý, *Conductivity Measurements during the Crystallization of* Bi_2S_3 *in* $Ge_{20}Bi_{15}S_{65}$ *Glass.* Journal of Materials Science Letters, 1986. **5**(2): p. 183-185.
155. Lyczko, N., et al., *Effect of Ultrasound on the Induction Time and the Metastable Zone Widths of Potassium Sulphate.* Chemical Engineering Journal, 2002. **86**(3): p. 233-241.
156. Sohnel, O. and J.W. Mullin, *A Method for the Determination of Fercipitation Induction Periods.* journal of crystal growth, 1978. **44**: p. 377-382.
157. Genceli, F.E., C. Himawan, and G.J. Witkamp, *Inline Determination of Supersaturation and Metastable Zone Width of MgSO4.12H2O with Conductivity and Refractive Index Measurement Techniques.* Journal of Crystal Growth, 2005. **275**: p. e1757-e1762.
158. Taguchi, K., J. Garside, and N.S. Tavare, *Nucleation and Growth Kinetics of Barium Sulphate in Batch Precipitation.* Journal of Crystal Growth, 1996. **163**(3): p. 318-328.
159. Casteel, J.F. and E.S. Amis, *Specific Conductance of Concentrated Solutions of Magnesium Salts in Water-ethanol System.* Journal of Chemical & Engineering Data, 1972. **17**(1): p. 55-59.
160. Yongsawatdigul, J., J.W. Park, and E. Kolbe, *Electrical Conductivity of Pacific Whiting Surimi Paste during Ohmic Heating.* Journal of Food Science, 1995.

60(5): p. 922-925.

161. Lyall, E., et al., *In Situ Ultrasonic Spectroscopy Study of the Nucleation and Growth of Copper Sulfate Pentahydrate Batch Crystallized from Supersaturated Aqueous Solutions.* Industrial & Engineering Chemistry Research, 2004. **43**(16): p. 4947-4956.
162. Nyvlt, J., *The Metastable Zone Width of Ammonium Aluminium Sulphate and Mechanisms of Secondary Nucleation.* Collections of the Czechoslovak Chemical Communications, 1982. **47**: p. 1184-1188.
163. Mougin, P., *In situ and On-line Ultrasonic Attenuation Spectroscopy for Particle Sizing during the Crystallization of Organic Fine Chemicals*, in *Mechanical and Chemical Engineering.* 2001, Heriot-Watt University.
164. Hipp, A.K., et al., *In-Situ Monitoring of Batch Crystallization by Ultrasound Spectroscopy.* Industrial & Engineering Chemistry Research, 2000. **39**(3): p. 783-789.
165. Mougin, P., D. Wilkinson, and K.J. Roberts, *In Situ Ultrasonic Attenuation Spectroscopic Study of the Dynamic Evolution of Particle Size during Solution-Phase Crystallization of Urea.* Crystal Growth & Design, 2002. **3**(1): p. 67-72.
166. Mougin, P., et al., *Characterization of Particle Size and Its Distribution during the Crystallization of Organic Fine Chemical Products as Measured in situ Using Ultrasonic Attenuation Spectroscopy.* J Acoust Soc Am, 2001. **109**(1): p. 274-282.
167. Tebbutt, J.S., T. Marshall, and R.E. Challis, *Monitoring of Copper(II) Sulfate Pentahydrate Crystallization Using Ultrasound.* Langmuir, 1999. **15**(9): p. 3356-3364.
168. Penchev, R.Y., *Monitoring and Controlling Crystal Size During Industrial Batch Crystallization Processes via the Use of ATR-FTIR and Acoustic Attenuation Spectroscpy Techniques*, in *School of Processes, Environmental and Materials Engineering.* 2007, University of Leeds: Leeds.
169. Karpinski, P. and K. Toyokura, *Nucleation and Growth of Copper Sulphate Crystals in A Fluidized Bed*, in *Industrial Crystallization 78*, E.J. Jong and S.J. Jancic, Editors. 1979, North-Holland: Amsterdam. p. 55-64.
170. Karpinski, P., *Mass Crystallization in a Fluidized Bed*, ed. W.P. Wrocawskiej. 1981, Wroclaw.
171. Toyokura, K., et al., *Secondary Nucleation of $KAl(SO_4)_2$ $12H_2O$, $MgSO_4$ H_2O, and $CuSO_4$ $5H_2O$*, in *Industrial Crystallization 81*, E.J. Jong and S.J. Jancic, Editors. 1982, North-Holland: Amsterdam. p. 87-96.
172. Tai, C.Y. and R.K. Pan, *Growth Kinetics of Copper Sulphate Pentahydrate Crystals in Pure and Impure Systems.* Journal of the Chinese Institute of Chemical Engineers, 1985. **16**: p. 379.
173. Zumstein, R.C. and R.W. Rousseau, *Anomalous Growth of Large and Small Copper Sulphate Pentahydrate Crystals.* Industrial & Engineering Chemistry Research 1989. **28**: p. 289-297.
174. Dukhin, A.S. and P.J. Goetz, *Bulk Viscosity and Compressibility Measurement*

using Acoustic Spectroscopy. The Journal of Chemical Physics, 2009. **130**(12): p. 124519-13.

175. Stokes, R. and R. Mills, *Viscosity of Electrolytes and Related Properties*. 1965, Oxford: Pergamon Press.
176. Breslau, B.R. and I.F. Miller, *On the Viscosity of Concentrated Aqueous Electrolyte Solution.* The Journal of Physical Chemistry, 1970. **74**(5): p. 1056-1061.
177. Hu, Y.F., *Prediction of Viscosity of Mixed Electrolyte Solutions Based on the Eyring's Absolute Rate Theory and the Equations of Patwardhan and Kumar.* Chemical Engineering Science, 2004. **59**(12): p. 2457-2464.
178. Zemansky, M. and R. dittman, *Heat and Thermodynamics*. 1997: London: McGraw- Hill.
179. Lide, D.R., *CRC Handbook of Chemistry and Physics 83 rd Edition*, ed. F.C.P.T. Boca Raton. 2002.
180. Holmes, M.J., N.G. Parker, and M.J.W. Povey. *Temperature Dependence of Bulk Viscosity in Water using Acoustic Spectroscopy.* in *6th Groupe De Recherche 2501 and 9th Anglo-French Physical Acoustics Joint Conference.* 2011.
181. Xu, J., et al., *Measurement of the Bulk Viscosity of Liquid by Brillouin Scattering.* Applied Optics, 2003. **42**(33): p. 6704-6709.
182. Pinfield, V.J. and M.J.W. Povey, *Thermal Scattering Must Be Accounted for in the Determination of Adiabatic Compressibility.* The Journal of Physical Chemistry B, 1997. **101**(7): p. 1110-1112.
183. Povey, M.J.W., et al., *Investigation of Bovine Serum Albumin Denaturation using Ultrasonic Spectroscopy.* Food Hydrocolloids, 2011. **25**(5): p. 1233-1241.
184. Umchid, S. *Frequency Dependent Ultrasonic Attenuation Coefficient Measurement*. 2008.
185. Bobber, R., *Underwater Electroacoustic Measurements*, ed. N.R. Laboratory. 1970.
186. Mohyuddin, I., *Development of A New Ultrasonic Spectrometer for In-process Particle Size Analysis*. 2006, University of Leeds.
187. Alba, F., *Method and Apparatus for Determining Particle Size Distribution and Concentration in a Suspension using Ultrasonics.* United states patent, 1992.
188. Khan, S., *Application of On-line ATR-FTIR Spectroscopy for Monitoring, Controlling and Scaling-up the Batch Crystallization of L-Glutamic Acid*, in *School of Process, Environmental and Materials Engineering*. 2008, University of Leeds: Leeds.